Understanding the pathophysiology of spinal muscular atrophy skeletal muscle

Justin G. Boyer

Thesis submitted to the
Faculty of Graduate and Postdoctoral Studies
in partial fulfillment of the requirements
for the Doctorate in Philosophy degree in Cellular and Molecular Medicine

Department of Cellular and Molecular Medicine

Faculty of Medicine

University of Ottawa

Abstract

The disruption of the survival motor neuron (*SMN1*) gene leads to the children's genetic disease spinal muscular atrophy (SMA). SMA is characterized by the degeneration of α-motor neurons and skeletal muscle atrophy. Although SMA is primarily considered a motor neuron disease, the involvement of muscle in its pathophysiology has not been ruled out. To gain a better understanding of the involvement of skeletal muscle pathophysiology in SMA, we have developed three aims: to identify cell-specific Smn-interacting proteins, to characterize postnatal skeletal muscle development in mouse models of SMA, and to assess the functional capacity of muscles from SMA model mice. We have used tandem affinity purification to discover Smn interacting partners in disease relevant cell types. We have identified novel cell-specific Smn interacting proteins of which we have validated myosin regulatory light chain as a muscle-specific Smn associated protein *in vivo*. We have taken advantage of two different mouse models of SMA, the severe *Smn*$^{-/-}$*;SMN2* mouse and the less severe *Smn*$^{2B/-}$ mouse, to study the postnatal development of skeletal muscle. Primary myoblasts from *Smn*$^{2B/-}$ mice demonstrate delayed myotube fusion and aberrant expression of the myogenic program. In addition, the expression of myogenic proteins was delayed in muscles from severe *Smn*$^{-/-}$*;SMN2* and less severe *Smn*$^{2B/-}$ SMA model mice. Muscle denervation and degeneration, however, are not the cause of the aberrant myogenic program. At the functional level, we demonstrate a significant decrease in force production in pre-symptomatic *Smn*$^{-/-}$*;SMN2* and *Smn*$^{2B/-}$ mice indicating that muscle weakness is an early event in these mice. Immunoblot analyses from hindlimb skeletal muscle samples revealed aberrant levels of developmentally regulated proteins important for muscle

function, which may impact muscle force production in skeletal muscle of SMA model mice. The present study demonstrates early and profound intrinsic muscle weakness and aberrant expression of muscle proteins in mouse models of SMA, thus demonstrating how muscle defects can contribute to the disease phenotype independently of and in addition to that caused by motor neuron pathology.

TABLE OF CONTENTS

LIST OF TABLES

LIST OF FIGURES

List of abbreviations:

ALS	Amyotrophic lateral sclerosis
ANOVA	analysis of variance
BTX	alpha-bungarotoxin
CCAC	Canadian Council on Animal Care
ChAT	choline acetyltransferase
DAPI	4', 6-diamidino-2-phenylindole
DSHB	Developmental Studies Hybridoma Bank
EBD	Evan's blue dye
GAPDH	glyceraldehyde 3-phosphate dehydrogenase
GLM	General Linear Model
hnRNP-A1	heterogeneous nuclear ribonucleoprotein A1
HSA	human skeletal-actin
L	lumbar
LAL	levator auris longus
MEF2	myocyte enhancer factor-2
MHC	myosin heavy chain
miRNA	micro-RNA
MRF	myogenic regulatory factor
MRF4	muscle-specific regulatory factor 4
Myf5	myogenic factor 5
MyoD	myoblast determination protein
MyoG	myogenin
MRLC	myosin regulatory light chain
NMJ	neuromuscular junction
NF	neurofilament
NF1	nuclear factor 1
P	postnatal day
Pax7	paired box transcription factor 7
PCR	polymerase chain reaction
PRMT	protein arginine methyltransferase
PrP	prion protein
QPCR	quantitative polymerase chain reaction
RA	rectus abdominis
RhoA-GTP	Ras homolog gene family, member A guanosine-5'-triphosphate
RyR1	ryanodine receptor 1
SERCA	sarcoplasmic reticulum Ca^{2+} ATPase
SDS-PAGE	sodium dodecyl sulfate polyacrylamide gel electrophoresis
SF2/ASF	splicing factor 2/alternative splicing factor
SBMA	Spinal bulbar muscular atrophy
Sm	Smith antigen
SMA	spinal muscular atrophy
SMN	survival motor neuron
snRNA	small nuclear RNAs
SnRNP	spliceosomal small nuclear ribonucleoprotein

SOD1	Cu/Zn superoxide dismutase 1
SV2	synaptic vesicle protein 2
TA	tibialis anterior
TAP	Tandem Affinity Purification
TEV	Tobacco Etch Virus
TVA	transversus abdominis
Unrip	UNR-interacting protein
ZEB	zinc-finger E box-binding protein

Authorization

Chapter 1 was adapted from Boyer et al. The many faces of SMN: deciphering the function critical to spinal muscular atrophy pathogenesis. Future Neurology. (2010) 5(6), 873-890 with permission from the copyright holder, Dr. Rashmi Kothary.

Chapter 2 was reprinted with permission from Shafey, D., J. G. Boyer, K. Bhanot and R. Kothary (2010). "Identification of novel interacting protein partners of SMN using tandem affinity purification." J Proteome Res **9**(4): 1659-1669. Copyright 2010 American Chemical Society.

Acknowledgments

The last few years have been very intensive and demanding and I would like to acknowledge some of the many people who have continuously supported me during the course of my studies. First and foremost, I would like to extend my sincere gratitude to my supervisor and mentor, Dr. Rashmi Kothary. His support and guidance throughout my PhD have been invaluable and I am grateful for the scientific freedom that he entrusted me with which allowed me to develop my potential as a researcher. I am grateful for our many conversations not only concerning my work, but also about my career choices and opportunities. I thank him for sharing his experiences about the joys and frustrations of being a scientist. Working with Dr. Kothary has been a very fulfilling and enriching experience for which I will be forever grateful.

I would like to acknowledge my lab co-workers: Yves De Repentigny, Dr. Lyndsay Murray, Dr. Melissa Bowerman, Dr. James Knight, Carrie Anderson, Ariane Beauvais, Marc-Oliver Deguise, Sabrina Gibeault, Armin Yazdani, Dr. Scott Ryan, and *The Core*: Kunal Bhanot, Andrew Ferrier, John-Paul Michalski, and Ryan O'Meara for their help. I thank them for our beneficial discussions and for making the laboratory atmosphere one that I enjoyed tremendously.

I thank my committee members: Dr. Jocelyn Côté, Dr. Lynn Megeney and Dr. Robin Parks for their guidance and inspiration throughout my PhD. A special thank you is given to Dr. Parks for the many conversations we had about his experiences as a researcher and for his advice regarding my applications to find a postdoc position.

I would like to thank the Canadian Institutes of Health Research and the Ontario Government for generously funding my graduate studies.

Finally, I want to express my heartfelt gratitude to my wonderful wife, my parents, my sister and my parents-in-law. Their love, support, patience and understanding throughout my PhD have been a great source of encouragement and have provided me a sense of relief in times of difficult decisions.

Chapter 1

General Introduction

1.1 Spinal muscular atrophy

Spinal muscular atrophy (SMA) is the most common genetic disease resulting in infant death, affecting approximately 1 in 6,000-10,000 births (Pearn 1978, Crawford and Pardo 1996). This autosomal recessive disease is characterized by a loss of α-motor neurons in the spinal cord and brain stem, accompanied by atrophy of the limb and trunk musculature, which eventually leads to paralysis and in severe cases, death (Crawford and Pardo 1996).

SMA is a heterogeneous disease and its clinical manifestations are classified based on age of onset and severity of symptoms (Table 1.1). Type 0 SMA has a prenatal onset and is typified by reduced fetal movements *in utero* and early neonatal death (Dubowitz 1999, MacLeod et al. 1999). Type I SMA (also known as Werdnig-Hoffmann disease) is the most severe form and afflicts patients with symptoms before 6 months of age. These patients are never able to sit up and usually die between 2-4 years of age due to respiratory distress. Technological advancements and proactive patient care such as the use of noninvasive pulmonary support and gastrostomy tube feeding have had a positive impact on the natural history of SMA (Oskoui et al. 2007). In fact, SMA type I patients diagnosed in the 2000s live significantly longer than type I patients from the 1980s because of the proactive disease management (Oskoui et al. 2007).

Type II and type III SMA (also known as Kugelberg-Welander disease) are milder forms where patients exhibit symptoms between 6 months and 17 years of age. Similar to type I, type II patients often develop serious pulmonary and orthopedic complications that require ventilation support to improve respiratory symptoms and surgical interventions to slow the progression of scoliosis (Montes et al. 2009). However,

type II children are generally able to stand and sit but not walk, while type III adults have the ability to walk if aided (Pearn 1980, Munsat and Davies 1992). Finally, individuals with type IV SMA, an adult onset form of the disease, develop symptoms after the age of 30 (Pearn 1978). Currently, SMA patients and physicians focus on disease management rather than a cure, as there is no effective medical treatment available.

Table 1.1. SMA types are classified based on the severity of the disease and the age of onset of the specific symptoms (Boyer et al. 2010).

SMA Type	**Age at onset**	**Physical characteristics that typify the disease**
Type 0	Prenatal	Fetus displays reduced movement
Type I (Werdnig-Hoffman disease)	< 6 months	Affected children are never able to sit
Type II	< 18 months	Affected children cannot stand or sit without aid
Type III (Kugelberg-Welander disease)	> 18 months	Affected children can walk without help
Type IV	Adulthood	Mild weakness of the proximal muscles

1.2 Survival motor neuron genes

At the genetic level, SMA is the result of homozygous mutations or deletions of the survival motor neuron 1 (*SMN1*) gene located on human chromosome 5q13 (Lefebvre et al. 1995). The full-length transcript produced by *SMN1* is 1.7-kilobase pairs and encodes a protein of 294 amino acids, approximately 38 kilodaltons (Liu and Dreyfuss 1996). *SMN* has been highly conserved throughout evolution with almost all eukaryotic organisms studied to date having one single copy of the gene. In humans, however, there is a duplication of the *SMN* gene resulting in two near identical copies called *SMN1* and *SMN2* (Lefebvre et al. 1995, Hahnen et al. 1996, van der Steege et al. 1996, DiDonato et al. 1997).

Both copies harbor 9 exons (1, 2a, 2b-8) and span approximately 20-kilobase pairs (Burglen et al. 1996, Chen et al. 1998). While deletions or mutations in *SMN1* but not *SMN2* cause SMA, the latter gene can modulate the severity of the disease through its copy number due to its production of a small amount of full-length protein (Lefebvre et al. 1995). Indeed, patients affected by the milder forms of SMA generally have a higher copy number of the *SMN2* gene (Lefebvre et al. 1997). For instance, it is reported that 70% of type I SMA patients harbor two copies of the *SMN2* gene, 82% of type II patients carry 3 copies of the gene while most type III patients have 4 copies of the *SMN2* gene (Wirth et al. 2006). Thus, SMA is considered to be a dosage sensitive disorder.

The critical difference between *SMN1* and *SMN2* is a C to T substitution in the *SMN2* gene at position 6 of exon 7 (Lorson et al. 1999). The nucleotide transition in *SMN2* negatively affects an exonic splicing enhancer sequence leading to an alternatively spliced variant (Cartegni et al. 2006). *SMN1* expresses a full-length protein while *SMN2*

predominantly expresses a truncated and unstable isoform of the protein, termed Δ7SMN, characterized by a deletion of exon 7 (Lefebvre et al. 1995). Recently, it was shown that the instability of the Δ7SMN protein is due to a degradation signal (degron) created by the exclusion of exon 7 in the *SMN2* transcript (Cho and Dreyfuss 2010). The exon 7 of the *SMN* gene contains the normal translational termination signal. Upon the exclusion of exon 7, the new translational completion signal is now at the 5' of exon 8 and results in production of the Δ7SMN protein (Lorson et al. 2010). The exonic splicing enhancer sequence found within exon 7 associates with the protein splicing factor 2/alternative splicing factor (SF2/ASF). The C to T transition in exon 7 leads to formation of an inhibitory sequence which affects the binding of SF2/ASF to the gene (Lorson et al. 2010). It is believed that the absence of the SF2/ASF – *SMN2* interaction is responsible for the limited inclusion of exon 7 in the *SMN2* gene (Cartegni and Krainer 2002). However, Kashima et al. (2007) showed that the C to T substitution in the *SMN2* sequence, as well as another single nucleotide substitution in intron 7, both form a new interacting sequence for a splicing repressor protein called heterogeneous nuclear ribonucleoprotein A1 (hnRNP-A1). This interaction is believed to repress the inclusion of exon 7 in *SMN2* splicing (Kashima and Manley 2003, Kashima et al. 2007). To date, therapeutic strategies targeting the *SMN* regulatory sequences using bifunctional RNAs have led to significant improvements in mouse models of SMA (Lorson et al. 2010).

1.3 The survival motor neuron protein

The full-length SMN protein is expressed in all cells of the developing embryo, albeit with a developmental modulation in levels (Liu et al. 2010). The SMN protein is involved

in several molecular and cellular processes including transcription, spliceosomal assembly, mRNA transport and neuromuscular junction (NMJ) formation to name a few (Kariya et al. 2008, Burghes and Beattie 2009). The SMN protein contains several protein motifs and domains that dictate its functions. For example, exon 2 encodes a nucleic acid-binding domain necessary to bind RNA and DNA (Lorson and Androphy 1998). Missense mutations in humans have been reported within exon 2 affecting RNA binding, demonstrating the functional importance of this domain (Lorson and Androphy 1998). A SMN binding site for the protein Gemin 2 is encoded by exon 2b and directly implicates SMN in the assembly of spliceosomal small nuclear ribonucleoproteins (snRNPs) (Fischer et al. 1997, Young et al. 2000). The SMN protein harbors a Tudor domain encoded by exon 3 which facilitates the direct binding to Smith antigen (Sm) proteins, an important step during snRNP assembly (Buhler et al. 1999). A sequence spanning exons 4-6 encodes a proline-rich motif capable of binding multiple profilin isoforms, thus implicating SMN in actin-dynamics (Giesemann et al. 1999). Missense mutations in SMA patients have been identified within the C-terminus of SMN leading to the discovery of a triplicated tyrosine-glycine (Y-G) peptide sequence within the SMN protein (Talbot et al. 1997). This sequence is proposed to associate with RNA binding proteins and links the SMN protein to RNA metabolism. Exon 6 codes for a modular oligomerization domain and biochemical analyses have demonstrated a direct correlation between the level of SMN self-association and disease severity (Lorson et al. 1998).

1.4 Mouse models of SMA

To better understand how deletions or mutations in *SMN1* lead to SMA pathogenesis, various mouse models have been developed (Park et al. 2010). Interestingly, the complete absence of the Smn protein in mice (*Smn*$^{-/-}$) proved to be embryonic lethal, emphasizing the necessity of the *Smn* gene for survival (Jablonka et al. 2000, Monani et al. 2000). In an innovative approach, the human *SMN2* gene was used to rescue the embryonic lethality in *Smn*$^{-/-}$ mice to give rise to *Smn*$^{-/-}$*;SMN2* mice (Hsieh-Li et al. 2000, Monani et al. 2000). This approach was useful in demonstrating that a high copy number of *SMN2* leads to a milder phenotype while mice having only two copies of the *SMN2* gene display a severe phenotype reminiscent of type I SMA (Hsieh-Li et al. 2000, Monani et al. 2000). Severe *Smn*$^{-/-}$*;SMN2* mice can survive up to 6 days and show a dramatic loss in motor neurons at P5 phenotype stage (Monani et al. 2000). Therapeutic approaches aimed at increasing full-length SMN protein levels from the *SMN2* gene would therefore also produce significantly more Δ7SMN protein relative to full-length SMN. In an effort to study whether increased levels of Δ7SMN would be detrimental or beneficial, researchers introduced a *Δ7SMN* transgene onto the *Smn*$^{-/-}$*;SMN2* background. The addition of the *Δ7SMN* transgene produced a slightly less severe mouse than the *Smn*$^{-/-}$*;SMN2* model and extended survival from 5 to 13 days (Le et al. 2005). Although the *Smn*$^{-/-}$*;SMN2* and *Smn*$^{-/-}$*;SMN2;Δ7* models are genetically representative of human patients, these mutant mice are very small in size and have a short life span making them difficult models to work with especially when assessing therapeutics.

Recently, our laboratory has generated an intermediate mouse model of SMA (*Smn*$^{2B/-}$) that does not contain a *SMN2* transgene but instead harbors a substitution of 3 nucleotides within the exonic splicing enhancer of exon 7 of the mouse *Smn* gene

(Hammond et al. 2010, Bowerman et al. 2012). The *Smn*$^{2B/-}$ mouse model displays a milder SMA phenotype than the *Smn*$^{-/-}$*;SMN2* and the *Smn*$^{-/-}$*;SMN2;Δ7* model due to slightly higher Smn protein levels. *Smn*$^{2B/-}$ mice display the key pathological characteristics of SMA such as fewer motor neurons, muscle denervation and muscle atrophy (Bowerman et al. 2012). The use of this model has proven favorable for testing Smn independent therapeutics because of the absence of the *SMN2* transgene (Bowerman et al. 2010, Bowerman et al. 2012). Numerous other mouse and animal models of SMA have been extremely useful in making progress towards identifying pathways important for the pathogenesis of SMA.

1.5 SMN functions and SMA pathogenesis

snRNP assembly

The full-length SMN protein is expressed in all cells studied to date, localizing in both the cytoplasm and in nuclear Gems (Liu and Dreyfuss 1996, Young et al. 2000). The SMN protein is part of a multiprotein nuclear complex which is comprised of SMN, Gemin2-8, UNR-interacting protein (Unrip) and Sm proteins, which together are essential for snRNP biogenesis (Paushkin et al. 2002, Battle et al. 2006, Burghes and Beattie 2009). In turn, snRNPs are the building blocks for the spliceosome. Following transcription, the pre-mRNA of protein-encoding genes is spliced to remove the introns, a RNA processing step mediated by the spliceosome (Will and Luhrmann 2001). The collective data to date suggest that the SMN complex is crucial for snRNP assembly. Whether the disruption of this complex and reduced snRNP assembly is responsible for SMA pathogenesis remains the focus of ongoing studies. Over the years, progress has

been made regarding the sequential steps involved in pre-mRNA splicing, specifically snRNP assembly.

The key function of the SMN complex in snRNP assembly is to serve as a catalyst in arranging the Sm proteins in a heptameric open-ring configuration and assist in the association of the Sm core to the Sm site of U small nuclear RNAs (snRNA), thus forming a spliceosomal complex (Liu et al. 1997, Meister et al. 2001, Pellizzoni et al. 2002, Chari et al. 2008). It is well established that the SMN Tudor domain is vital for Sm protein binding (Buhler et al. 1999). The direct interaction between the SMN Tudor domain and Sm proteins is mediated through the protein arginine methyltransferase (PRMT)-induced symmetrical dimethylated arginine of Sm proteins, a critical step for snRNP assembly (Côté and Richard 2005, Gonsalvez et al. 2007). Furthermore, Sm protein methylation regulates the nuclear localization of snRNPs (Côté and Richard 2005). A role for SMN has previously been proposed as a recruiter and docking station for trimethylguanosine synthase 1 (Mouaikel et al. 2003). The hypermethylation of snRNA by this enzyme allows the SMN complex and associated snRNPs to interact with importin-β and snurportin, and to be imported into the nucleus (Palacios et al. 1997, Huber et al. 1998, Narayanan et al. 2002, Narayanan et al. 2004). Once in the nucleus, snRNPs and the SMN complex localize to Cajal bodies through their interaction with coilin (Carvalho et al. 1999, Hebert et al. 2001, Tucker et al. 2001). The recruitment of SMN to Cajal bodies appears to be methyl-dependent possibly through the methylation of the coilin C-terminal RG motif (Hebert et al. 2001, Boisvert et al. 2002). At present, the function of the SMN complex upon nuclear entry is not well defined and warrants investigation to further our understanding of pre-mRNA splicing. SMN depletion could

thus affect any and/or all of the above-mentioned interactions necessary for precise snRNP biogenesis.

Based on the involvement of SMN in mRNA maturation via its role in snRNP assembly, many research groups have focused on identifying the biological relevance and importance of snRNP assembly to the pathogenesis of SMA. Aberrant snRNP biosynthesis has been reported in cells from SMA patients as well as in vertebrate models of SMA (Pellizzoni et al. 1999, Wan et al. 2005, Winkler et al. 2005, Gabanella et al. 2007). However, work in zebrafish and drosophila models of SMA demonstrates that the SMA phenotype and the function of Smn in snRNP biogenesis appear to be mutually exclusive (Carrel et al. 2006, Praveen et al. 2012). Nonetheless, a correlation has been established between general snRNP assembly activity in the spinal cord of SMA model mice and disease severity (Gabanella et al. 2007).

Pre-mRNA Splicing

Pre-mRNA splicing involves the excision of introns, and in the context of SMA, defects in this molecular process were first reported over a decade ago when a mutated form of SMN produced robust splicing inhibition in pre-mRNA *in vitro* assays (Pellizzoni et al. 1998). More recently, splicing defects have been at the forefront of various studies to determine if defects in RNA metabolism are responsible for SMA pathology. Zhang and colleagues (2008) have observed that SMN reduction produces cell-type-specific changes in snRNA expression and profiles. To address the possible consequence of this aberrant snRNP assembly, the authors studied pre-mRNA splicing patterns in the brain, spinal cord and kidney of SMA model mice (Zhang et al. 2008).

They demonstrated that, at the peak of disease progression, large scale tissue-specific defects in intron-exon splicing are apparent when SMN levels are reduced to pathogenic levels (Zhang et al. 2008). These results suggest that in SMA, the pre-mRNA splicing accuracy is compromised and that widespread aberrant splicing may explain the disease pathology. However, as these analyses were only performed in the later stages of disease progression, and none of the aberrantly spliced genes were linked to SMA pathology, the relevance of these findings still requires further investigation.

In another study, Bäumer and colleagues (2009) performed exon-array analyses to assess whether splicing defects preceded the onset of the SMA phenotype. In agreement with other studies, the authors concluded that the splicing changes observed in mouse models of SMA (*Smn*$^{-/-}$*;SMN2*;*SMN*Δ*7* and *Smn*$^{-/-}$*;SMN2* mice) are a late feature of the disease and thus are likely secondary to the disease mechanism (Baümer et al. 2009, Liu et al. 2010). Recently, Smn-deficiency has been linked to splicing and expression disruptions of *stasimon,* a gene involved neurotransmitter release at the drosophila NMJ (Lotti et al. 2012). Lotti *et al.* (2012) demonstrate that *stasimon* can rescue several aspects of pathology in drosophila and zebrafish models of SMA. However, the mis-splicing of *stasimon* and particularly the aberrant mRNA levels of the gene are evident only in late stages of disease in SMA model mice. At the moment, it is unknown whether *stasimon* can lead to phenotype improvement in a mammalian model of SMA.

With regards to snRNP assembly and RNA splicing, several questions remain to be answered to convincingly link the housekeeping functions of SMN to SMA pathogenesis. Perhaps the most important realization is that no causal link has yet been established between the identified aberrantly spliced mRNA targets and the specificity of

SMA pathogenesis in mammalian model. Collectively, these concerns have pushed forward the search for roles of SMN in motor neuron processes where its function is much less understood, leaving open the possibility that the nuclear role of SMN is not the primary pathogenic origin of SMA.

1.6 SMN function and SMA pathology in motor neurons

In addition to the role of SMN in snRNP biogenesis, interactions with numerous cytoplasmic proteins unrelated to snRNPs or splicing, suggests that SMN has additional functions. Furthermore, defects in the general housekeeping role of SMN in the regulation of RNA metabolism do not explain how deletions or mutations in *SMN1* specifically affect the α-motor neurons in SMA patients. Thus, various groups have focused their efforts on assessing the effects of SMN depletion in neuronal models and how this might result in SMA pathogenesis. Collectively, these studies suggest a role for SMN in neurite outgrowth and axonal pathfinding, as well as in the regulation of actin dynamics (Fan and Simard 2002, McWhorter et al. 2003, Bowerman et al. 2007, Shafey et al. 2008).

Fan and Simard (2002) reported that SMN localizes in growth cones of mouse embryonal teratocarcinoma P19 cells during neuronal differentiation. In cultured mouse neurons, SMN is found in granules within neurites and at growth cones (Fan and Simard 2002, Zhang et al. 2003). The expression and distribution profiles of SMN in these cells therefore suggest a role for SMN in neurons. The inclusion of exon7 is necessary for the distribution of SMN in motor neuron processes. The absence of this exon leads to the nuclear retention of SMN and consequently a decrease in neurite outgrowth (Zhang et al.

2003, van Bergeijk et al. 2007). Furthermore, knockdown of the SMN protein in zebrafish resulted in aberrant motor axon outgrowth and pathfinding (McWhorter et al. 2003). These findings in various cell culture and animal models suggest a neuronal-specific role for SMN in motor neuron outgrowth. However, it is not clear how SMN modulates axonal outgrowth and identifying the biochemical pathways involved would provide us with a better understanding of the neuronal-specific function of SMA.

1.7 SMN regulates actin dynamics in motor neurons

The actin cytoskeleton and its regulation play a crucial role in neuritogenesis (Bray and Chapman 1985, da Silva and Dotti 2002, Cingolani and Goda 2008). Actin is the most abundant pre-synaptic protein, playing roles in synaptic vesicle organization, mobilization, and trafficking (Fifkova and Delay 1982, Landis et al. 1988, Shupliakov et al. 2002, Sakaba and Neher 2003, Dillon and Goda 2005). Considering the phenotypic defects observed in SMN-depleted neuronal cells, a role for SMN in the regulation of actin dynamics, whether direct or indirect, has been investigated.

Defects in actin dynamics were identified in Smn-knockdown PC12 cells. Depletion of Smn led to aberrant differentiation and neurite outgrowth defects (Bowerman et al. 2007). The defects were associated with abnormally high expression of profilin IIA and Ras homolog gene family, member A guanosine-5'-triphosphate (RhoA-GTP) which are both involved in the regulation of actin dynamics. Through its polyproline motif, Smn interacts with profilin IIa in the cytoplasm, neurite-like extensions and in growth cones of PC12 cells (Giesemann et al. 1999, Sharma et al. 2005). *In vitro* experiments show that Smn can modulate actin dynamics by binding to

profilin IIa and inhibiting its negative regulation of neurite sprouting and elongation (Da Silva et al. 2003, Sharma et al. 2005). Subsequent analyses in *Smn*$^{2B/-}$ mice confirmed the aberrant up-regulation of profilin II and RhoA *in vivo* (Bowerman et al. 2009, Bowerman et al. 2010). The genetic reduction of profilin II levels in *Smn*$^{2B/-}$ mice did not rescue the lifespan or the phenotype of these mice (Bowerman et al. 2009). However, administration of inhibitors of Rho-kinase, a direct downstream effector of RhoA, increased lifespan in the *Smn*$^{2B/-}$ mouse model of SMA and improved NMJ maturity and myofiber size (Bowerman et al. 2010, Bowerman et al. 2012). This work suggests that the manipulation of actin cytoskeletal dynamics could be a valuable therapeutic approach for the treatment of SMA.

Plastin 3 as a SMA modifier

Another recently identified actin regulator and potential modifier of SMA pathology is plastin 3 (Oprea et al. 2008). Plastin 3 is involved in bundling, turnover, and assembly of actin (Glenney et al. 1981, Giganti et al. 2005). Analysis of SMA-discordant families identified plastin 3 as a positive modifier of SMA pathology, with asymptomatic females carrying the exact *SMN1* mutations as affected siblings displaying a significant increase in plastin 3 mRNA and protein levels (Oprea et al. 2008). The authors also show that SMN, plastin 3 and actin form a complex in mouse spinal cord and overexpression of plastin 3 in SMN-depleted PC12 cells and primary motor neurons from mouse models of SMA led to significant rescue of the defects in neurite length (Oprea et al. 2008).

The findings described above strongly support the hypothesis that mis-regulation of actin and its regulators are central to SMA pathogenesis. However, it remains to be

seen if actin dynamics are affected elsewhere in the motor unit such as the NMJ and skeletal muscle.

1.8 SMN function and SMA pathology at the NMJ

In light of the motor neuron defects and muscle atrophy characterizing SMA, recent research has focused on the NMJ, the results of which are summarized in Table 1.2. Indeed, various groups have shown that SMN depletion results in abnormal endplate morphology, endplate denervation, neurofilament (NF) accumulation and perturbed function (Table 1.2) (Kariya et al. 2008, Murray et al. 2008, Kong et al. 2009, Murray et al. 2010).

At the pre-synapse in a zebrafish model of SMA, a decrease in synaptic vesicle protein 2, a protein responsible for normal neuronal transmission, has been reported (Boon et al. 2009). Moreover, Kong and colleagues (2009) report a decrease in synaptic vesicle density in NMJs of a mouse model of SMA. Neurofilament accumulation at the pre-synaptic terminal and pre-terminal axon has been described in multiple mouse models of SMA (Cifuentes-Diaz et al. 2002, Kariya et al. 2008, Murray et al. 2008, Kong et al. 2009). It thus appears that SMN depletion also affects the expression and localization of proteins important for normal functioning of the NMJ. Several studies describe denervated NMJs in animal models of SMA, characterized by reduced endplate occupancy and even complete endplate vacancy (Murray et al. 2010) (Table 1.2). The denervation of the motor axon appears to be particularly associated with proximal muscles, which correlates with the proximal weakness observed in patients (Kariya et al. 2008, Kong et al. 2009). It is well established that post-synaptic defects are also present

in SMA. Immature motor endplates, assessed by their reduction in size and their decreased number of perforations, are prevalent in SMA (Kariya et al. 2008, Murray et al. 2008, Kong et al. 2009). Interestingly, in *drosophila*, SMN localizes at the motor endplate but its function in this region has not yet been determined (Chang et al. 2008). It is plausible that SMN has a specific role at the post-synapse and that its depletion contributes to the reported motor endplate defects, independent of pre-synaptic abnormalities (Murray et al. 2008). Future research should be aimed at confirming this finding in mice as well as further investigate the function of Smn at the NMJ.

In light of the many morphological NMJ defects observed in model organisms of SMA, it is not surprising that its function is also perturbed. Indeed, excitatory post-synaptic currents are reduced in *drosophila* and mouse models of SMA, a finding likely attributable to a decrease in vesicle release (Chan et al. 2003, Kong et al. 2009). Moreover, in response to a repetitive stimulation protocol, a greater number of NMJs from mouse models of SMA experienced intermittent transmission failures compared to controls (Kariya et al. 2008). It thus appears that loss of the SMN protein profoundly impacts proper NMJ function. Thus, deciphering if NMJ defects are at the origin of SMA pathogenesis and what molecular mechanisms are responsible for these defects may be key in identifying novel targets and developing therapeutics to cure or alleviate the symptoms of SMA.

Table 1.2. NMJ defects reported in various models of SMA (Boyer et al. 2010).

Model	Neurofilament accumulation	Abnormal motor endplates	Denervation	Neuromuscular Junction Synaptic function	Reference
Mouse Conditional Neuronal KO	Yes	Yes	Yes	Not tested	(Cifuentes-Diaz et al. 2002)
Drosophila	Not determined	Yes	Not determined	Abnormal	(Chan et al. 2003)
Mouse *Smn*$^{-/-}$*;SMN2;Δ7*	Not determined	Yes	Yes (mild)	Not tested	(Le et al. 2005)
Mouse *Smn*$^{-/-}$*;SMN2* and *Smn*$^{-/-}$*;SMN2;Δ7*	Yes	Yes	Yes	Not tested	(Murray et al. 2008)
Mouse *Smn*$^{-/-}$*;SMN2;Δ7*	Yes	Yes	Yes (mild)	Abnormal	(Kariya et al. 2008)
Drosophila	Not determined	Yes	Not determined	Not tested	(Chang et al. 2008)
Mouse *Smn*$^{-/-}$*;SMN2;Δ7*	Yes	Yes	No (very limited denervation)	Abnormal	(Kong et al. 2009)
Zebrafish	Not determined	No	Not determined	Not tested	(Boon et al. 2009)
Mouse *Smn*$^{-/-}$*;SMN2* (N11/N46)	Yes	Yes	Yes (not quantified)	Abnormal	(Michaud et al. 2010)
Mouse *Smn*$^{2B/-}$	Yes	Yes	Yes	Not tested	(Bowerman et al. 2012)
Mouse *SMN*^{RT}	Not determined	Yes	Yes	Not tested	(Cobb et al. 2013)

1.9 SMN function and SMA pathology in skeletal muscle

Muscle intrinsic defects

While SMA is traditionally considered to be a motor neuron disease, a possible involvement of skeletal muscle in SMA pathogenesis has been investigated (Braun et al. 1995, Cifuentes-Diaz et al. 2001, Shafey et al. 2005). Current research has focused on determining if the SMN protein has a specific and independent role in skeletal muscle. In a study by Shafey *et al*., (2005), C2C12 myoblasts with reduced SMN expression displayed defects such as abnormal proliferation, aberrant myoblast fusion and malformed myotubes. These findings demonstrate that reduced SMN levels can result in intrinsic muscle defects. The muscle-specific depletion of SMN in various conditional knockout mouse models also suggests a role for SMN in skeletal muscle. These mice show a severe dystrophic phenotype, myofibers with compromised sarcolemma, a decrease in muscle force as well as a reduced lifespan (Cifuentes-Diaz et al. 2001, Nicole et al. 2003). However, the limitations of the above-mentioned mouse and cell culture models are that they are not necessarily representative of the true SMA pathogenesis. Indeed, the C2C12 cell model lacks a motor neuron signal while the muscle-specific SMN-depleted mice do not have the residual full-length SMN protein normally present in SMA patients. The relevance of the mouse model has also been put into question due to the fact that a liver-specific depletion of the SMN protein resulted in mice with liver defects not normally present in SMA (Vitte et al. 2004). This implies that complete absence of SMN in any tissue may lead to severe defects and therefore, does not convincingly argue for a role for the SMN protein in skeletal muscle in the context of SMA pathogenesis.

Studies demonstrating muscle intrinsic defects have however been performed using human primary myoblasts from SMA patients. Upon differentiation of human myoblasts, myotubes were unable to fuse properly, a result reminiscent of what was observed in C2C12 Smn-knockdown cells (Arnold et al. 2004). Furthermore, skeletal muscle defects such as vacuolization and compromised sarcomere structures were reported in human SMA muscle cells co-cultured with rat spinal cord explants (Braun et al. 1995). Although these primary cell culture studies were fairly concise, they nonetheless provide valuable insight into intrinsic muscle abnormalities. Collectively the cell and conditional mouse studies were the first to show muscle intrinsic defects in SMA and establish and validate a strong rationale to study muscle defects in the context of SMA.

Abnormal skeletal muscle development in SMA mice

A growing body of evidence suggests that Smn-depletion leads to aberrant skeletal muscle development in SMA model mice. In the *Smn$^{-/-}$;SMN2;Δ7* mouse model, Lee and colleagues (2011) showed that the cross-sectional area of myofibers did not increase from P5 to P13 suggesting impaired muscle growth. Delayed myofiber growth is evident in the severe *Smn$^{-/-}$;SMN2* as well. Tibialis anterior (TA) muscle from phenotype stage *Smn$^{-/-}$;SMN2* show similar cross-sectional area than pre-symptomatic mice (Dachs et al. 2011). These studies imply retarded muscle growth is present in SMA model mice. However, the evidence presented is based on indirect measures of development and does not rule out the contributions of muscle atrophy mechanisms. A study on patient samples confirms that SMA muscles demonstrate impaired growth and maturation characterized

by smaller and disorganized myotubes (Martinez-Hernandez et al. 2009). The study on human patients however, was solely based on muscle histology, therefore no evidence was presented to provide insight into the molecular alterations underlying aberrant muscle development in SMA patients. Delayed muscle development is also supported by the increased expression of immature myosin heavy chain (MHC) isoform. Sustained expression of the embryonic and perinatal MHC isoforms has been detected at the transcript and protein level in phenotype stage *Smn*$^{-/-}$*;SMN2;Δ7* mice (Kong et al. 2009, Lee et al. 2011). This aberrant MHC expression profile is also associated with a delay in postsynaptic endplate development. The expression of the immature acetylcholine receptor persists in *Smn*$^{-/-}$*;SMN2;Δ7* mice and is accompanied by impaired postsynaptic maturation at the morphological level (Kong et al. 2009, Dachs et al. 2011).

Recently, Hayhurst et al. (2012) have provided evidence suggesting that Smn-depletion leads to accelerated muscle differentiation *in vivo*. Satellite cells, identified by the paired-box transcription factor Pax7, were increased in number and expressed myogenic markers earlier in *Smn*$^{-/-}$*;SMN2* mice compared to controls. Despite the accelerated expression of the myogenic regulatory factors in *Smn*$^{-/-}$*;SMN2* satellite cells, these cells failed to grow upon differentiation in culture (Hayhurst et al. 2012). At the moment, it is unclear how premature myogenic differentiation leads to reduced myofiber size in SMA.

A role of SMN in mature myofibers

In *drosophila*, Smn was shown to be a sarcomeric protein (Rajendra et al. 2007). Moreover, it interacts with α-actinin, a cross-linking protein that stabilizes actin

microfilaments (Rajendra et al. 2007). Follow-up experiments in mice confirm these findings and specifically identify Smn as a Z-disc component in skeletal and cardiac muscle (Walker et al. 2008). Other proteins such as Gemins and Unrip are also present at Z-discs, likely forming a muscle-specific Smn complex (Walker et al. 2008). However, the absence of snRNPs in purified myofibrils suggests that Smn might have a function other than snRNP biogenesis at the Z-disc (Walker et al. 2008). Indeed, the levels of snRNP assembly activity significantly decrease during C2C12 myoblast differentiation, suggesting unique functions for SMN during growth and differentiation of muscle cells (Gabanella et al. 2005).

When compared to wild type muscle, myofibrils from SMA model mice showed morphological defects such as vacuoles and abnormal Z-disc spacing. Although such structural defects were observed, it is unlikely that Smn plays a role in maintaining sarcomeric integrity given that the domain organization of the Smn protein does not support such an idea. It therefore remains unclear if Smn has a functional role at the sarcomere and if it has any impact on SMA pathology.

Increased cell death in SMA muscle

Increasing evidence suggests that the depletion of Smn in skeletal muscle renders it susceptible to cell death. To gain insight into intrinsic molecular changes in skeletal muscle prior to motor neuron degeneration, Mutsaers and colleagues (2011) performed a proteomic screen using the rostral band of the levator auris longus muscle in pre-symptomatic severe SMA model mice. Several proteins involved in cell death pathways were aberrantly expressed, some of which were validated in skeletal muscle from human

patients. Furthermore, the authors highlighted changes in protein expression that were not identified in muscle samples from denervated mice. In a separate study, increased apoptotic cell death was observed in muscles from phenotype stage *Smn*$^{-/-}$*;SMN2* mice but was not detected at the pre-symptomatic P0-P1 time point. To demonstrate that the overt presence of apoptotic cell death was a muscle intrinsic phenomenon, Dachs et al. (2011) performed sciatic nerve denervation in neonatal mice. Forty-eight hours post-denervation, no increase in apoptotic cells was observed in the experimentally denervated muscles compared to sham controls. Therefore, the increased cell death correlates with disease progression in *Smn*$^{-/-}$*;SMN2* mice and is not attributed to muscle denervation. That said, an investigation of cell death in C2C12 cells depleted of Smn and cultured satellite cells isolated from *Smn*$^{-/-}$*;SMN2* mice revealed normal proportion of apoptotic cells. Furthermore, the number of apoptotic cells in type 1 human SMA muscle samples was comparable to controls (Martinez-Hernandez et al. 2009). Therefore, it would appear that increased cell death in skeletal muscle might be limited to mouse models of SMA. At the moment, how the absence of Smn leads to increased apoptosis and whether apoptosis is primary or secondary to the SMA pathogenesis is unclear and requires further study.

The therapeutic requirements of SMN in skeletal muscle

The aforementioned studies have thus begun to shed light on the function of SMN in muscle. To further assess the impact of SMN expression in muscle or neurons on SMA disease pathogenesis, a transgene encoding SMN was introduced in a severe mouse model (*Smn*$^{-/-}$*;SMN2*) under the control of a muscle or a neuron-specific promoter (Gavrilina et al. 2008). A high expression of *SMN* in muscle was achieved using the

human skeletal-actin (*HSA*) promoter. This strategy produced a modest increase in survival in the *Smn*$^{-/-}$*;SMN2* mice. Conversely, expression of *SMN* in neurons using the prion protein (*PrP*) promoter had a greater impact on survival, but only when expressed at high levels. However, considerable leaky SMN expression was observed in spinal cord and skeletal muscle using the *HSA* and *PrP* promoters respectively. Furthermore, it is possible that the *HSA* promoter expresses SMN too late during myogenesis to produce maximal benefits. More recently, a similar study was performed using conditional SMA model mice expressing tissue-specific Cre drivers; the motor neuron-specific choline acetyltransferase promoter (*ChAT*^{cre}) and the muscle-specific myogenic determination 1 (*MyoD*^{cre}) and myogenic factor 5 (*Myf5*^{cre}). MyoD and Myf5 are myogenic regulatory factors expressed very early during myogenesis and may therefore yield more significant improvements in the survival of SMA mice (Martinez et al. 2012). Interestingly, restoring Smn expression in motor neurons of *ChAT*^{cre} mice led to a very modest increase in survival compared to the survival reported using the *PrP* promoter. The *ChAT*^{cre} extended survival 2 days more than the muscle-specific promoters *MyoD*^{cre} and *Myf5*^{cre}. *ChAT*^{cre} conditional mice showed increased SMN expression in motor neurons and improved NJM function and morphology. Despite these improvements, only the *MyoD*^{cre} and the *Myf5*^{cre} lines produced a robust increase in the cross-sectional area of myofibers. It should be noted that Smn expression from the *Myf5*^{cre} driver was detectable in the nervous system making it somewhat difficult to interpret the results from this mouse model (Martinez et al. 2012). Nonetheless, the results form *MyoD*^{cre} and *Myf5*^{cre} demonstrate the importance of restoring Smn expression in skeletal muscle and suggest that a combinatorial expression of Smn in both myofibers and motor neurons may

provide a more impressive extension of life in mouse models of SMA. In a *drosophila* model of SMA, the importance of SMN expression in both neurons and muscle has clearly been established. While reduction of SMN in either neurons or muscle proved to be lethal, its reduction in muscle accelerated lethality (Chan et al. 2003, Chang et al. 2008). Thus, restoration of Smn expression in skeletal muscle should not be overlooked when developing therapeutic strategies.

1.10 Rationale and hypothesis

Currently, there is increased agreement within the SMA field to support the notion that multiple tissues are affected in SMA and a systemic approach should be envisaged when developing therapeutics. To date, several studies have highlighted that Smn-depletion leads to defects along the entire motor unit including in motor neurons, at the NMJ and in skeletal muscle (Figure 1.1). However, despite these advances, there is still a lack of understanding in the pathogenesis and pathophysiology of diseased skeletal muscle in SMA that needs to be addressed. How muscle defects contribute to SMA pathology and phenotype is not fully understood since no thorough studies have uncovered the extent of muscle defects in mouse models of SMA. The primary objective of this doctoral thesis is therefore to further our understanding of SMA pathogenesis and pathophysiology in skeletal muscle.

Hypothesis: *We hypothesize that Smn-depletion will result in muscle-intrinsic defects in the context of SMA*.

To test this hypothesis, four independent aims were established:

Aim 1: To validate myosin regulatory light chain as a Smn interacting protein in skeletal muscle.

Aim 2: To characterize muscle histology in mouse models of SMA.

Aim 3: To assess the functional capacities of diseased skeletal muscle from mouse models of SMA.

Aim 4: To characterize the molecular pathology of muscles from mouse models of SMA.

NUCLEUS
SMN is present in Gems

SMN with Gemins 2-8 and Unrip form the SMN complex

SMN complex regulates snRNP assembly

MOTOR AXON
SMN is localized in neurites and growth cones

SMN regulates actin dynamics in motor neurons

NMJ/SKELETAL MUSCLE
SMN is a Z-disc protein

SMN localizes at the motor endplate in drosophila

SMN appears to have a role other than snRNP assembly

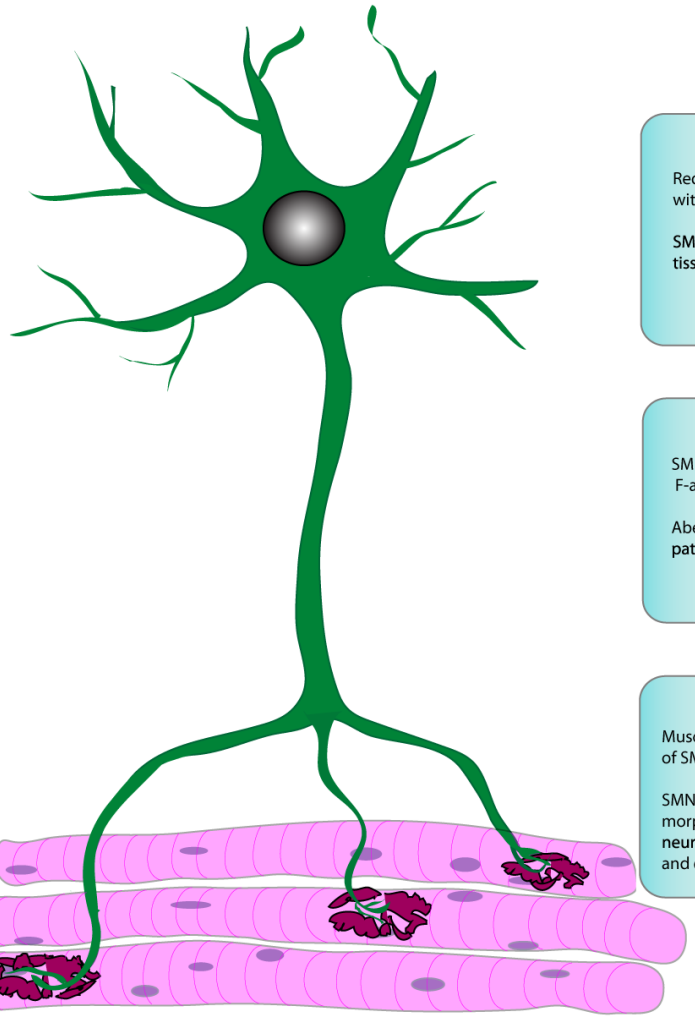

NUCLEUS
Reduced snRNP assembly activity correlates with severity of SMA disease

SMN deficiency is associated with tissue-specific pre-mRNA splicing defects

MOTOR AXON
SMN depletion results in defects of β- and F-actin expression and localization

Aberrant motor axon outgrowth and pathfinding

NMJ/SKELETAL MUSCLE
Muscle atrophy is a pathological hallmark of SMA

SMN depletion results in abnormal endplate morphology, endplate denervation, neurofilament accumulation, and defects in vesicle release

Figure 1.1. SMN function and SMA pathology. Schematic diagram highlighting our understanding of SMN function and the consequences of SMN-depletion at the motor unit (Boyer et al. 2010).

Chapter 2

Identification of novel interacting protein partners of SMN using Tandem Affinity Purification

Author Contributions

DS and RK conceived of and designed the project. DS generated the clones, established the stable cell lines and performed the TAP experiments. DS, JGB and RK analyzed the proteomic data. DS performed the work for figures 2.1, 2.2, 2.3, 2.4 and 2.7. J.G.B. performed the work for figures 2.5, 2.6 and all the MRLC *in vivo* staining (data not shown). KB assisted JGB with figure 2.5. DS and JGB wrote the paper and RK revised and edited the manuscript. RK supervised DS and JGB.

Identification of novel interacting protein partners of SMN using Tandem Affinity Purification

Dina Shafey[1,2,*], Justin Boyer[1,2,*], Kunal Bhanot[1] and Rashmi Kothary[1,2,3,#]

[*]these authors contributed equally to the work

[1]Ottawa Hospital Research Institute, Ottawa, ON, Canada K1H 8L6 and The University of Ottawa Center for Neuromuscular Disease

[2]Department of Cellular and Molecular Medicine, University of Ottawa, Ottawa, ON, Canada K1H 8M5

[3]Department of Medicine, University of Ottawa, Ottawa, ON, Canada K1H 8M5

[#]To whom correspondence should be addressed

Published in: Journal of Proteome Research. (2010) 9(4): 1659-1669

Abstract

Mutations in the survival motor neuron (SMN) gene cause Spinal Muscular Atrophy (SMA), a neuromuscular disease associated with muscle weakness that progresses to paralysis, respiratory distress, and ultimately death. Both neurons and muscle are severely affected in this disease. Tandem Affinity Purification (TAP) has emerged as a useful tool for studying protein complexes *in vitro*. We have used this purification system to discover novel SMN interacting partners in C2C12 muscle and PC12 neuronal cells. To do so, we fused a TAP-tag, consisting of a HIS hexamer and FLAG epitope separated by the Tobacco Etch Virus (TEV) protease cleavage site, to either the N- or C-terminal region of SMN. Interestingly, the profile of SMN interacting proteins varies depending on the cell type and stage. We have identified a number of novel SMN interacting proteins in both C2C12 and PC12 cells, and from among these we have validated Annexin II and myosin regulatory light chain (MRLC). The discovery of these proteins will lead to a better understanding of the mechanisms underlying the pathophysiology of SMA.

Keywords: Spinal Muscular Atrophy, Survival Motor Neuron, Tandem Affinity Purification, Annexin, MRLC

Introduction

Spinal muscular atrophy (SMA) is a genetic disorder characterized by the degeneration of α-motor neurons in the spinal cord and skeletal muscle atrophy. The loss of α-motor neurons causes proximal, symmetrical limb and trunk muscle weakness that progresses to paralysis and ultimately to death. SMA is caused by mutations in the survival motor neuron 1 gene (*SMN1*) (Melki et al. 1994, Bussaglia et al. 1995, Lefebvre et al. 1995, Brahe et al. 1996, Parsons et al. 1996, Hahnen et al. 1997). SMN has been largely characterized in HeLa cells to be part of at least one large multiprotein complex, which includes Gemin2 (Liu and Dreyfuss 1996, Fischer et al. 1997, Charroux et al. 1999, Charroux et al. 2000), Gemin3 (Charroux et al. 1999, Campbell et al. 2000), Gemin4 (Charroux et al. 2000, Meister et al. 2000), and spliceosomal U snRNP proteins of the Smith antigen (Sm) class (Fischer et al. 1997, Liu et al. 1997, Buhler et al. 1999, Pellizzoni et al. 1999, Meister et al. 2000). The association of SMN with U snRNAs and Sm proteins revealed a role for SMN in the biogenesis and function of spliceosomal U snRNPs (Fischer et al. 1997, Buhler et al. 1999, Selenko et al. 2001). The nuclear SMN also contributes to pre-mRNA splicing (Pellizzoni et al. 1998, Meister et al. 2000, Pellizzoni et al. 2001, Zhang et al. 2008). However, the role of SMN in snRNP assembly and in RNA splicing appears essential for all cell types and does not explain why motor neurons and muscle are specifically affected in SMA. Thus, additional functions may be relevant in the context of the disease. In addition to the components of the complex mentioned above, SMN has been identified to directly interact with profilins (Giesemann et al. 1999), fibrillarin, GAR1 (Jones et al. 2001, Pellizzoni et al. 2001), hnRNP-R, hnRNP-Q (Rossoll et al. 2002), papillomavirus nuclear transcription activator E2

(Strasswimmer et al. 1999) and nucleolin (Lefebvre et al. 2002). These interactions were identified in non-muscle or non-neuronal cell types, however, these interactions demonstrate that SMN may be involved in functions other than mRNA splicing such as helicase activity, RNA metabolism and nuclear transcription. Further supporting this idea is data demonstrating the absence of key Sm-class snRNPs with Smn in mouse myofibrils (Walker et al. 2008). Despite recent progress in the understanding of the function of SMN in pre-mRNA splicing, very little is known about the cause of the motor neuron and skeletal muscle atrophy specific pathology in SMA. Identifying SMN interacting proteins in neuronal and muscle cell types should lead us to a better understanding of SMA pathogenesis.

In this report, we have used the Tandem Affinity Purification (TAP) system (Knuesel et al. 2003, Cherasse et al. 2007) to identify novel interactors of SMN. The TAP method permits the rapid and efficient purification of epitope-tagged protein complexes from crude extracts under native conditions. This system coupled with mass spectrometric analysis allows for the reproducible identification of novel interactors, while reducing the number of non-specific proteins, due to its two-step purification process. The goal of this study was to identify those interactors that may have neuronal or muscle relevance. We have therefore focused our attention on the study of the SMN complex during different stages of growth and differentiation in C2C12 muscle and PC12 neuronal cells, and have identified known and novel SMN interacting partners.

Materials and methods

Generation of NTAP-SMN and CTAP-SMN constructs

The retroviral expression constructs pBRIT-LoxP-CTAP HIS-FLAG and pBRIT-LoxP-NTAP FLAG-HIS were originally designed by Dr. Greenblatt and subsequently modified and generously supplied to us by Dr. Iain McKinnell and Dr. Michael Rudnicki (McKinnell et al. 2007). The coding sequence for Human SMN was PCR amplified for insertion into the NTAP construct with 5'-GGA GAA TTC ATG GCG ATG AGC AGC GGC GGC AGT-3' (forward primer) and 5'-GGA CTC GAG ATT CCT TAC ACT CGT GGA AGG AAG AAA-3' (reverse primer) and with 5'-GGA GAA TTC GCC GCC ATG ATG GCG ATG AGC AGC GGC GGC AGT-3' (forward primer) and 5'-GGA CTC GAG ATT CCT TAC ACT CGT GGA AGG AAG AAA-3' (reverse primer) for insertion into the CTAP construct. The amplified SMN cDNA was gel purified and digested with the restriction enzymes EcoRI and XhoI. The pBRIT-LoxP-CTAP HIS-FLAG and pBRIT-LoxP-NTAP FLAG-HIS vectors were also digested with EcoRI and XhoI. The appropriate amplified SMN cDNA was ligated to the appropriate vector to generate our NTAP-SMN and CTAP-SMN constructs.

Cell Culture

C2C12 myoblasts and PC12 neuronal cells were cultured as previously described (Shafey et al. 2005, Bowerman et al. 2007). The retroviral packaging cell line, Phoenix-eco was maintained in DMEM (Wisent) supplemented with 5% FBS, and 1% penicillin/streptomycin (Invitrogen).

Establishment of stable cell lines expressing the NTAP-SMN and CTAP-SMN constructs

High titer infectious retrovirus stocks were generated by transfecting the NTAP-SMN and CTAP-SMN constructs into Phoenix-eco cells using Lipofectamine 2000 (Invitrogen). Polybrene-enhanced retroviral infection of the above stocks into C2C12 and PC12 cells was used to obtain stable lines with NTAP-SMN or CTAP-SMN expression similar to endogenous levels. These cells were subjected to drug selection with 2 μg/ml puromycin (Invitrogen), plated at low density, and single colonies were isolated. Several drug-resistant C2C12 and PC12 cell lines were established for both constructs, and their Smn protein levels determined by immunoblotting. Cell culture lysates used for immunoblotting were collected in ice-cold lysis buffer (50 mM Tris-HCl pH 7.4, 150 mM NaCl, 1 mM EDTA, 1% Nonidet P-40 [NP-40], and 1% glycerol) containing 10 mM Na_2VO_4, 1 mM phenylmethylsulfonyl fluoride (PMSF), 0.01 mg/ml aprotinin, 0.01 mg/ml pepstatin, and 0.01 mg/ml leupeptin on ice. Lysates were resolved on 10% sodium dodecyl sulfate polyacrylamide gel electrophoresis (SDS-PAGE) and transferred to a PVDF membrane (Millipore). Smn protein levels were determined by probing with a monoclonal Smn antibody (Transduction Laboratories), and an actin-antibody (Research Diagnostics) was used to ensure equal protein loading. Bands were detected using the enhanced chemiluminescence (ECL) system (Amersham Biosciences).

TAP-tag purification

Approximately 1 g of cells was collected at growth, one, three, five, and seven days of differentiation from both the C2C12 and PC12 cell clones. Cells were flash frozen and lysed in 1.3 volumes (ml/g of cell pellet) of Buffer A (10 mM Tris-HCl pH 7.9, 0.1 M

NaCl, 1.5 mM $MgCl_2$, 0.18% NP40) supplemented with protease inhibitors (2.4 μg/ml chymostatin, 1.5 μg/ml pepstatin A, 88 μg/ml PMSF, 0.5 μg/ml leupeptin, 17 μg/ml aprotinin, 310 μg/ml benzamidine). Once the cells had been homogenized in Buffer A, one volume of Buffer B (50 mM Tris-HCl pH 7.9, 0.6 M NaCl, 1.5 mM $MgCl_2$, 25% glycerol) was added and cells were homogenized again. This was followed by the addition of 1 μl of benzonase nuclease (Novogen) and the homogenate was rotated at 4°C for 30 minutes. The homogenate was then spun at 40,000 g for one hour in an ultracentrifuge and the supernatant dialyzed with Slide-A-Lyzer Dialysis Cassette (PIERCE) for 3 hours in dialysis buffer (10 mM Tris-HCl pH 7.9, 0.1 M NaCl, 0.1 mM EDTA, 10% glycerol). Once dialyzed, the extract was spun at 14,000 g for 20 minutes and the supernatant was removed and placed into a Low Retention Microcentrifuge Tube (Fisher Scientific). CTAP-SMN fusion protein and its associated components were recovered from extracts by affinity selection on anti-Flag M2 agarose beads (Sigma). M2-agarose beads (50 μl/sample) were washed twice with AFC Buffer (10 mM Tris-HCl pH 7.9, 100 mM NaCl, 0.1% NP40), then resuspended in equal volume of AFC buffer. The 50 μl of beads (100 μl of slurry) were added to the extract and rotated overnight at 4°C. The beads were then washed three times in AFC buffer and twice in TEV buffer (20 mM Tris-HCl pH 7.9, 100 mM NaCl, 0.1 mM EDTA, 0.1% NP40). Beads were resuspended in 100 μl of TEV buffer, 2 mg/ml acTEV protease (Invitrogen) and 2 mg/ml Flag peptide (Sigma) and rotated for 30 minutes at 4°C. The beads were pelleted and the supernatant was kept for later use. The beads were resuspended again in 100 μl of TEV buffer, 2 mg/ml acTEV protease and 2 mg/ml Flag peptide. This process was repeated three times, each time the supernatant was kept for later use. Ni-NTA agarose beads

(Qiagen) (60 µl/sample) were washed twice in Ni-NTA wash buffer (20 mM Tris-HCl pH 7.9, 100 mM NaCl, 0.1 mM EDTA, 5 mM imidazole) and then resuspended in an equal volume of Ni-NTA wash buffer. The Ni-NTA beads were then added to the TEV cleavage supernatant and rotated overnight at 4°C. The beads were washed three times in Ni-NTA wash buffer and eluted with 4 x 100 µl Ni-NTA elution buffer (20 mM Tris-HCl pH 7.9, 100 mM NaCl, 0.1 mM EDTA, 0.4 M imidazole). The recovery of NTAP-SMN fusion protein and its associated components was similar to the CTAP-SMN recovery, however the order of purification is different. For the NTAP-SMN purification, the complex was first bound to the Ni-NTA beads and then following elution and TEV cleavage, the complex was bound to the M2 agarose beads. The final purified complex was eluted in 4 x 100 µl AFC buffer with 2 mg/ml Flag peptide.

Sample preparation for mass spectrometry

The protein complexes recovered from the TAP-tag purification were concentrated using Microcon Centrifugal Filter device for protein concentration (Millipore). The concentrated purified complexes were resolved on a 12% SDS-PAGE gel. The gel was stained in a non-fixing silver stain, fixed in 50% ethanol, 5% acetic acid solution for 30 minutes, washed in 50% ethanol for 10 minutes, then washed in water twice for 10 minutes, sensitized for 2 minutes in 0.02% sodium thiosulphate, washed twice for 5 minutes, stained with chilled 0.1% silver nitrate for 30 minutes, and then washed in water for 2 minutes. After this, a small amount of developer (0.04% formalin, 2% sodium carbonate) was added to the water and swirled briefly to remove excess silver. The water was replaced with developer and the gel was shaken slowly until bands appeared. At that

point, the developer was discarded and a stop solution (5% acetic acid) was added to the gel for at least 5 minutes. The gel was then stored in 1% acetic acid. Protein bands were excised from the gel and stored in 1% acetic acid.

Mass spectrometric analysis

In-gel digestion was performed using trypsin as previously described (Wilm et al. 1996). Sixteen-hour digestions were performed using sequencing grade trypsin (Promega). Peptides from gel bands were extracted and hydrated in 20 ml of 5% formic acid and analyzed by LC-MS (Liquid chromatography-mass spectrometry) as follows. Peptides were loaded at a rate of 5 μl/min onto a 200 μm x 50 mm precolumn packed with 5 μm YMC ODS-A C_{18} beads (Waters) using an Agilent 1100 series HPLC system (Agilent Technologies). Subsequent to the desalting step, the flow was split and peptides were eluted through a second 75 μm x 50 mm column, packed with the same beads, at approximately 200 nl/min using a 5-80% gradient of acetonitrile with 0.1% formic acid for 1 hr. The LC effluent was electrosprayed into an LTQ linear ion-trap mass spectrometer (Thermo-Electron). MS spectra were acquired in a data-dependant acquisition mode that automatically selected and fragmented the four most intense peaks from each MS spectrum generated.

Peptide and MS mass tolerances were set at ± 2 and 0.8 Da, respectively. MS data were then analyzed and matched to human protein sequences in the NCBI database (nrdb) using the MASCOT database search engine version 2.2.04 (MatrixScience) with carbamidomethyl as a fixed modification and oxidation as a variable modification. A mascot score cut-off of 40 was selected to ensure a false positive rate of less than 1%.

This cut-off was based on a previous large scale proteomic analysis that demonstrated that tryptic peptides with +2 and +3 charges could be identified with roughly 99% precision using mascot cut-off scores of 30 and 26 (Elias et al. 2005).

Animals

All experimental protocols were performed in accordance with the University of Ottawa Animal Care Committee. SMA mice were generated from males and females of the genotype *Smn*$^{+/-}$;*SMN2*$^{+/+}$ on an FVB/n background (Monani et al. 2000). This mouse model of SMA does not express any endogenous Smn protein but has low level of human SMN protein expressed from a low copy human *SMN2* transgene. This is sufficient to allow the mice to develop to term but they display neurological deficits soon thereafter. The tibialis anterior muscle was dissected and allowed to equilibrate in 30% sucrose diluted in 1X phosphate buffered saline before being frozen in tissue embedding medium for immunostaining. Hindlimb muscles were dissected and flash frozen immediately and stored for subsequent protein analysis. All tissues were acquired from end-stage mice at postnatal day 5 (P5).

Immunoprecipitation assays

Wild type C2C12 and PC12 cells at growth, and 1, 3, 5 and 7 days of differentiation, and hindlimb muscles from P5 *Smn*$^{+/+}$;*SMN2*$^{+/+}$ and *Smn*$^{-/-}$;*SMN2*$^{+/+}$ mice were lysed in NP-40 buffer. Lysates were incubated overnight at 4°C with protein A or protein G sepharose beads (Amersham Biosciences), and with either Smn (Transduction Laboratories), Gemin2 (Abcam), MRLC (Abcam), Nucleolin (Abcam), Profilin-1 (Abcam), or Annexin-

II (Abcam) antibodies. Controls were processed in parallel and consisted of muscle lysate alone, antibodies incubated with the appropriate sepharose beads, and muscle lysate incubated with either protein A or G sepharose beads. Bound fractions were washed and solubilized in 2X Laemmli SDS sample buffer and separated on a 10% SDS polyacrylamide gel. The separated proteins were analyzed by immunoblot analysis using one of the following antibodies: Smn (1:2500), Gemin2 (1:1000), MRLC (1:1000), Nucleolin (1:1000), Profilin-1 (1:1000), and Annexin-II (1:1000) and detected by ECL (Amersham Biosciences).

Immunoblotting

Cell culture lysates used for immunoblotting were collected in ice-cold lysis buffer on ice. Hindlimb muscle tissue lysates from P5 mice were obtaining by grinding the tissue with a liquid nitrogen cooled mortar and pestle and subsequently adding the ice-cold lysis buffer. Protein concentrations were assessed by using the Bradford method. The separated proteins were analyzed by immunoblot using one of the following antibodies: Smn (1:2500), GAPDH (1:5000) (Abcam), MRLC (1:1000) or Annexin II H-50 (1:1000) (Santa Cruz Biotechnology). Bands were detected using ECL (Amersham Biosciences).

Immunofluorescence

Cells were stain as previously described (Shafey et al. 2005). The primary antibodies used were diluted as follows: Smn (1:100) (Transduction Laboratories, USA), Annexin II (1:50) (Santa Cruz Biotechnology), and MLC2 (1:20) (Santa Cruz Biotechnology).

Longitudinal muscle sections (10 μm) and teased fibers were collected from P5 *Smn*$^{+/-}$*;SMN2* and *Smn*$^{-/-}$*;SMN2* mice using a previously described technique (Rezniczek et al. 2007). Tissue sections and teased fibers were blocked with buffer (1X PBS, 0.15% glycine and 0.5% BSA) containing 10% horse serum for 30 min at room temperature and incubated overnight at 4°C with antibodies targeting Smn (1:100) (Transduction Laboratories) or MRLC (1:20) diluted in buffer. Secondary antibodies, Alexa Fluor 488-conjugated donkey anti-rabbit antibody (Molecular Probes) and an Alexa Fluor 555-conjugated donkey anti-mouse antibody (Molecular Probes) were diluted in buffer and incubated with the samples for 1 hour. Hoechst staining of nuclei was also performed in parallel. Fluorescent images were captured on a Zeiss confocal microscope (LSM 510 META DuoScan).

Proximity ligation assay

The Duolink proximity ligation assay (PLA) kit which includes an anti-rabbit PLA plus probe, an anti-mouse PLA minus probe, and the 563 detection kit was purchased from Olink Bioscience (Sweden). Paraformaldehyde fixed C2C12 cells grown on coverslips in a 12-well plate were blocked for 1 hour in 10% goat serum. The cells were then incubated with SMN and MRLC antibodies in antibody solution (1XPBS, 0.4% Triton X-100, 0.05% bovine serum albumin) overnight at 4°C. All subsequent reagent incubations were performed in a humidity chamber at 37°C. PLA probes were diluted in antibody solution (1:5) and all other duolink reagent dilutions were performed according to the manufacturer's specifications. Following a 2 hour incubation with the PLA probes, the cells were incubated with a series of hybridization, ligation, amplification and detection

mixtures with multiple washes between each step in accordance with the manufacturer's specifications. After air-drying in a light-protected enclosure, the coverslips were mounted on slides using Olink mounting media containing DAPI nuclear stain. Each experiment was performed in duplicate. A positive control involved incubating Smn with the known direct interacting partner Gemin2. For the negative controls, the PLA was performed with Smn and α-Parvin, a protein not previously shown to bind to Smn but expressed in C2C12 cells (data not shown). An additional negative control was performed in which one of the primary antibodies was not added to the assay. Detection of the PLA signals (red dot) using the Zeiss LSM 510 confocal microscope indicated that the proteins were within 40 nm of each other within the cell.

Results

Generation of NTAP-SMN and CTAP-SMN stable cell lines

The TAP-tag vector consists of a HIS and a FLAG epitope separated by a Tobacco Etch Virus (TEV) protease cleavage site. The N-terminal TAP-tag (NTAP) has the HIS epitope on the outside and the C-Terminal TAP-tag (CTAP) has the FLAG epitope on the outside (Fig. 2.1A). Recombinant retroviruses carrying the NTAP-SMN and CTAP-SMN constructs were prepared to infect C2C12 muscle and PC12 neuronal cells. Stable cell lines that maintain the expression of the fusion protein at similar to endogenous levels were generated (Fig. 2.1B-E). Clones N5 and C12 were selected from the C2C12 stable cell lines expressing NTAP-SMN and CTAP-SMN, respectively for all subsequent experiments. Similarly, clones N4 and C1 from the PC12 stable cell lines expressing NTAP-SMN and CTAP-SMN, respectively were selected for all subsequent experiments.

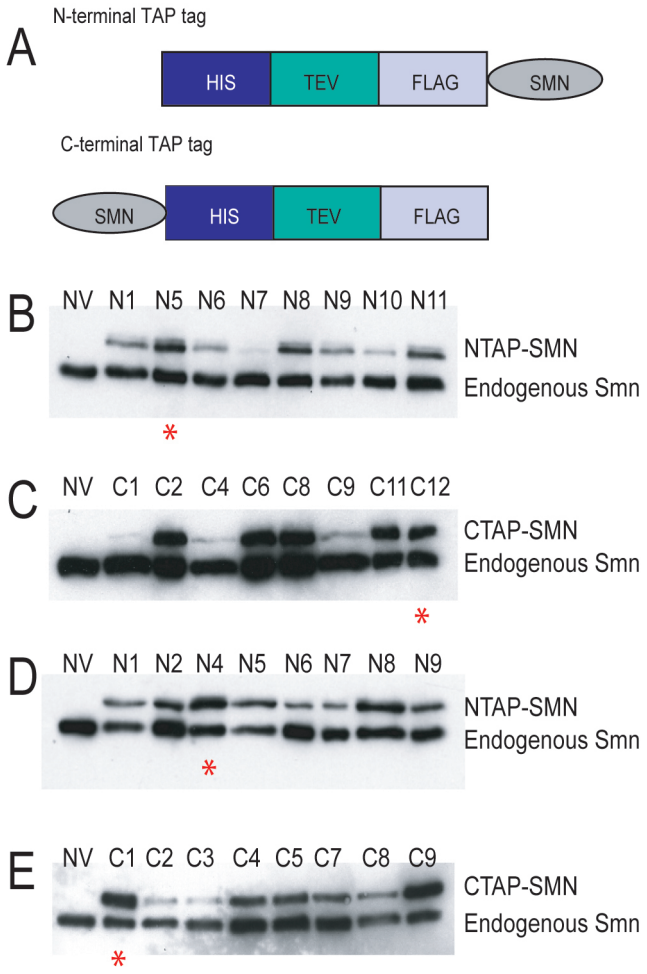

Figure 2.1. NTAP and CTAP-SMN constructs and clones. A. Schematic of the N-terminal (NTAP) and C-terminal (CTAP) SMN constructs. Cell lysates of C2C12 (B,C) and PC12 (D,E) cell clones expressing NTAP-SMN and CTAP-SMN were blotted with an anti-Smn antibody. The endogenous Smn protein migrates faster than the tagged fusion protein. The asterisk (*) indicates the clones that were used for the subsequent studies (NV: no vector control).

Purification of SMN complexes

Cell extracts from all four clones were collected at growth, one, three, five, and seven days of differentiation. The tagged SMN proteins, as well as any associated components, were recovered by tandem affinity purification. Interestingly, in C2C12 cells the SMN complex constituents vary depending on whether the analysis is done at growth, early differentiation, or late differentiation (Fig. 2.2A and Supplemental Fig. 2.1A). By contrast, in PC12 cells the SMN complex remains relatively invariant during growth and differentiation (Fig. 2.2B and Supplemental Fig. 2.1B). In addition, in both the C2C12 and PC12 purification, the NTAP-SMN fusion was more efficient at purifying interacting proteins than the CTAP-SMN fusion. This difference could be due to possible interference of the TAP-tag at the C-terminal end of SMN.

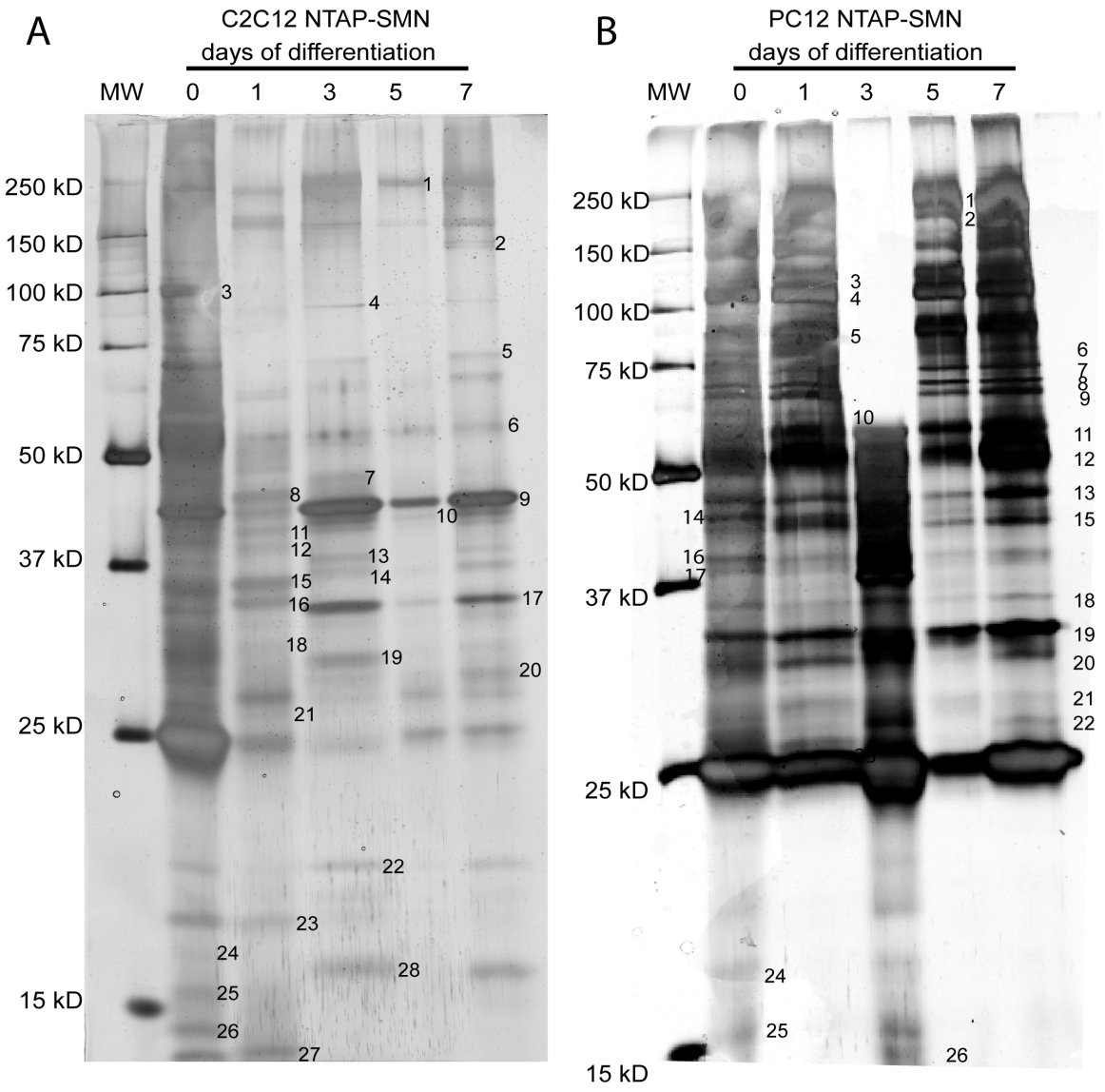

Figure 2.2. NTAP-SMN complex purified from C2C12 (A) and PC12 (B) cell clones during growth, and 1, 3, 5 and 7 days of differentiation were resolved on SDS-PAGE and silver stained. The numbers indicate the bands that were excised from the gel and identified by mass spectrometry. Molecular weight markers are indicated on the left.

Identification of co-purifying proteins

To identify the proteins that were co-purified with NTAP-SMN and CTAP-SMN, silver stained visible bands were excised from gels and subjected to tryptic digestion. An LTQ linear ion trap mass spectrometer was used for identification of the resulting peptides. In this manner, we not only detected known binding partners for SMN, such as Gemin2, SnrpD1, and profilin, but we have in addition identified new binding partners (summarized in Tables 2.1-4). There were many SMN interacting proteins that were specific to the C2C12 cell or PC12 cell sample, however some SMN interacting proteins were identified in both C2C12 and PC12 cells and these are listed in Table 5.

Table 2.1. Identification of proteins recovered from the NTAP-SMN tandem affinity purification in C2C12 cells.

BAND	Protein Identification	Days of Differentiation					C2C12 CTAP-SMN [a]	PC12 TAP-tag SMN [b]
		0	1	3	5	7		
1	Myh9 Myosin-9	-[c]	-	+[d]	+	+	-	-
2	Myh10 Myosin, heavy polypeptide 10, non-muscle	-	-	-	-	+	-	-
3	Actn4 Alpha-actinin-4 Actn1 Alpha-actinin-1	+ +	- -	- -	- -	- -	- -	- -
4	Actn1 Alpha-actinin-1 Actn4 Alpha-actinin-4 Sfpq Splicing factor, proline Gsn Isoform 1 of Gelsolin precursor	+ + + +	+ + + +	+ + + +	+ + + +	+ + + +	- - - +	- - + -
5	Gsn Isoform 1 of Gelsolin precursor Sfpq Splicing factor, proline	+ +	+ +	+ +	+ +	+ +	+ -	- +
6	Myh7 Myosin-7	+	+	+	+	+	-	-
7	Ppm1b Protein phosphatase 1B2 53 kDa isoform Myh6 Myosin-6	- -	- -	+ +	- -	- -	- -	+ -
8	Ppm1a Protein phosphatase 2C isoform alpha	-	+	-	-	-	-	-
9	Isoform C of Lamin-A/C	+	+	+	+	+	+	-
10	Wdr77 Methylosome protein 50	-	-	+	+	+	-	-
11	Mapk1 Mitogen-activated protein kinase 1 Fus RNA-binding protein FUS Smn1 Survival motor neuron protein	+ + +	+ + +	- - -	- - -	- - -	- - +	+ - +
12	Dnajb11 DnaJ homolog subfamily B member 11 Efha1 EF-hand domain-containing family member A1	+ +	+ +	- -	- -	- -	- -	- -
13	Tpm2 Isoform 1 of Tropomyosin beta chain Tpm1 Isoform 1 of Tropomyosin-1 alpha chain	- -	- -	+ +	+ +	+ +	- -	- -
14	Tpm2 Isoform 1 of Tropomyosin beta chain Tpm1 Isoform 1 of Tropomyosin-1 alpha chain	- -	- -	+ +	+ +	+ +	- -	- -
15	Nono Isoform 1 of Non-POU domain-containing Fn1 Fibronectin precursor	+ +	+ +	- -	- -	- -	- -	+ -
16	Pspc1 Paraspeckle protein 1 Nono Isoform 1 of Non-POU domain-containing	+ +	+ +	- -	- -	- -	- -	- +
17	Tpm1 Isoform 2 of Tropomyosin-1 alpha chain Tpm1 Isoform 1 of Tropomyosin-1 alpha chain	- -	- -	+ +	+ +	+ +	- -	- -
18	Gemin 2 (SIP1)	+	+	-	-	-	-	+
19	Tpm3 Isoform 2 of Tropomyosin alpha-3 chain Tpm3 2 days neonate thymus thymic cells cDNA Tpm4 Tropomyosin alpha-4 chain Tpm1 28 kDa protein	- - - -	- - - -	+ + + +	- - - -	- - - -	- - - -	- - - -
20	Tpm1 28 kDa protein Tpm3 Isoform 1 of Tropomyosin alpha-3 chain	- -	- -	+ +	+ +	+ +	- -	- -
21	Spin1 Isoform 1 of Spindlin-1	+	+	-	-	-	-	+
22	myosin regulatory light chain	+	-	+	+	+	-	-

23	Nme2 Nucleoside diphosphate kinase B Nme1 Nucleoside diphosphate kinase A	+ +	+ +	- -	- -	- -	+ +	- -
24	Nme1 Nucleoside diphosphate kinase A Myl6 Isoform Smooth muscle of Myosin light	+ +	- -	- -	- -	- -	+ +	- -
25	Snrpd2 Small nuclear ribonucleoprotein Sm D2 Snrpd1 Small nuclear ribonucleoprotein Sm D1	+ +	- -	- -	- -	- -	- -	+ -
26	Pdlim2 PDZ and LIM domain protein 2	+	-	-	-	-	-	-
27	Snrpf small nuclear ribonucleoprotein	+	+	-	-	-	-	-
28	EG546101 similar to myosin, light polypeptide 6	-	-	+	+	+	-	-

[a] In the C2C12 CTAP-SMN column, the '+' indicates that the band is present and the '-' indicates that the band is absent at any time point analyzed

[b] In the PC12 TAP-tag SMN column, the '+' indicates that the band is present and the '-' indicates that the band is absent at any time point and in either the CTAP-SMN or NTAP-SMN purification

[c] - indicates the absence of the band

[d] + indicates the presence of the band

Table 2.2. Identification of proteins recovered from the CTAP-SMN tandem affinity purification in C2C12 cells.

BAND	Protein Identification	Days of Differentiation				C2C12 NTAP-SMN [a]	PC12 Tap-tag SMN [b]
		0	1	3	5		
1	Spna2 similar to Spectrin alpha chain	-[c]	+[d]	-	-	-	-
2	Golga3 Isoform 1 of Golgin subfamily A member 3	+	-	-	-	-	-
3	Spna2 similar to Spectrin alpha chain	+	-	-	-	-	-
4	Rrbp1 ribosome binding protein 1 isoform a	+	-	-	-	-	-
5	Ivns1abp influenza virus NS1A binding protein	+	+	+	+	-	-
6	Eef1a2 Elongation factor 1-alpha 2	+	-	-	-	-	+
7	Actb Actin, cytoplasmic 1 Lmna Isoform C of Lamin-A/C	- -	+ +	+ +	- -	+ +	+ -
8	Acta1 Actin	-	+	-	-	+	+
9	Hnrpab S1 protein C2	+	-	-	-	-	+
10	Anxa1 Annexin A1 Acta1 Actin, alpha skeletal muscle	- -	+ +	- -	- -	- +	- +
11	Anxa2 Annexin A2	+	-	-	-	-	+
12	Ldha L-lactate dehydrogenase A chain	-	+	+	-	-	+
13	Actb Actin, cytoplasmic 1 Acta1 Actin, alpha skeletal muscle	- -	+ +	+ +	- -	+ +	+ +
14	EG622339 similar to GAPDH	-	+	+	-	-	+

[a] In the C2C12 NTAP-SMN column, the '+' indicates that the band is present and the '-' indicates that the band is absent at any time point analyzed

[b] In the PC12 TAP-tag SMN column, the '+' indicates that the band is present and the '-' indicates that the band is absent at any time point and in either the CTAP-SMN or NTAP-SMN purification

[c] - indicates the presence of the band

[d] + indicates the absence of the band

Table 2.3. Identification of proteins recovered from the NTAP-SMN tandem affinity purification in PC12 cells.

BAND	Protein Identification	Days of Differentiation					PC12 CTAP-SMN [a]	C2C12 Tap-tag SMN [b]
		0	1	3	5	7		
1	Eif5b eukaryotic translation initiation factor	+[c]	+	-[d]	+	+	+	-
2	Eif5b eukaryotic translation initiation factor	+	+	-	+	+	+	-
3	Ipo8 Isoform 1 of Importin-8	+	+	-	+	+	-	-
4	Ipo8 Isoform 1 of Importin-8	+	+	-	+	+	-	-
5	Sfpq Splicing factor, proline	+	+	-	+	+	-	+
6	Pfkm 6-phosphofructokinase	+	+	-	+	+	-	-
	Pfkp Isoform 1 of 6-phosphofructokinase type C	+	+	-	+	+	-	-
	Vps35 Vacuolar protein sorting-associated	+	+	-	+	+	-	-
	Sec23a Protein transport protein Sec23A	+	+	-	+	+	-	-
	Sec23b Protein transport protein Sec23B	+	+	-	+	+	-	-
	Dhx15 Putative pre-mRNA-splicing factor	+	+	-	+	+	-	+
	Ddx1 ATP-dependent RNA helicase DDX1	+	+	-	+	+	-	-
	Nin Isoform 1 of Ninein	+	+	-	+	+	-	-
7	Hspa5 78 kDa glucose-regulated protein precursor	+	+	-	+	+	-	-
	Ddx3x ATP-dependent RNA helicase DDX3X	+	+	-	+	+	-	-
	Prmt5 Protein arginine N-methyltransferase 5	+	+	-	+	+	-	-
8	Hspa8 Heat shock cognate 71 kDa protein	+	+	-	+	+	-	+
	Lmna Isoform A of Lamin-A/C	+	+	-	+	+	-	-
	Hspa9 Stress-70 protein, mitochondrial precursor	+	+	-	+	+	-	-
	Prmt5 Protein arginine N-methyltransferase 5	+	+	-	+	+	-	-
	Ddx3x similar to DEAD (Asp-Glu-Ala-Asp) box	+	+	-	+	+	-	-
	Pabpc2 poly A binding protein, cytoplasmic 2	+	+	-	+	+	-	-
9	Prmt5 Protein arginine N-methyltransferase 5	+	+	-	+	+	-	-
	Vgf VGF nerve growth factor inducible	+	+	-	+	+	-	-
	Ddx5 Probable ATP-dependent RNA helicase	+	+	-	+	+	-	-
	DDX5	+	+	-	+	+	-	-
	Hnrpl Heterogeneous nuclear ribonucleoprotein L							
10	Hnrpl Heterogeneous nuclear ribonucleoprotein L	+	+	-	+	+	-	-
	Ddx5 Probable ATP-dependent RNA helicase	+	+	-	+	+	-	-
	DDX5	+	+	-	+	+	-	-
	Lmna Isoform C of Lamin-A/C	+	+	-	+	+	-	-
	Cct3 T-complex protein 1 subunit gamma							
11	Nono Isoform 1 of Non-POU domain-containing	+	+	+	+	+	-	+
	Cct8 T-complex protein 1 subunit theta	+	+	+	+	+	-	-
	G6pdx Glucose-6-phosphate 1-dehydrogenase X	+	+	+	+	+	-	-
12	Serbp1 Isoform 1 of Plasminogen activator	+	+	+	+	+	-	-
	Ppm1b Protein phosphatase 1B2 53 kDa isoforms	+	+	+	+	+	-	+
	Prph1 Isoform 3u of Peripherin	+	+	+	+	+	-	-
13	Eef1a1 Elongation factor 1-alpha 1	+	+	+	+	+	-	-
	Eef1a2 Elongation factor 1-alpha 2	+	+	+	+	+	+	+
	Dnaja2 DnaJ homolog subfamily A member 2	+	+	+	+	+	-	-
	Prph1 Isoform 3u of Peripherin	+	+	+	+	+	-	-
14	Tufm Isoform 1 of Elongation factor Tu,	+	-	-	-	-	-	-
	Eif4a1 Eukaryotic initiation factor 4A-I	+	-	-	-	-	-	-
	U2af2 Splicing factor U2AF 65 kDa subunit	+	-	-	-	-	-	-
15	Acta1 Actin, alpha skeletal muscle	+	+	+	+	+	-	+
16	Mapk1 Mitogen-activated protein kinase 1	+	+	+	+	+	-	+
	Idh3b Tumor-related protein	+	+	+	+	+	-	-
	Csnk2a1 Casein kinase II subunit alpha	+	+	+	+	+	-	-
17	Idh3g Isocitrate dehydrogenase [NAD] subunit	+	+	-	-	-	-	-

	Lancl1 LanC-like protein 1	+	+	-	-	-	-	-
	Pcbp1 Poly(rC)-binding protein 1	+	+	-	-	-	-	-
18	GAPDH Glyceraldehyde 3 phosphate	+	++	+	-	+	-	-
	dehydrogenase	+	+	+	-	+	-	-
	Eif2s1 Eukaryotic translation initiation factor	+		+	-		+	+
	Smn1 Survival motor neuron protein							
19	Smn1 Survival motor neuron protein	+	+	+	+	+	+	+
	Ldha L-lactate dehydrogenase A chain	+	+	+	+	+	-	+
	Ldhb L-lactate dehydrogenase B chain	+	+	+	+	+	-	-
20	Gemin 2 (Sip1)	+	+	+	-	+	-	+
21	cytokine-like nuclear factor n-pac	+	+	-	-	-	-	-
	Spin1 Isoform 1 of Spindlin-1	+	+	-	-	-	-	+
	Mtap S-methyl-5-thioadenosine phosphorylase	+	+	-	-	-	-	-
22	Psph Phosphoserine phosphatases	+	-	-	-	-	-	-
23	Psph Phosphoserine phosphatases	+	+	+	-	+	-	-
	Prdx4 Peroxiredoxin-4	+	+	+	-	+	-	-
24	Rbm3 Putative RNA-binding protein 3	+	-	-	-	-	-	-
25	Snrpd2 Small nuclear ribonucleoprotein Sm D2	+	-	-	-	-	-	+
26	Phf5a PHD finger-like domain-containing protein	-	-	+	-	-	-	-

[a] In the PC12 CTAP-SMN column, the '+' indicates that the band is present and the '-' indicates that the band is absent at any time point analyzed

[b] In the C2C12 TAP-tag SMN column, the '+' indicates that the band is present and the '-' indicates that the band is absent at any time point and in either the CTAP-SMN or NTAP-SMN purification

[c] + indicates the presence of the band

[d] - indicates the absence of the band

Table 2.4. Identification of proteins recovered from the CTAP-SMN tandem affinity purification in PC12 cells.

BAND	Protein Identification	Days of Differentiation					PC12 NTAP-SMN [a]	C2C12 Tap-tag SMN [b]
		0	1	3	5	7		
1	Eif5b eukaryotic translation initiation factor	- [c]	-	-	-	+ [d]	+	-
2	Nucleolin	-	+	-	-	-	-	-
3	Actg1 Gamma actin-like protein	+	+	-	-	+	-	-
4	EG432946 similar to heterogeneous nuclear ribonucleoprotein A3	+	+	+	+	+	-	-
5	Anxa2 Annexin A2 Pfn1 Profilin-1	+ +	- -	- -	- -	- -	- +	+ -
6	Ftl2 Ferritin light chain 2	+	+	+	+	+	-	-

[a] In the PC12 NTAP-SMN column, the '+' indicates that the band is present and the '-' indicates that the band is absent at any time point analyzed

[b] In the C2C12 TAP-tag SMN column, the '+' indicates that the band is present and the '-' indicates that the band is absent at any time point and in either the CTAP-SMN or NTAP-SMN purification

[c] - indicates the absence of the band

[d] + indicates the presence of the band

Table 2.5. SMN interacting proteins that were identified in both the PC12 and C2C12 cells.

Protein identified	C2C12		PC12	
	Growth	Differentiation	Growth	Differentiation
Smn1	+[a]	+	+	+
Gemin2	+	+	+	+
Small nuclear ribonucleoprotein Sm D2	+	+	+	+
Ppm1b Protein phosphatase 1B2	-[b]	+	+	+
Splicing factor, proline	+	+	+	+
Actb Actin, cytoplasmic 1	+	+	+	+
Isoform C of Lamin-A/C	+	+	+	+
Mapk1 Mitogen-activated protein kinase 1	+	+	+	+
Annexin A2	+	-	+	+
Eef1a2 Elongation factor 1-alpha 2	+	-	+	+
Nono Isoform 1 of Non-POU domain-containing	+	+	+	+
Spin1 Isoform 1 of Spindlin-1	+	+	+	+
Ldha L-lactate dehydrogenase A chain	+	+	+	+

[a] indicates the presence of the protein
[b] indicates the absence of the protein

Validation of novel SMN interacting proteins

Of the many novel SMN interacting proteins identified, we chose to validate Annexin II and myosin regulatory light chain (MRLC) in C2C12 cells and Annexin II in PC12 cells. Annexin II was identified as an interacting protein in both C2C12 and PC12 cells, whereas MRLC was specific to C2C12 cells. To confirm that Annexin II and MRLC are associated with Smn in C2C12 cells, we performed immunoprecipitation experiments with the endogenous Smn, Gemin2, MRLC and Annexin II proteins. The associated complexes were analyzed by immunoblot for the presence of Smn (Fig. 2.3B). As expected, control immunoprecipitates did not contain any of the proteins (Fig. 2.3A). As a further validation of any interaction, we performed the reciprocal immunoprecipitation with Smn in the C2C12 cell lysates from growth, and 1 and 3 days of differentiation, and the associated complexes were analyzed for the presence of Smn, Gemin2, Annexin II and MRLC (Fig. 2.3C). From these experiments, we demonstrate that Gemin2 immunoprecipitates with Smn in C2C12 cells at all time points studied, and that Annexin II and MRLC immunoprecipitate with Smn in C2C12 cells only during growth and 1 day of differentiation (Fig. 2.3B and C).

Similarly, we performed reciprocal immunoprecipitations to confirm Annexin II association with Smn in PC12 cells. Included in the analysis were immunoprecipitations with Gemin2, nucleolin, and profilin-1, known interactors of Smn. Our results demonstrate that all four proteins immunoprecipitate with Smn in PC12 cells during growth and 3 days of differentiation (Fig. 2.4B and C). No bands were detected in control experiments for PC12 cells (Fig. 2.4A).

To further dissect the interaction between Smn and MRLC we have performed a series of proximity ligation assays. This method is used to identify whether proteins are within 40 nm of one another in the cell and is indicative of a direct interaction. The presence of distinct fluorescent dots using the PLA in C2C12 cells at growth with MRLC and Smn antibodies indicates that these proteins are indeed within 40 nm of each other in the cell and are likely direct interactors (Fig. 2.5A). The positive control (Smn and Gemin2 interaction in the nucleus) showed that the assay works (Fig. 2.5B) and the negative controls (Fig. 2.5C and D) showed that the Smn-MRLC interaction was specific.

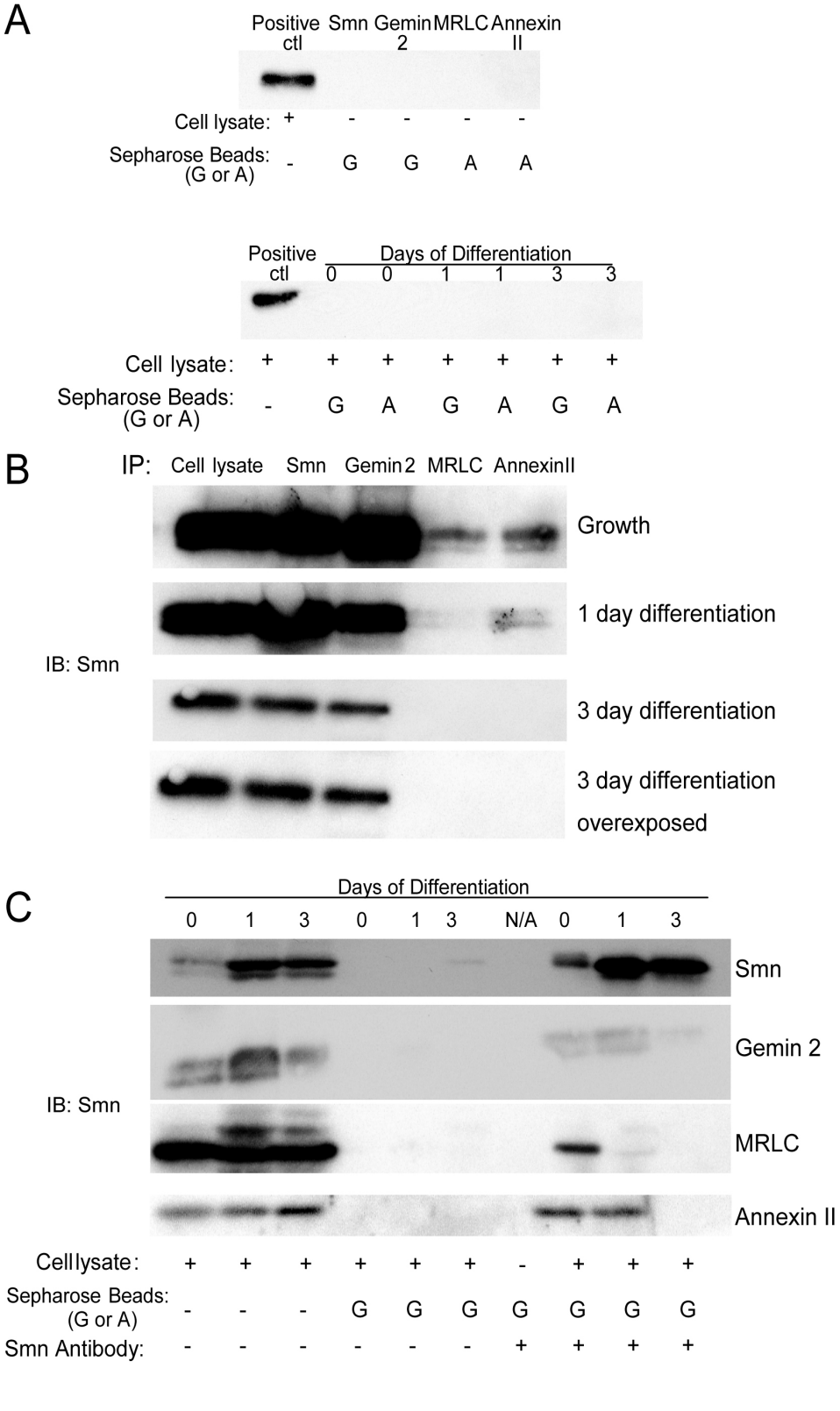
A
Positive ctl
Smn
Gemin 2
MRLC
Annexin II
Cell lysate: + - - - -
Sepharose Beads: (G or A) - G G A A
Positive ctl
Days of Differentiation
0 0 1 1 3 3
Cell lysate: + + + + + + +
Sepharose Beads: (G or A) - G A G A G A
B
IP: Cell lysate Smn Gemin2 MRLC AnnexinII
Growth
1 day differentiation
IB: Smn
3 day differentiation
3 day differentiation overexposed
C
Days of Differentiation
0 1 3 0 1 3 N/A 0 1 3
Smn
Gemin 2
IB: Smn
MRLC
Annexin II
Cell lysate: + + + + + + - + + +
Sepharose Beads: (G or A) - - - G G G G G G G
Smn Antibody: - - - - - - + + + +

Figure 2.3. Annexin II and myosin regulatory light chain interact with Smn in cultured C2C12 cells. A. Controls for the immunoprecipitation of Smn, Gemin2, MRLC and Annexin II in C2C12 cells. Controls are lysate alone, antibodies incubated with the appropriate sepharose beads, and lysate incubated with either protein A or G sepharose beads. These gels were then immunoblotted for Smn. B. Immunoprecipitation of Smn, Gemin2, MRLC and Annexin II during growth, and 1 and 3 days of differentiation in C2C12 cell lysates. Immunoblot analysis was performed using an Smn antibody. C. Immunoprecipitations of Smn during growth (0), 1 and 3 days of differentiation in C2C12 cell lysates were resolved on SDS-PAGE. Controls included lysate incubated with protein G sepharose beads and Smn antibody with protein G sepharose beads. Immunoblot analysis was performed using Smn, Gemin2, MRLC and Annexin II antibodies. (IB: immunoblot)

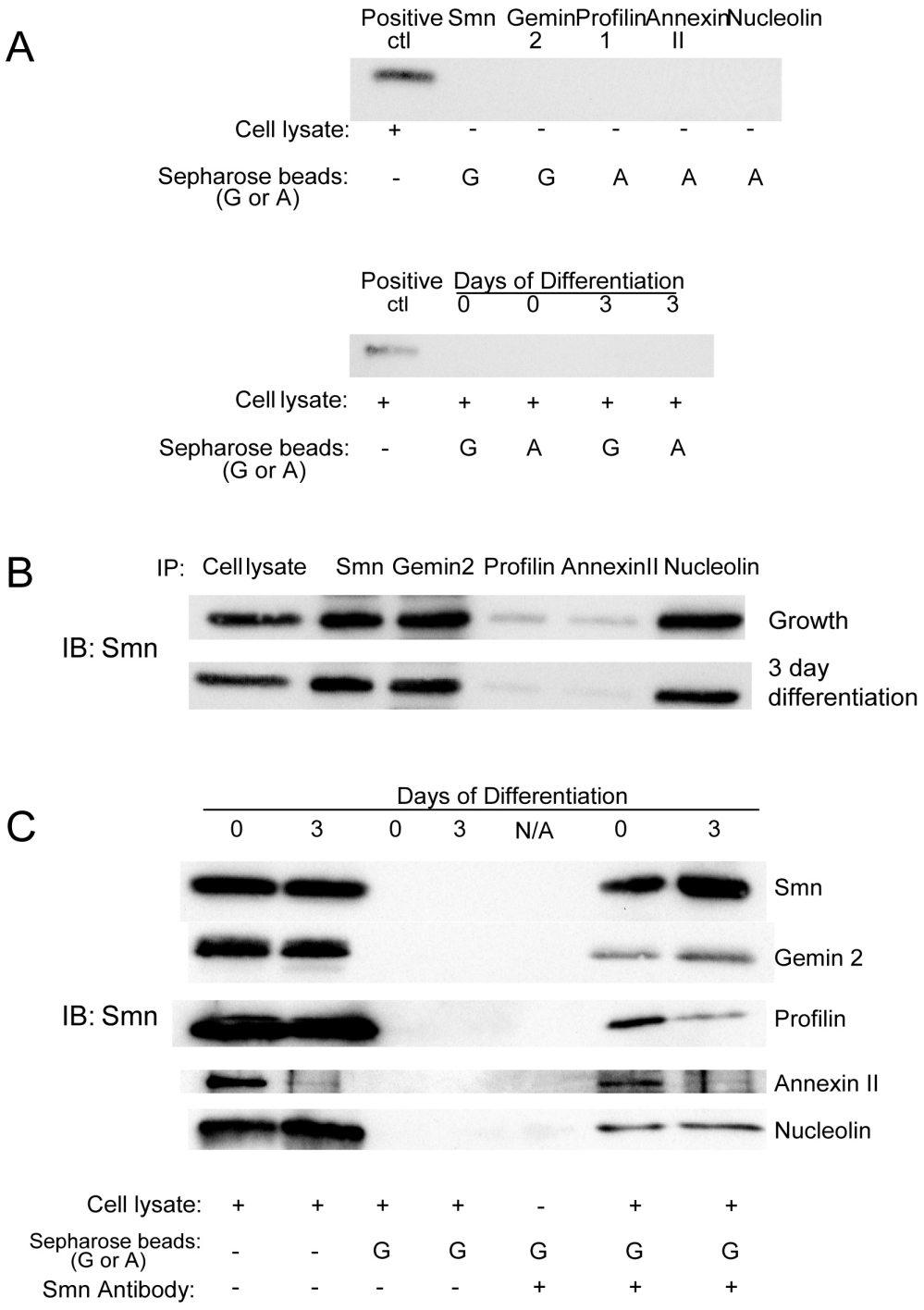
A
Positive ctl
Smn
Gemin 2
Profilin 1
Annexin II
Nucleolin
Cell lysate: + - - - - -
Sepharose beads: (G or A) - G G A A A
Positive ctl
Days of Differentiation
0 0 3 3
Cell lysate: + + + + +
Sepharose beads: (G or A) - G A G A
B
IP: Cell lysate
Smn
Gemin2
Profilin
AnnexinII
Nucleolin
IB: Smn
Growth
3 day differentiation
C
Days of Differentiation
0 3 0 3 N/A 0 3
Smn
Gemin 2
IB: Smn
Profilin
Annexin II
Nucleolin
Cell lysate: + + + + - + +
Sepharose beads: (G or A) - - G G G G G
Smn Antibody: - - - - + + +

Figure 2.4. Annexin II and nucleolin interact with Smn in cultured PC12 cells. A. Controls for the immunoprecipitation of Smn, Gemin2, profilin, Annexin II, and nucleolin in PC12 cells. Controls are lysate alone, antibodies incubated with the appropriate sepharose beads, and lysate incubated with either protein A or G sepharose beads. These gels were then immunoblotted for Smn. B. Immunoprecipitation of Smn, Gemin2, Profilin, Annexin II, and nucleolin during growth and 3 days of differentiation in PC12 cell lysates were resolved on SDS-PAGE blotted for Smn. C. Immunoprecipitation of Smn during growth (0) and 3 days of differentiation in PC12 cell lysates were resolved on SDS-PAGE. Controls include lysate incubated with protein G sepharose beads and Smn antibody with protein G sepharose beads. Immunoblot analysis was performed using Smn, Gemin2, Profilin, Annexin II, and nucleolin antibodies. (IB: immunoblot)

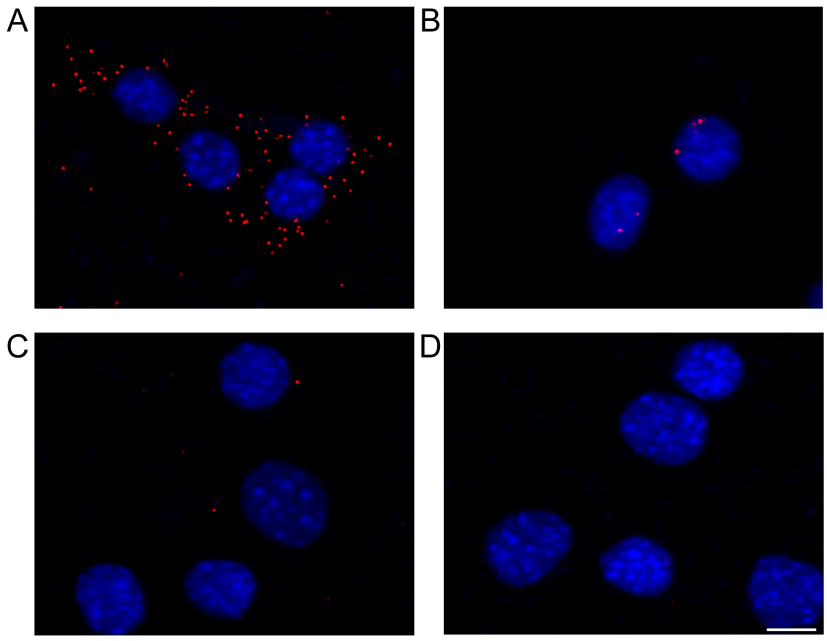

Figure 2.5. Smn is in close proximity to MRLC in C2C12 cells. A. Proximity ligation assay performed with Smn and MRLC antibodies demonstrates the presence of several PLA signals in the cytoplasm of the myoblasts. B. As a positive control, the PLA method was performed using Smn and Gemin2, a known direct interacting partner of Smn. Fluorescent dots were observed in the nucleus as expected based on the known localization of this interaction. C and D. Negative controls were performed in parallel which consisted of the PLA without one of the primary antibodies (C) or with α-Parvin, a protein not previously shown to interact with Smn (D). Minimal background fluorescence was detected in C, while virtually no fluorescence was observed in D. Scale bar = 10 μm.

Validation in SMA mouse models

To confirm that MRLC is associated with Smn in mouse muscle, we performed immunoprecipitation experiments with the endogenous proteins. Tissue lysates from P5 tibialis anterior muscle from *Smn*$^{+/+}$*;SMN2* and *Smn*$^{-/-}$*;SMN2* mice were used to immunoprecipitate complexes with MRLC. The associated complexes were analyzed for the presence of Smn (Fig. 2.6A). Control immunoprecipitates did not contain any of the proteins (Fig. 2.6A). As a further validation of the interaction, we performed the reciprocal immunoprecipitation with Smn in the tissue lysates and the associated complexes were analyzed for the presence of MRLC (Fig. 2.6B). From these experiments, we demonstrate that MRLC immunoprecipitates with Smn in muscle tissue extracts.

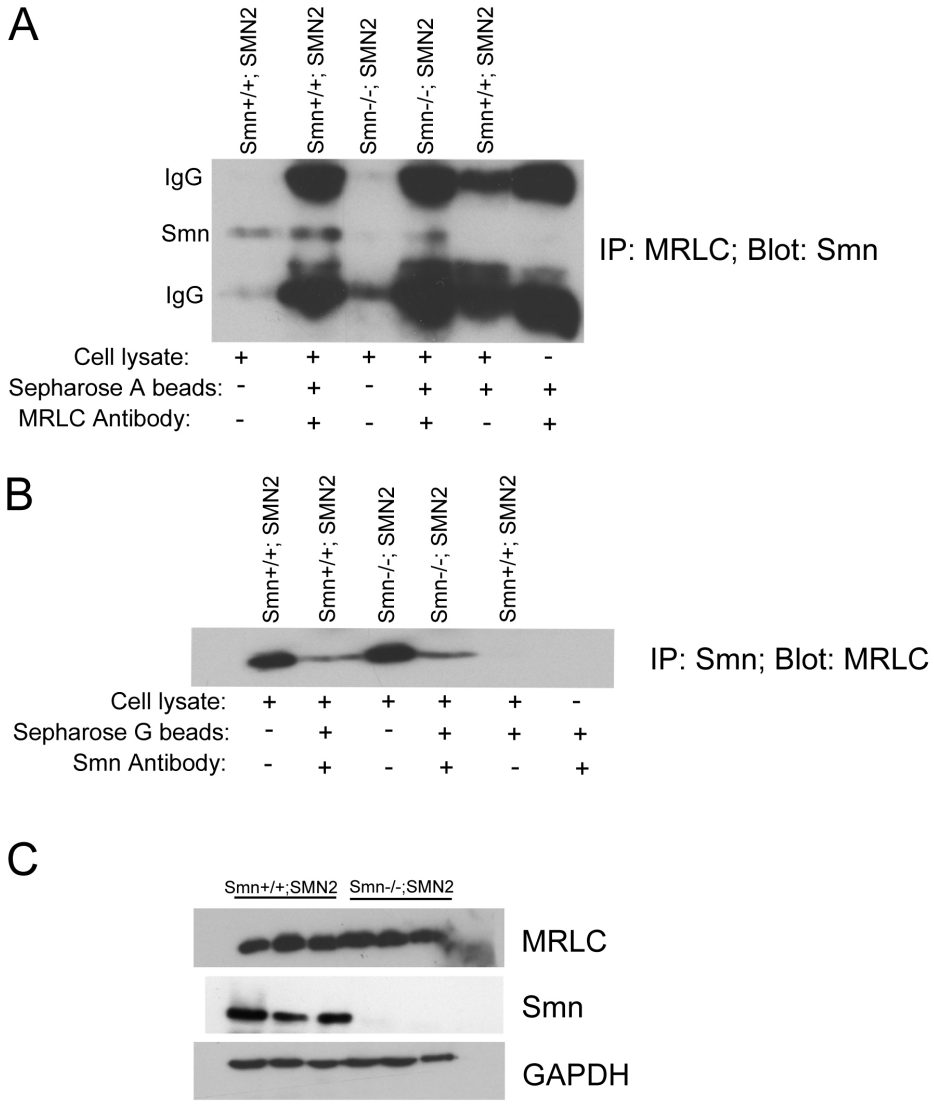

Figure 2.6. MRLC and SMN immunoprecipitate together in mouse skeletal muscle lysate. A and B. Reciprocal immunoprecipitation of Smn and MRLC using extracts from hindlimb skeletal muscle from P5 mice. Controls were prepared in parallel and consisted of lysate alone, antibodies incubated with the appropriate sepharose beads, and lysate incubated with either protein A or G sepharose beads. C. Immunoblot analysis of Smn, MRLC as well as GAPDH which served as an internal control (N = 6).

Myosin Regulatory Light Chain levels are increased and it is mis-localized in Smn depleted cells but not in Smn$^{-/-}$;SMN2 skeletal muscle

Having identified Annexin II and MRLC as two Smn interacting proteins in C2C12 cells, we next performed experiments to determine if Smn depletion had any impact on these proteins. We took advantage of our previously described C2C12 cell line, 2B3, in which Smn is knocked down by approximately 90% (Shafey et al. 2005). We first assessed the levels of Annexin II and MRLC in wild type and 2B3 C2C12 cells. The level of Annexin II was unaffected in the Smn knockdown cells, however the level of MRLC is noticeably increased in the 2B3 cells (Fig. 2.7A).

We further analyzed the distribution of Annexin II and MRLC to determine if these proteins are still properly localized in the 2B3 cells. Annexin II is found in the cytoplasm and around the nucleus in both the wild type and 2B3 cells (Fig. 2.7B). In contrast, MRLC localization is dramatically affected in 2B3 cells. Normally, MRLC is present in the cytoplasm of wild type C2C12 cells at relatively low levels (Fig. 2.7B). However, in 2B3 cells, in addition to being localized in the cytoplasm, MRLC is also found clustered in the nucleus, and it is present at relatively higher levels than in the wild type cells (Fig. 2.7B). The abnormal localization is particularly prominent at 3 days of differentiation.

To confirm these data in vivo, we performed analysis on skeletal muscle tissues from wild type, *Smn*$^{+/+}$*;SMN2* and *Smn*$^{-/-}$*;SMN2* mice. In contrast to the C2C12 cells, MRLC protein levels were unchanged in muscle from *Smn*$^{-/-}$*;SMN2* mice compared to the control as determined by immunoblotting (Fig. 2.6C). Furthermore, we analyzed by

immunofluorescence the distribution of MRLC and observed no aberrant MRLC localization in *Smn*$^{-/-}$*;SMN2* skeletal muscle (data not shown).

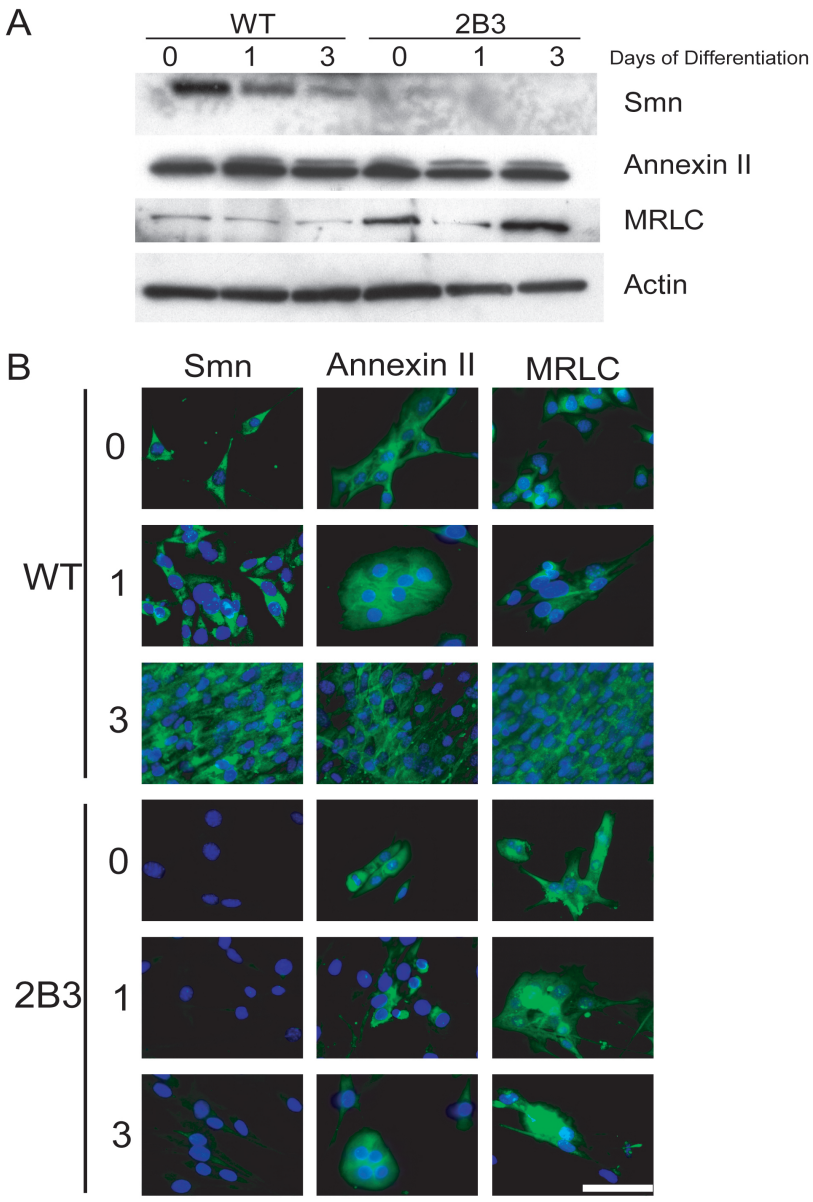

Figure 2.7. Level and localization of myosin regulatory light chain is affected in Smn-depleted C2C12 cells. A. Immunoblot analysis of Smn, Annexin II and MRLC in wild type and 2B3 Smn knockdown C2C12 cells (N=3). B. Immunocytochemistry of Smn, Annexin II and MRLC in wild type and 2B3 Smn knockdown C2C12 cells. The same microscope settings were used for images at all stages of differentiation. Scale bar, 50 μm (N = 3).

Discussion

Previous studies have determined that mutations or deletions in the *SMN1* gene are the primary cause of SMA (Melki et al. 1994, Bussaglia et al. 1995, Lefebvre et al. 1995, Brahe et al. 1996, Parsons et al. 1996, Hahnen et al. 1997). Understanding how SMN functions and in particular how its depletion leads to pathogenesis in SMA patients is an intense field of study. Among the many questions being addressed is why systemically reduced levels of functional SMN protein lead to specific degeneration of motor neurons and muscle atrophy. It is possible that in addition to the reported role in splicing and transcriptional regulation, SMN could be playing a motor neuron and/or muscle specific function through differences in the constituents that make up the SMN complex in these relevant cell types. Thus, determining if SMN is part of diverse complexes in neurons and muscle, and if these complexes are dynamic or static should lead us to a better understanding of SMA pathophysiology. Therefore, we chose to examine whether Smn interacting proteins change during different stages of growth and differentiation of C2C12 muscle and PC12 neuronal-like cells.

Cellular functions are the result of the coordinated action of several proteins in macromolecular assemblies. Protein complex composition varies with time to adapt to changing cellular requirements. Therefore, the analysis of protein complex composition is an important step in elucidating the pathophysiology of a disease. Mass spectrometry-based proteomic tools have proven to be successful in the identification of multicomponent complexes formed under native conditions (Puig et al. 2001, Aebersold and Mann 2003). The TAP system is an affinity purification technique originally developed in yeast that enables the purification of protein complexes under close to

physiological conditions (Rigaut et al. 1999, Knuesel et al. 2003, Yang et al. 2006). This approach has emerged as a useful tool for studying protein complexes *in vitro* (Rigaut et al. 1999, Knuesel et al. 2003) and *in vivo* (Yang et al. 2006). We used this approach to study the changes in SMN complex constituents during different stages of growth and differentiation in C2C12 and PC12 cells. In C2C12 cells, there are several changes to the nature of SMN associated proteins from growth, to early differentiation, and then to late differentiation. The dynamic nature of the SMN complex in C2C12 cells indicates the possibility for a change in the role that SMN plays at different stages of muscle development and/or differentiation.

However, in contrast to C2C12 cells, the SMN complex appears to be relatively static in PC12 cells, with the purified complex remaining essentially unchanged over time. The reason for this relatively invariant pattern in the SMN associated proteins is that for the most part the PC12 cell remains morphologically unchanged during differentiation, except for the establishment of neurite processes. Since this latter structure only makes up a minor proportion of the cell in terms of volume, any change in the SMN complex may be masked.

We have discovered that Smn forms different complexes in different cell types and at different stages of differentiation. From our analysis, we identified many known SMN interacting proteins, including Gemin2, sm proteins, snRNPs, α-actinin and profilin. We also identified many novel SMN associated proteins in both the C2C12 and PC12 cells. Some of these proteins, like Annexin II, were identified as SMN interactors in both cell lines. However, many interacting proteins such as MRLC are specific to one cell type. The identification of these cell-specific interactors may imply a unique role for

Smn in those cell types. We have validated the interaction between Smn and Gemin2, profilin, nucleolin and Annexin II in PC12 cells and we have validated the interaction between Smn and Gemin2, Annexin II and MRLC in C2C12 cells and mouse skeletal muscle tissue. Of importance, these results were validated by performing reciprocal immunoprecipitation experiments targeting the endogenous proteins. Annexin II is part of a family of structurally similar proteins that bind to phospholipids and may be involved in regulation of membrane transport, membrane channel activity, and interaction of the cell membrane with the extracellular matrix (Waisman 1995), (Menell et al. 1999). A pair of MRLCs, myosin essential light chains as well as two heavy chains makes up the actin-based motor known as myosin II. In skeletal muscle, the phosphorylation of MRLC by its kinase affects Ca^{2+} sensitivity and influences force development (Szczesna et al. 2002).

Although Annexin II levels and localization were not perturbed in Smn depleted C2C12 cells, MRLC was found to be present at elevated levels and its localization was affected. To corroborate these findings we analyzed the interaction of MRLC with Smn, as well as its expression and localization in tibialis anterior muscle from *Smn*$^{+/+}$;*SMN2*$^{+/+}$ and *Smn*$^{-/-}$;*SMN2*$^{+/+}$ mice. We also determined whether the expression and localization of MRLC was affected in the *Smn*$^{-/-}$;*SMN2*$^{+/+}$ mice. In comparison to the Smn depleted C2C12 cells, we did not observe any differences in the expression of MRLC in the Smn depleted mouse model. This result can likely be attributed to the developmental differences between the muscle cells in culture and mature myocytes *in vivo*. In addition, a major difference between the *Smn*$^{-/-}$;*SMN2* mouse model and the Smn knockdown C2C12 myoblasts relates to the absence of the human *SMN2* transgene in the 2B3 C2C12

cell line. The *SMN2* transgene produces a truncated SMN protein which may influence MLRC levels *in vivo*. Understanding why MRLC is up regulated and mis-localized in cultured muscle cells may lead us to a better understanding of the specific role of Smn in muscle and how this affects SMA pathophysiology.

In our previous study, we had demonstrated that Smn deficiency in C2C12 myoblasts leads to abnormal myoblast fusion (Shafey et al. 2005), which is corroborated by findings that SMA patient derived myoblasts have fusion abnormalities (Arnold et al. 2004). Myoblast fusion is a critical process for the terminal differentiation of skeletal muscle. An important regulator of this process is the small GTPase protein Rho (Nishiyama et al. 2004, Charrasse et al. 2006). Rho GTPases are molecular switches that control a variety of cytoskeleton-dependent cell functions such as actin cytoskeleton organization, microtubule dynamics, membrane transport, cell polarity and transcriptional activity (Etienne-Manneville and Hall 2002). Rho activity, which is high in proliferating myoblasts, decreases during myogenesis (Charrasse et al. 2006). If Rho is constitutively active, myoblast fusion is blocked (Nishiyama et al. 2004). Consistent with this, the activity of Rho's effector, the Rho-associated kinase (ROCK), is also decreased in differentiating C2C12 cells, and constitutively active ROCK blocks myoblast fusion (Nishiyama et al. 2004). Thus, the down regulation of Rho/ROCK signaling is required for proper myoblast fusion. When RhoA is in its active state, it activates ROCK, resulting in phosphorylation and activation of MRLC, which in turn regulates the assembly of stress fibers (Kimura et al. 1996, Totsukawa et al. 2000, Ueda et al. 2002). Our group has previously shown that Smn-depletion in mice is associated with the improper activation of the RhoA/ROCK pathway in a neuronal cell line leading to defects in

differentiation and neuritogenesis (Bowerman et al. 2007). Based on our findings, the association between MRLC and Smn in muscle may play a role in properly regulating the RhoA/ROCK pathway in the context of myoblast fusion or actin dynamics (Bowerman et al. 2009). However, for the moment it remains to be seen if this pathway is perturbed in SMA muscle. Further investigation on the functional relationship of MRLC and other proteins identified in our TAP-tag screen should lead to a better understanding of the mechanisms that lead to motor neuron degeneration and muscle atrophy in SMA.

Using the Tandem Affinity Purification method, we have been able to elucidate many novel SMN interacting proteins in disease relevant cell types. The discovery of these proteins will lead to a better understanding of the pathophysiology of SMA and may lead us to the identification of new drug targets.

Funding

This project was funded by grants from the Canadian Institutes of Health Research (CIHR), Muscular Dystrophy Association, and Families of SMA Canada (FSMAC) to R.K. D.S. is a recipient a Canada Graduate Scholarship from the CIHR and J.G.B is a recipient of an Ontario Graduate Scholarship. R.K. is a recipient of a University Health Research Chair from the University of Ottawa.

Supporting Information Available:

Supplementary information can be downloaded for free at http://pubs.acs.org.

Acknowledgements

We are grateful to Dr. Lynn Megeney for critical reading of the manuscript, and the rest of the Kothary laboratory for helpful discussions. We also thank Dr. Iain McKinnell for his extensive help with the Tap-Tag purification process, James Knight for his help with the gel preparation for mass spectrometry analysis, and Julian Vasilescu for his prompt and extensive mass spectrometry analysis.

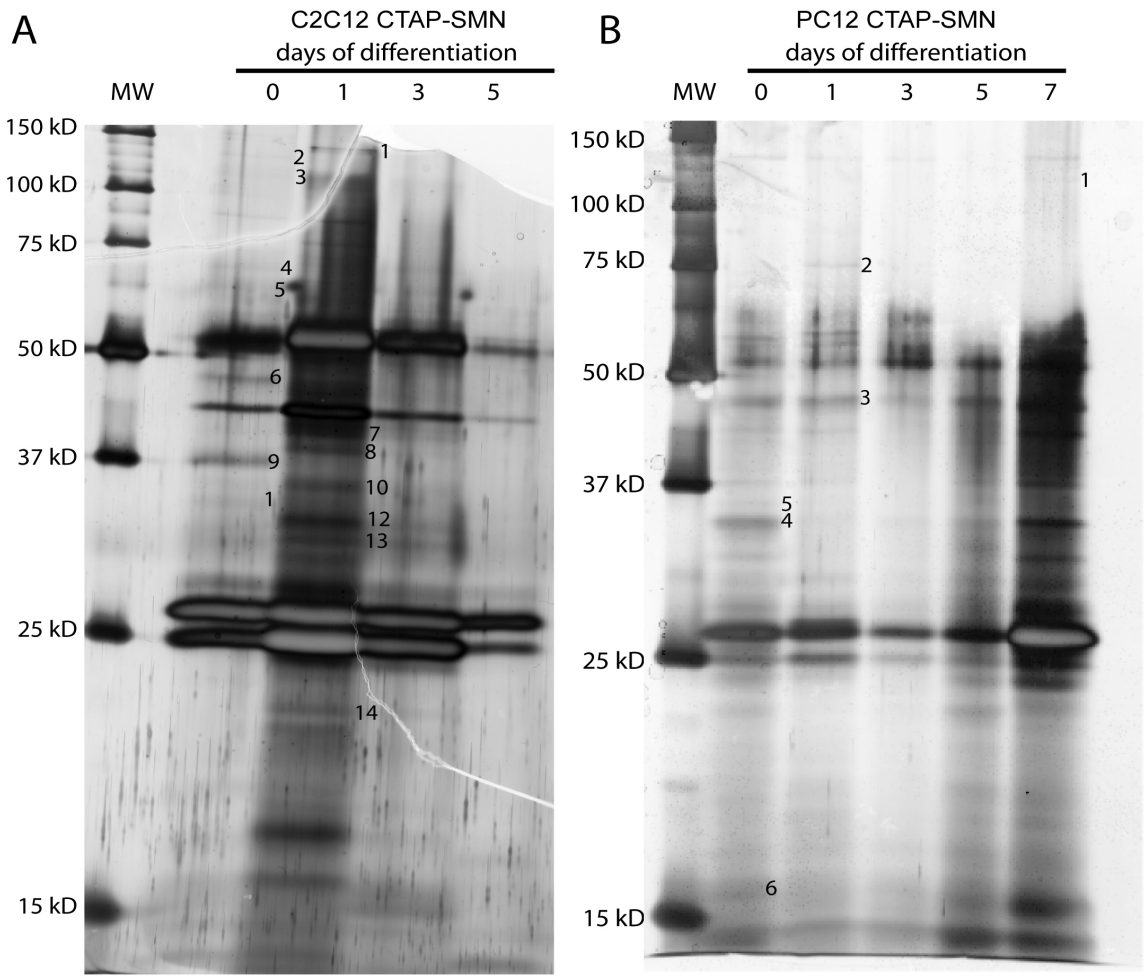

Supplemental Figure 2.1. CTAP-SMN complex purified from C2C12 (A) and PC12 (B) cell clones during growth, and 1, 3, 5 and 7 days of differentiation were resolved on SDS-PAGE and silver stained. The numbers indicate the bands that were excised from the gel and identified by mass spectrometry. Molecular weight markers are indicated on the left.

Chapter 3

Impaired skeletal muscle development in mouse models of spinal muscular atrophy

Author Contributions

JGB and RK conceived of and designed the project. JGB performed and analyzed most of the experiments and was assisted by MOD for figures 3.2 and 3.4 and by YDR for panel D of figure 3.5. JGB performed the denervation experiments while in CBL's laboratory. JGB wrote the paper and RK revised and edited the manuscript.

Impaired skeletal muscle development in mouse models of spinal muscular atrophy

Justin G. Boyer[1,2], Marc-Olivier Deguise[1], Yves De Repentigny[1], Céline Boudreau-Larivière[3], and Rashmi Kothary[1,2,4#]

[1]Ottawa Hospital Research Institute, Regenerative Medicine Program, Ottawa, ON, Canada K1H 8L6

[2]Department of Cellular and Molecular Medicine, University of Ottawa, Ottawa, ON, Canada K1H 8M5

[3]School of Human Kinetics, Laurentian University, Sudbury, ON, Canada, P3E 2C6

[4]Department of Medicine, University of Ottawa, Ottawa, ON, Canada K1H 8M5

[#]To whom correspondence should be addressed

Abstract

The disruption of the survival motor neuron (*SMN1*) gene leads to the neuromuscular disease spinal muscular atrophy (SMA). Although SMA is primarily considered a motor neuron disease, the importance of muscle defects in its pathogenesis has not been fully investigated. Previous studies have demonstrated that the pathological reduction of Smn leads to developmental defects in C2C12 cells. However, very little is known about muscle defects caused by Smn-depletion in the context of SMA pathology. Here, we investigated postnatal muscle development in mouse models of SMA. We use both primary cell culture and SMA model mice to demonstrate that reduced levels of Smn lead to a profound disruption in the myogenic program. There was aberrant expression of Pax7 and myogenic regulatory factors (MyoD, myogenin) in primary myoblasts isolated from $Smn^{2B/-}$ mice during stages of growth and differentiation, leading to myotube fusion defects. Similarly, a time course analysis in severe $Smn^{-/-}$;*SMN2* mice revealed decreased expression of the myogenic program. By comparison, skeletal muscle from the less severe $Smn^{2B/-}$ mice also displayed a decreased expression and a delay in the onset of the myogenic program. The molecular mis-regulation of the myogenic program was associated with a decrease in myofiber size and an increased presence of immature myofibers in both mouse models of SMA, suggesting that Smn is crucial for early muscle development. Importantly, a disruption in the myogenic program and decrease in fiber maturity could be detected at a time point prior to any neuromuscular junction degeneration, and in muscles which show no denervation at late stages of disease. Taken together, we demonstrate delayed muscle maturation in mouse models of SMA at the

molecular and histological levels, which occur independent of muscle denervation. These defects likely have a significant contribution to the muscle weakness observed in SMA.

Key words: Survival motor neuron, myogenic regulatory factors, denervation.

Introduction

Spinal muscular atrophy (SMA) is an autosomal recessive disorder characterized by the degeneration of α-motor neurons in the spinal cord and is a major leading genetic cause of infant deaths (Boyer et al. 2010). The deletion, rearrangement, or mutation of the disease causing gene, survival motor neuron 1 (*SMN1*), is the cause of SMA in over 95% of patients (Hahnen et al. 1995, Lefebvre et al. 1995, Burghes and Beattie 2009). There are two virtually identical copies of the *SMN* gene, a telomeric copy, *SMN1*, and a centromeric copy, *SMN2* (Rochette et al. 2001). Compared to the *SMN1* gene, a single nucleotide substitution identified in *SMN2* has a profound functional impact as only 10% of *SMN2* translated products are full-length and stable (Lorson et al. 1999). In contrast to humans, mice have only a single *Smn* gene and the homozygous deletion of the gene leads to death early during pre-implantation embryonic development (Schrank et al. 1997). The addition of the human *SMN2* transgene onto the *Smn*-null background leads to a severe phenotype in mice (Monani et al. 2000). These mice, designated $Smn^{-/-}$;*SMN2*, live up to 6 days before succumbing to the disease. The addition of the *Δ7SMN* transgene onto the $Smn^{+/-}$;*SMN2* background produced a slightly less severe mouse and extended survival from 5 to 13 days (Le et al. 2005). We have previously generated an intermediate mouse model of SMA ($Smn^{2B/-}$) that survives to 4 weeks of age due to slightly higher Smn protein levels than the severe models (Bowerman et al. 2012). The *2B* mutation consists of a three-nucleotide substitution in the exon splicing enhancer of exon 7 of the endogenous mouse *Smn* gene (Hammond et al. 2010).

Although SMA is primarily considered a motor neuron disease, the involvement of muscle in its pathogenesis has not been fully investigated. C2C12 myoblasts with

reduced Smn protein display abnormal proliferation, aberrant myoblast fusion, and malformed myotubes (Shafey et al. 2005). Skeletal muscle is severely affected by Smn depletion as demonstrated in a conditional knockout mouse model (Cifuentes-Diaz et al. 2001). These mice display a severe dystrophic phenotype and myofibers with compromised sarcolemma. In a separate study, a proteomic screen identified intrinsic molecular changes in pre-symptomatic skeletal muscles from mouse models of SMA prior to motor neuron degeneration (Mutsaers et al. 2011). More recently, muscle defects have been highlighted *in vivo* in a severe mouse model of SMA. Increased cell death, independent of muscle denervation, was observed in various skeletal muscles of *Smn*$^{-/-}$*;SMN2* mice (Dachs et al. 2011). The idea of delayed muscle development in mouse models of SMA has been suggested by several groups, however this has, for the most part, been proposed on the basis that myofibers do not appear to grow in size shortly after birth in severe mouse models of SMA (Dachs et al. 2011, Lee et al. 2011). For instance, Dachs et al. (2011) demonstrate that myofiber size of P5 phenotypic *Smn*$^{-/-}$*;SMN2* muscles are the same size as P0-P1 muscles from pre-symptomatic *Smn*$^{-/-}$*;SMN2* mice.

The maturation of muscle is coordinated by the sequential expression of myogenic regulatory factors namely, myoblast determination 1 (MyoD), myogenin and the muscle-specific regulatory factor 4 **(**MRF4; also known as Myf6). MyoD is an early marker of myogenesis while myogenin and MRF4 are expressed later and mark muscle differentiation. During postnatal muscle development, a high proportion of paired box protein 7 (Pax7) positive satellite cells undergo proliferation and differentiation, and profoundly contribute to muscle growth (Seale et al. 2000).

Whether skeletal muscle defects contribute to the SMA phenotype has only recently begun to be investigated. Much remains to be uncovered in diseased skeletal muscles including why they are smaller in SMA. Mechanisms underlying muscle weakness in SMA can be targeted therapeutically to increase muscle strength, regardless of whether they are attributed to intrinsic defects, or the consequence of motor neuron pathology.

Here, we show abnormal expression of myogenic regulatory factors during growth and differentiation of primary myoblasts from *Smn*$^{2B/-}$ mice. These observations were extended *in vivo*, where we demonstrate the presence of delayed skeletal muscle development at the molecular and histological level independent of myofiber degeneration and muscle denervation in several mouse models of SMA. These data demonstrate that Smn is required for proper perinatal muscle development.

Materials and Methods

Mice and tissue extraction

In the present study, we took advantage of three different SMA mouse models, the *Smn*$^{-/-}$*;SMN2* mice (Jackson Labs) that die around postnatal day (P) 6, the *Smn*$^{-/-}$*;SMN2;Δ7* mice (Jackson Labs) that die at P13-P15, and the less severe *Smn*$^{2B/-}$ mice that die around 4 weeks of age (Monani et al. 2000, Le et al. 2005, Bowerman et al. 2012). The *Smn*$^{2B/-}$ mice were established in our laboratory and maintained in our animal facility on a C57BL/6 x CD-1 hybrid background. The *Smn*$^{+/-}$ mice (Jablonka et al. 2000) obtained from Jackson Labs were crossed with *Smn*$^{2B/2B}$ mice to produce *Smn*$^{2B/-}$ affected mice and *Smn*$^{2B/+}$ control littermates (Bowerman et al. 2012). The mice were housed and cared for according to the Canadian Council on Animal Care (CCAC) guidelines and the University of Ottawa Animal Care Committee protocols. Pre-symptomatic tissues were collected at P0 and P2 for severe *Smn*$^{-/-}$*;SMN2* mice, and P2, P6 (early pre-symptomatic) and P9 (late pre-symptomatic) for the *Smn*$^{2B/-}$ mice. Tissues were collected from phenotypic stages at P5 in *Smn*$^{-/-}$*;SMN2* mice, P13 in *Smn*$^{-/-}$*;SMN2;Δ7* mice, and at P15 and P21 in *Smn*$^{2B/-}$ mice. Muscles used for RNA or protein extractions were flash frozen in liquid nitrogen, while muscles used for immunofluorescence and histology were embedded in optimum cutting temperature medium (Fisher) and frozen in cryomolds (Tissue-Tek). All tissues were stored at -80°C.

Primary cell isolation and culture

Smn$^{2B/-}$ primary myoblasts were isolated from hindlimb muscles of 3-week-old mice as originally described (Rando and Blau 1994). Cells were cultured on collagen-coated

plates (Gibco) and maintained under growth conditions using Ham's F10 (Wisent) media supplemented with 20% fetal bovine serum, 2.5 ng/ml human recombinant basic fibroblast factor (Invitrogen), and 2% penicillin/streptomycin (Gibco). Primary myoblasts seeded at equal density were induced to differentiate with Dulbecco's Modified Eagle Medium (Wisent) supplemented with 5% horse serum (Gibco) and 1% penicillin/streptomycin. In all experiments, cells were maintained at 37°C with 5% CO_2 and were provided fresh media every other day.

Hindlimb denervation

Denervation surgeries were performed in accordance with the guidelines set by the CCAC and the Laurentian University Animal Care Committee. Young adult mice were anaesthetized by inhalation of isofluorane. The hindlimb muscles were bilaterally denervated by surgically exposing the sciatic nerve and removing a 2-3 mm segment of the nerve. This ensured that nerve transmission to hindlimb muscles was blocked and nerve regeneration was prevented. A sham procedure was performed as a control and consisted of exposing the mice to the same surgical procedures except for the sciatic nerve sectioning. Gastrocnemius muscles were collected and flash frozen from denervated and sham operated mice one and seven days following surgery.

Evan's blue dye injection

Phenotype stage *Smn*$^{-/-}$*;SMN2* and *Smn*$^{2B/-}$ mice were injected with Evan's blue dye (1%) diluted in phosphate buffered saline. The dye was administered by an intraperitoneal injection and at a concentration of 100 µl per 10 g of body weight for *Smn*$^{2B/-}$ mice, and

50 µl per 10 g of body weight for *Smn*$^{-/-}$;*SMN2* mice. Tissues from *Smn*$^{2B/-}$ mice were harvested 24 hrs post-injection and 6 hrs post-injection for *Smn*$^{-/-}$;*SMN2* mice. Skeletal muscles were sectioned using a cryostat, fixed with ice-cold acetone at -20°C for 10 min, and stained with laminin to visualize the myofibers. Degenerating fibers could be detected by the presence of a red signal using a fluorescence microscope. *mdx* mice, a model of Duchenne muscular dystrophy, were injected at phenotype stage with Evan's blue dye in parallel and served as a positive control for the presence of degenerating myofibers.

Histological analysis of skeletal muscles

Histological analyses were performed on hematoxylin and eosin stained cross-sections (10 µm) from frozen tibialis anterior (TA) muscles of P2 and P5 *Smn*$^{-/-}$;*SMN2*, and P2, P9 and P21 *Smn*$^{2B/-}$ mice. Sections were stained with hematoxylin and eosin using a standard protocol, images taken with a Zeiss Axioplan2 microscope, and the centrally located nuclei were counted using ImageJ software (NIH). The centrally located nuclei data are presented relative to the total number of myofibers present in a given field of view. Images to assess central nucleation were taken at 20x for P5, P9, P21 and at 40x for P2 data. The cross-sectional area of the TA muscle from phenotypic mice was calculated by tracing the contour of myofibers using the tracing tool in ImageJ. A minimum of 200 myofibers was traced. Cross-sections from control and SMA model mice were collected from the same area of the TA muscle.

Immunofluorescence

Cross-sections (10-12 μm) were collected using a cryostat (Leica) and fixed with 4% paraformaldehyde and then stained as previously described (Boyer et al. 2010a). A mouse on mouse kit (Vector Labs), and the primary antibodies targeting Pax7 (Developmental Studies Hybridoma Bank, DSHB) and laminin (Abcam) were used to highlight satellite cells and the basal lamina respectively. Control and $Smn^{2B/-}$ primary myotubes were stained with myosin heavy chain (MHC) antibody (DSHB). All secondary antibodies were purchased from Molecular Probes and nuclei were visualized using 4',6-diamidino-2-phenylindole (DAPI, Sigma). Immunofluorescence images were captured using a Zeiss Axioplan fluorescence microscope or a Zeiss Confocal microscope (LSM 510 Meta DuoScan). Pax7 positive cells were quantified from 2 different fields of view taken at 20x and expressed relative to the total number of myofibers present as assessed by laminin staining. The fusion capacity of primary myoblasts was determined by counting the number of nuclei per myotube using the ImageJ counting tool. For each sample, the data were averaged from 5 different fields of view taken at 10x.

RNA extraction and reverse-transcription

Flash frozen hindlimb muscle samples were homogenized and RNA was isolated using a column-based technique with the RNeasy kit (Qiagen) as per the manufacturer's protocol. RNA concentrations were obtained for each sample using a Nanophotometer spectrophotometer (MBI Lab Equipment). Samples were treated with DNase (gDNA wipeout buffer, Qiagen) to eliminate any potential DNA contamination. RNA was reverse transcribed using the quantitect reverse transcription kit (Qiagen) as per the

manufacturer's protocol. A negative control sample comprised of RNase/DNase free water in lieu of RNA was prepared and processed in parallel.

Polymerase Chain Reaction (PCR) and quantitative polymerase chain reaction (QPCR)

PCR was performed to assess the expression of pre-miR-206 using conditions and primer sequences previously described (Williams et al. 2009). PCR products were electrophoresed on a 2% agarose gel and densitometry was performed using ImageJ. QPCR was performed to assess the mRNA expression of myogenic transcription factors such as paired box protein 7 (Pax7)**,** myoblast determination 1 (MyoD), myogenin and the muscle-specific regulatory factor 4 **(**MRF4; also known as Myf6) in skeletal muscles from control and mutant mice. Each QPCR was performed in triplicate using primers described in Supplemental Table 3.1. Each QPCR reaction contained 50 ng of cDNA, 2x SyBR Green JumpStart Taq ReadyMix for QPCR (Sigma Aldrich), RNase/DNase-free water and appropriate primers (200 nM) in a final volume of 25 µl. Each reaction was heated at 94°C for 3 minutes followed by 40 cycles of denaturing at 94°C for 30 sec, annealing at 60°C for 30 sec and elongation at 72°C for 30 sec. To confirm amplicon specificity and size, a melting curve analysis was performed and the final QPCR products were migrated on a 2% agarose gel for each primer set. Two negative controls were included in every QPCR plate and consisted of water in lieu of cDNA and RNA free cDNA. QPCR results from each plate were generated from a standard curve with known amounts of cDNA. Quantified results were normalized to glyceraldehyde 3-phosphate dehydrogenase (GAPDH) transcript levels to control for loading.

Protein analysis

Protein concentrations were determined using the Bradford method. Immunoblot analysis was performed as previously described (Shafey et al. 2010). Primary antibodies used were: GAPDH (Abcam), MHC (MF20), MRF4 (Santa Cruz), MyoD (BD Transduction Laboratories), myogenin (BD Transduction Laboratories), Pax7, Smn (BD Transduction Laboratories), and tubulin (DSHB). Densitometric analyses were performed using ImageJ software. Immunoblot data are expressed as ratios using GAPDH or tubulin (for the differentiated myotube data) as a loading control for normalization.

Statistical analyses

Data are presented as the mean ± standard error of the mean. A Student's *t* test was performed using Excel to compare the means of all other data. Significance was set at $p < 0.05$.

Results

Decreased levels of myogenic regulatory factors and fusion defects in $Smn^{2B/-}$ primary myoblasts

Previous work from our group demonstrated abnormal myogenesis upon reduction of Smn in C2C12 myoblasts (Shafey et al. 2005). To study myogenesis in a genetically relevant manner and in an intrinsic way by eliminating the negative contribution that motor neuron degeneration might have on muscle cells, we isolated primary myoblasts from $Smn^{2B/-}$ mice. As expected, the protein expression of Smn was dramatically reduced in $Smn^{2B/-}$ myoblasts (Fig. 3.1A). Surprisingly, myoblasts under normal growth conditions displayed a 4-fold decrease in Pax7, and a 28-fold decrease in MyoD (Fig. 3.1A). To assess whether the mis-regulation of Pax7 and MyoD might have an impact on myoblast differentiation, cells were seeded at equal densities, grown to confluence, and induced to differentiate by serum deprivation for 5 days. Cell lysate from control and $Smn^{2B/-}$ differentiated cells were analyzed for myogenic differentiation markers. We observed a significant decrease (2.6-fold) in the level of myogenin, an early marker of myogenic differentiation, and a similar decrease (1.6-fold) in MHC, a late marker of myogenic differentiation (Fig. 3.1B). To assess whether the aberrant expression of the myogenic program had any biological consequences, we examined the fusion potential of $Smn^{2B/-}$ myoblasts. Upon differentiation, we observed a general decrease in fusion in $Smn^{2B/-}$ myotubes as evidenced by an increased number of mononucleated MHC positive cells and a corresponding decrease in myotubes with 8 or more nuclei in $Smn^{2B/-}$ myotubes compared to control myotubes (Fig. 3.1C). These results are reminiscent of those we have previously obtained using the hypomorphic Smn knockdown C2C12 cells

(Shafey et al. 2005). Together, our results suggest that in culture, myoblasts from *Smn*$^{2B/-}$ mice have differentiation and fusion defects.

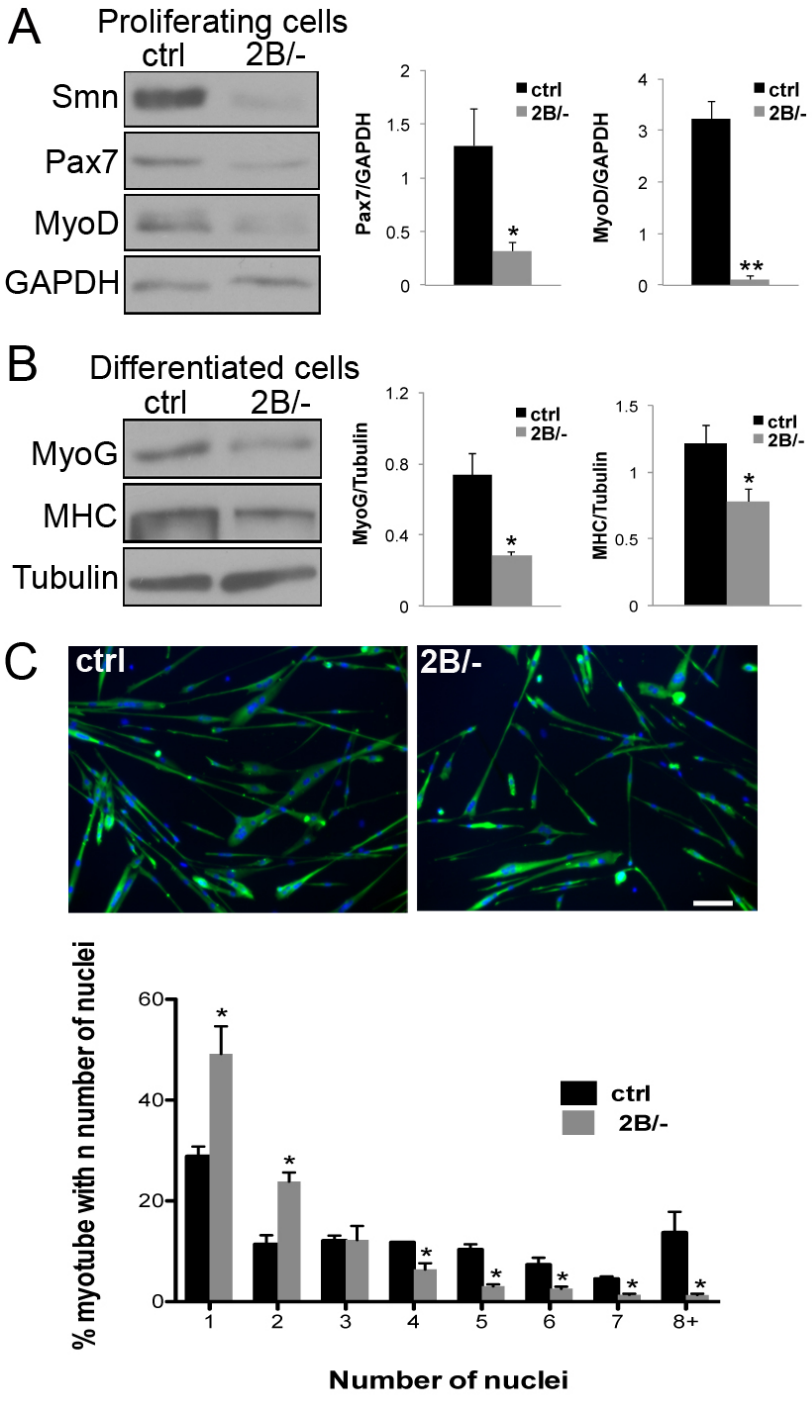
A
Proliferating cells
ctrl
2B/-
Smn
Pax7
MyoD
GAPDH
Pax7/GAPDH
MyoD/GAPDH
ctrl
2B/-
B
Differentiated cells
MyoG
MHC
Tubulin
MyoG/Tubulin
MHC/Tubulin
C
ctrl
2B/-
% myotube with n number of nuclei
Number of nuclei
1
2
3
4
5
6
7
8+

Figure 3.1. Altered myogenic program expression and aberrant myotube formation in primary cells from *Smn*$^{2B/-}$ mice.

(A) Immunoblot analysis reveals decreased Smn, Pax7 and MyoD protein levels in proliferating primary myoblasts established from control and *Smn*$^{2B/-}$ mice. Bar graph showing a significant decrease in Pax7 and MyoD protein levels. (B) Immunoblot analysis and quantification reveals significantly decreased levels of myogenic differentiation markers, namely myogenin (MyoG) and myosin heavy chain (MHC), in cultured primary cells differentiated for 5 days. (C) Representative images of control and *Smn*$^{2B/-}$ myoblasts differentiated into myotubes for 72 hours and stained for MHC. Quantification of the number of nuclei per myotube revealed that there is a decrease in myoblast fusion in *Smn*$^{2B/-}$ cells compared to controls. Scale bar = 50 μm. N = 3 for all experiments, *, $p < 0.05$; **, $p < 0.01$.

Aberrant myogenic program mRNA expression in skeletal muscle from SMA model mice

The decrease in the levels of the myogenic regulatory factors in *Smn*$^{2B/-}$ primary myoblasts led us to investigate myogenic gene expression in mouse models of SMA. We examined the expression of *Pax7*, *MyoD*, *myogenin* and *MRF4* by QPCR. These transcription factors are essential for proper myogenesis and their individual expression pattern marks specific stages of myogenesis (Bentzinger et al. 2012).

In hindlimb muscle samples from phenotype stage P5 *Smn*$^{-/-}$*;SMN2* mice, we observed an 81% decrease in *Pax7* transcript levels in comparison to controls, while *MyoD* and *myogenin* transcript levels were decreased 47% and 36% respectively (Fig. 3.2A). No significant change was detected in *MRF4* mRNA levels between *Smn*$^{-/-}$*;SMN2* and control muscle samples. We also assessed the expression of the myogenic program in skeletal muscle from the less severe *Smn*$^{2B/-}$ model at P21 phenotype stage. Interestingly, *Pax7* mRNA levels were increased 12-fold and those of *MyoD* 31-fold. Transcripts for the markers of myogenic differentiation, *myogenin* and *MRF4*, were increased by 7- and 11-fold respectively (Fig. 3.2B). The difference observed in *Smn*$^{2B/-}$ versus *Smn*$^{-/-}$*;SMN2* mice likely reflects the substantial decrease in expression of the myogenic program by P21 in normal mice, and thus likely reflects a potential delay in the establishment of this program in the *Smn*$^{2B/-}$ mice.

The proper temporal expression of these myogenic transcription factors is essential for the subsequent expression of genes involved in muscle function. We investigated whether the aberrant expression of the myogenic program affected the expression of MHC isoforms in muscle from mouse models of SMA. The expression of the embryonic and neonatal *MHC* transcripts followed the same trend as that of the

myogenic regulatory factors. That is, compared to control counterparts, a decrease in the mRNA expression of embryonic and neonatal *MHC* was detected in phenotype stage *Smn*$^{-/-}$*;SMN2* mice, while these transcripts were increased in *Smn*$^{2B/-}$ samples at P21 (Fig. 3.2C and D). As with the myogenic factors, the mis-regulation of the embryonic and neonatal *MHC* transcripts suggests a delay in skeletal muscle development.

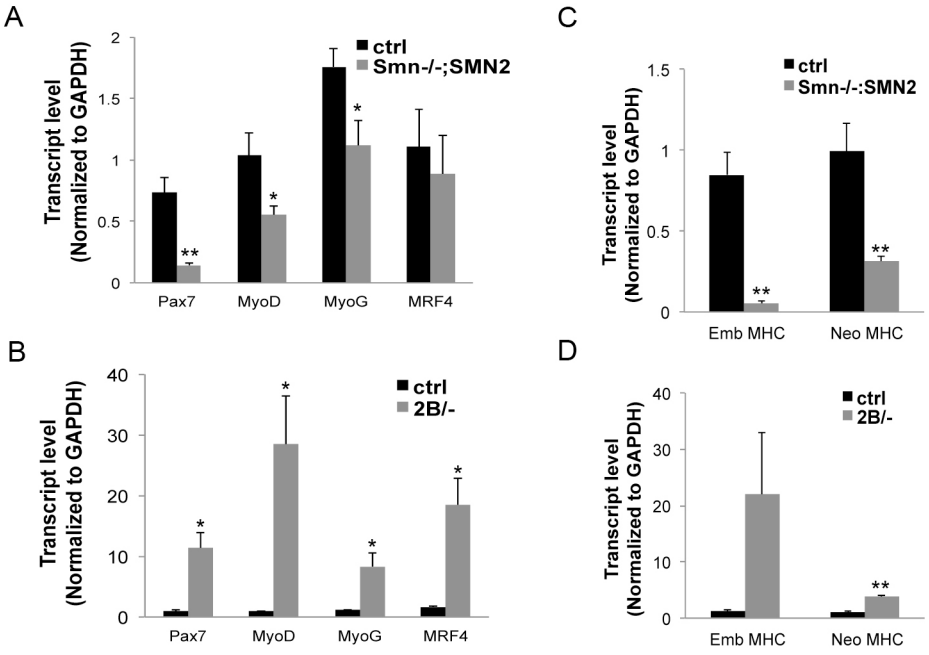

Figure 3.2. Mis-regulated myogenic gene expression in mouse models of SMA.

(A) QPCR was performed with RNA extracted from hindlimb muscle from phenotypic SMA model mice. A decrease in expression of *Pax7*, *MyoD* and *myogenin* transcripts was observed in severe P5 phenotype stage $Smn^{-/-}$;*SMN2* mice. (B) In contrast, transcript levels of *Pax7*, *MyoD* and *myogenin* were increased in P21 phenotype stage $Smn^{2B/-}$ mice compared to controls. (C, D) Changes in the levels of transcripts of the embryonic (Emb MHC) and neonatal (Neo MHC) myosin heavy chain isoforms in $Smn^{-/-}$;*SMN2* (C) and $Smn^{2B/-}$ (D) mice compared to controls. N = 5 for all experiments. *, $p < 0.05$; **, $p < 0.01$. (Myogenin, MyoG).

The myogenic program is delayed in skeletal muscle from mouse models of SMA

To better understand the apparent difference in the expression of the myogenic regulatory factors between the two mouse models of SMA, we performed a time course analysis to assess the protein levels for these factors. The myogenic regulatory factors are normally highly expressed early during postnatal skeletal muscle development and their levels decrease significantly over time. By P21 these factors are difficult to detect relative to P2 (Fig. 3.3A). Interestingly, Smn protein expression from P2 to P21 follows a very similar trend suggesting a need for Smn early in muscle development (Fig. 3.3A).

The expression of myogenic proteins was assessed at P0, P2 and P5 in hindlimb muscle from *Smn$^{-/-}$;SMN2* and control mice (Fig. 3.3B and Supp. Fig. 3.1A). In this model, no differences were observed at P0, however, a significant decrease in Pax7 was observed at P2 compared to controls and, a trend towards decreased levels of MyoD and myogenin was also observed but did not reach significance (Supp. Fig. 3.1A). In P5 phenotypic *Smn$^{-/-}$;SMN2* mice, we observed a significant decrease in the protein levels of Pax7, MyoD and myogenin compared to controls. The level of MRF4 was unchanged at all time points assessed. These changes are in agreement with our mRNA data (Fig. 3.2).

Immunoblot analysis was also performed on hindlimb skeletal muscle from *Smn$^{2B/-}$* mice at early pre-symptomatic (P2 and P6), late pre-symptomatic (P9), and phenotype stage (P15 and P21) time points (Fig. 3.3C and Supp. Fig. 3.1B). Similar to what was observed in *Smn$^{-/-}$;SMN2* mice, Pax7 and MyoD levels were significantly decreased in *Smn$^{2B/-}$* skeletal muscle at P2 compared to controls. In addition, myogenin and MRF4 were also decreased at P2 compared to controls. At P6, Pax7 and MyoD both showed a trend towards decreased expression in *Smn$^{2B/-}$* muscle, however only myogenin

was statistically significantly decreased compared to controls (Supp. Fig. 3.1B). We observed a shift in the expression of myogenic factors at P9 in pre-symptomatic *Smn*$^{2B/-}$ skeletal muscle where Pax7 and MyoD were increased compared to control counterparts (Fig. 3.3C). However, myogenin and MRF4, which are markers of terminal differentiation, remained low in *Smn*$^{2B/-}$ mice compared to controls. At P15, Pax7 and MyoD expression in *Smn*$^{2B/-}$ muscle remained higher than controls while myogenin and MRF4 protein levels were unchanged. Finally at P21, Pax7, MyoD, myogenin and MRF4 were all increased in *Smn*$^{2B/-}$ muscle. The delay in expression of the myogenic regulatory factors becomes even more apparent when control and *Smn*$^{2B/-}$ samples from P2, P9 and P21 are processed together (Fig. 3.3D).

We have also extended our analysis to the commonly used *Smn*$^{-/-}$*;SMN2;Δ7* mouse model. Using skeletal muscle lysate collected from phenotypic P13 *Smn*$^{-/-}$*;SMN2;Δ7* and control mice, we show a decrease in the protein levels of Pax7, MyoD and myogenin, and to a lesser extent MRF4 (Supp. Fig. 3.2). Taken together, the levels of the myogenic factors are low soon after birth in all mouse models of SMA examined, and never have the chance to establish themselves in the severe mice as is the case, albeit much later, in skeletal muscles of the less severe *Smn*$^{2B/-}$ mice. These data suggest that the pathological reduction of Smn leads to muscles having an immature molecular profile in mice.

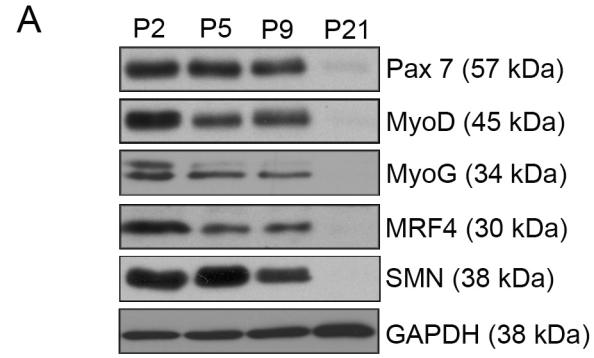
A
P2
P5
P9
P21
Pax 7 (57 kDa)
MyoD (45 kDa)
MyoG (34 kDa)
MRF4 (30 kDa)
SMN (38 kDa)
GAPDH (38 kDa)

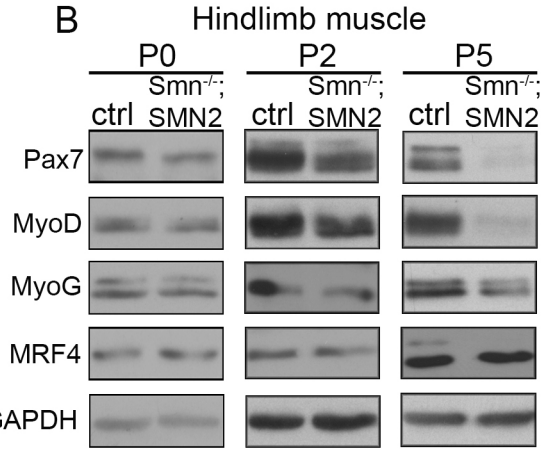
B
Hindlimb muscle
P0
P2
P5
ctrl
Smn-/-; SMN2
Pax7
MyoD
MyoG
MRF4
GAPDH

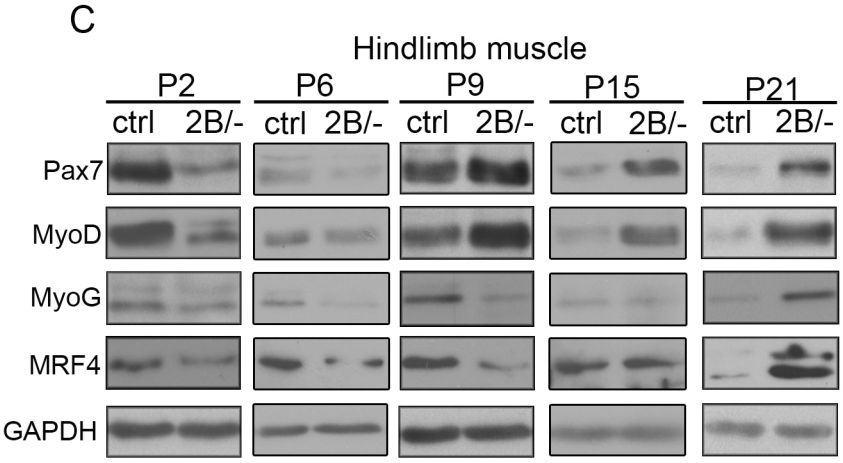
C
Hindlimb muscle
P2
P6
P9
P15
P21
ctrl
2B/-
Pax7
MyoD
MyoG
MRF4
GAPDH

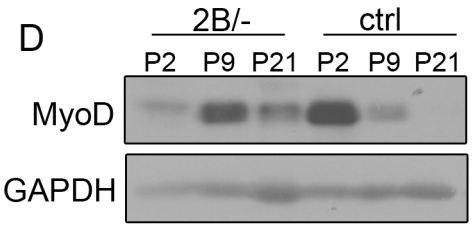
D
2B/-
ctrl
P2
P9
P21
MyoD
GAPDH

Figure 3.3. Delayed expression of myogenic proteins in mouse models of SMA.

(A) Time-course analysis of myogenic program expression in wild type hindlimb protein samples. The protein levels of Pax7, MyoD, myogenin, MRF4 and Smn were assessed at P2, P5, P9 and P21 by immunoblot and show a robust decrease during postnatal muscle development. (B) Representative immunoblots in muscle from P0, P2 and P5 *Smn*$^{-/-}$*;SMN2* mice revealed a robust decrease over time in Pax7, MyoD and myogenin protein levels compared to controls. The expression of MRF4 was unchanged at all time points. (C) Representative immunoblot showing aberrant expression of myogenic proteins at different time points in *Smn*$^{2B/-}$ mice. The levels of myogenic factors are decreased in P2 muscles and increased at P21. At P6, MyoG protein expression was decreased. The expression pattern of Pax7 and MyoD were high at P9 in *Smn*$^{2B/-}$ compared to controls, while those of MyoG were low. Only Pax7 expression was mis-regulated at P15 compared to controls. (D) Time course analysis of MyoD protein expression reveals a delay in the peak expression from P2 in control samples to P9 in *Smn*$^{2B/-}$ muscle. N = 3 for all experiments. (Myogenin, MyoG).

Altered satellite cell number in skeletal muscle of mouse models of SMA

The aberrant Pax7 mRNA and protein expression suggests that the pool of satellite cells may be altered in mouse models of SMA. The importance of satellite cells to postnatal muscle growth has previously been demonstrated in *Pax7*-null mice where small musculature and fewer myofibers were major characteristics of this mouse model (Seale et al. 2000). We therefore investigated whether satellite cell populations were affected in pre-symptomatic and phenotypic stages in SMA model mice. Immunofluorescence studies showed that pre-symptomatic P2 $Smn^{-/-}$;*SMN2* muscle had 47% fewer satellite cells than littermate controls (Fig. 3.4A and B). In P5 phenotypic severe $Smn^{-/-}$;*SMN2* mice, we observed 57% fewer Pax7 positive cells in comparison to controls (Fig. 3.4A and C). By comparison, although there was a trend towards fewer satellite cells, no significant difference was detected in the number of Pax7 positive cells in P2 $Smn^{2B/-}$ muscle (Fig. 3.4A and B). By P21, phenotype stage P21 $Smn^{2B/-}$ muscle had 47% more Pax7 positive cells compared to littermate controls (Fig. 3.4A and C), consistent with the Pax7 protein levels detailed above.

The microRNA-206 directly influences Pax7 expression in muscle (Chen et al. 2010). We therefore assessed whether mis-regulation of miR-206 could explain the abnormal Pax7 expression observed in SMA model mice. For example, in the $Smn^{-/-}$;*SMN2* model, decreased Pax7 expression could be due to increased expression of miR-206 while the opposite situation could apply to the $Smn^{2B/-}$ model. However, we observed significantly less miR-206 precursor in P5 $Smn^{-/-}$;*SMN2* muscle and significantly more miR-206 precursor at P21 in the $Smn^{2B/-}$ model (Fig. 3.4E and F). These data suggest that the altered Pax7 expression in mouse models of SMA is not attributed to the mis-

regulation of miR-206. The aberrant satellite cell number may contribute to decreased muscle size in SMA, especially in *Smn*$^{-/-}$*;SMN2* mice where we observed significantly fewer satellite cells.

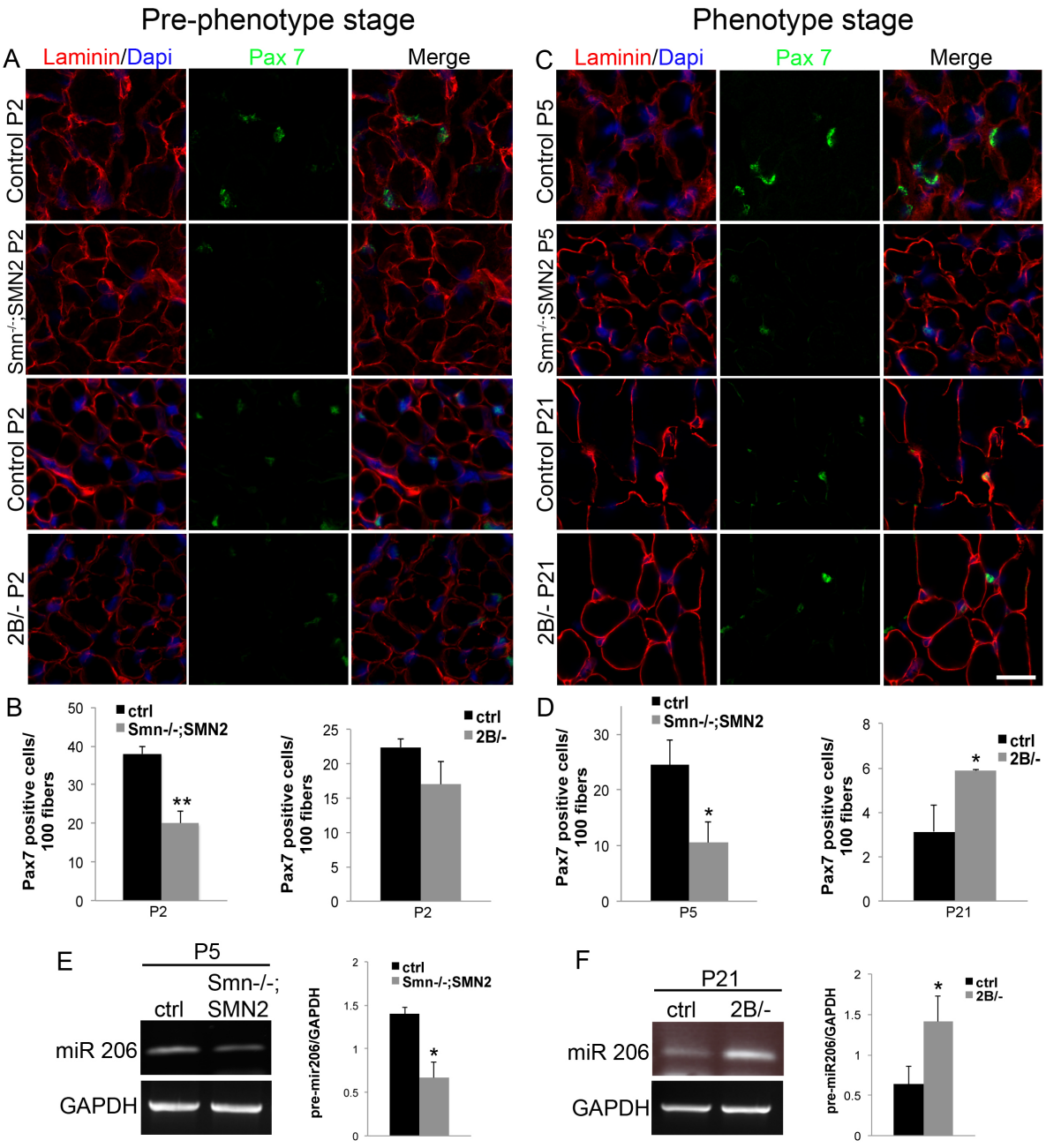
Pre-phenotype stage
Phenotype stage
A
Laminin/Dapi
Pax 7
Merge
Control P2
Smn-/-;SMN2 P2
Control P2
2B/- P2
C
Laminin/Dapi
Pax 7
Merge
Control P5
Smn-/-;SMN2 P5
Control P21
2B/- P21
B
Pax7 positive cells/ 100 fibers
ctrl
Smn-/-;SMN2
**
P2
ctrl
2B/-
P2
D
Pax7 positive cells/ 100 fibers
ctrl
Smn-/-;SMN2
*
P5
ctrl
2B/-
*
P21
E
P5
ctrl
Smn-/-; SMN2
miR 206
GAPDH
pre-mir206/GAPDH
ctrl
Smn-/-;SMN2
*
F
P21
ctrl
2B/-
miR 206
GAPDH
pre-miR206/GAPDH
ctrl
2B/-
*

Figure 3.4. Altered satellite cell number in TA muscles from SMA model mice.

(A) Representative immunofluorescence images of pre-phenotype P2 *Smn*$^{-/-}$*;SMN2*, P2 *Smn*$^{2B/-}$, phenotypic P5 *Smn*$^{-/-}$*;SMN2*, P21 *Smn*$^{2B/-}$ and control TA muscles showing laminin (red), nuclei (DAPI, blue), and Pax7 (green) staining. (B) Bar graph demonstrating a 47% decrease in the number of Pax7 positive cells in severe P2 *Smn*$^{-/-}$*;SMN2* muscle compared to control samples. No statistically significant change was observed between P2 *Smn*$^{2B/-}$ and control samples, although a trend towards a decrease was noted. (C) Bar graph showing 57% fewer Pax7 positive cells in severe P5 *Smn*$^{-/-}$*;SMN2* muscle compared to controls. As well, quantification revealed a 47% increase in Pax7 positive cells in P21 *Smn*$^{2B/-}$ TA muscles compared to control. (D) Representative RT-PCR results and quantification of miR-206 precursor in phenotype stage *Smn*$^{-/-}$*;SMN2* mice showing decreased expression. (F) RT-PCR analysis and quantification demonstrating a significant increase in pre-miR-206 expression in P21 *Smn*$^{2B/-}$ compared to controls. N = 3 for all experiments and scale bar = 10 μm. *, $p < 0.05$; **, $p < 0.01$.

Increased immature myofibers in skeletal muscles of mouse models of SMA

Our time course protein expression analysis of the myogenic program suggested a delay in skeletal muscle development in mouse models of SMA. We therefore performed a histological analysis to assess the consequence of this molecular phenotype. The TA muscle was selected as it is spared from histological denervation in mouse models of SMA and therefore it would likely not be influenced by muscle denervation induced atrophy (Kong et al. 2009, Bowerman et al. 2010). The cross-sectional area of TA myofibers from P5 *Smn*$^{-/-}$*;SMN2* and P21 *Smn*$^{2B/-}$ mice was significantly decreased compared to control muscles (Fig. 3.5A).

During this analysis, we noticed a higher proportion of myofibers with centrally located nuclei. This was observed in both *Smn*$^{-/-}$*;SMN2* and *Smn*$^{2B/-}$ mice at phenotypic (P5 and P21 respectively) stages. Importantly, this was also seen at pre-phenotypic stages, demonstrating that centrally located nuclei are an early feature in disease pathogenesis (Fig. 3.5B and C).

Central nucleation is observed both during muscle development but can also be a histological hallmark of muscle fiber regeneration following a bout of degeneration. In order to investigate whether this central nucleation was due to regeneration following degeneration, we performed the Evan's blue dye assay to assess whether skeletal muscles from mouse models of SMA have degenerating myofibers which would in turn lead to newly formed fibers with centrally located nuclei. We did not observe any degenerating fibers present in phenotype stage *Smn*$^{-/-}$*;SMN2* and *Smn*$^{2B/-}$ TA muscles (Fig. 3.5D). Furthermore, we did not observe any degenerating myofibers in the other more proximal muscles such as the rectus abdominis (RA) and transversus abdominis (TVA) and the

levator auris longus (LAL) (Supp. Fig. 3.3). In contrast, muscle fibers from the *mdx* mouse model of muscular dystrophy display numerous examples of degeneration (Fig. 3.5D). These data suggest that TA muscle fibers from mouse models of SMA are not undergoing degeneration, but rather that the increase in central nucleation observed is indicative of an impairment in muscle development.

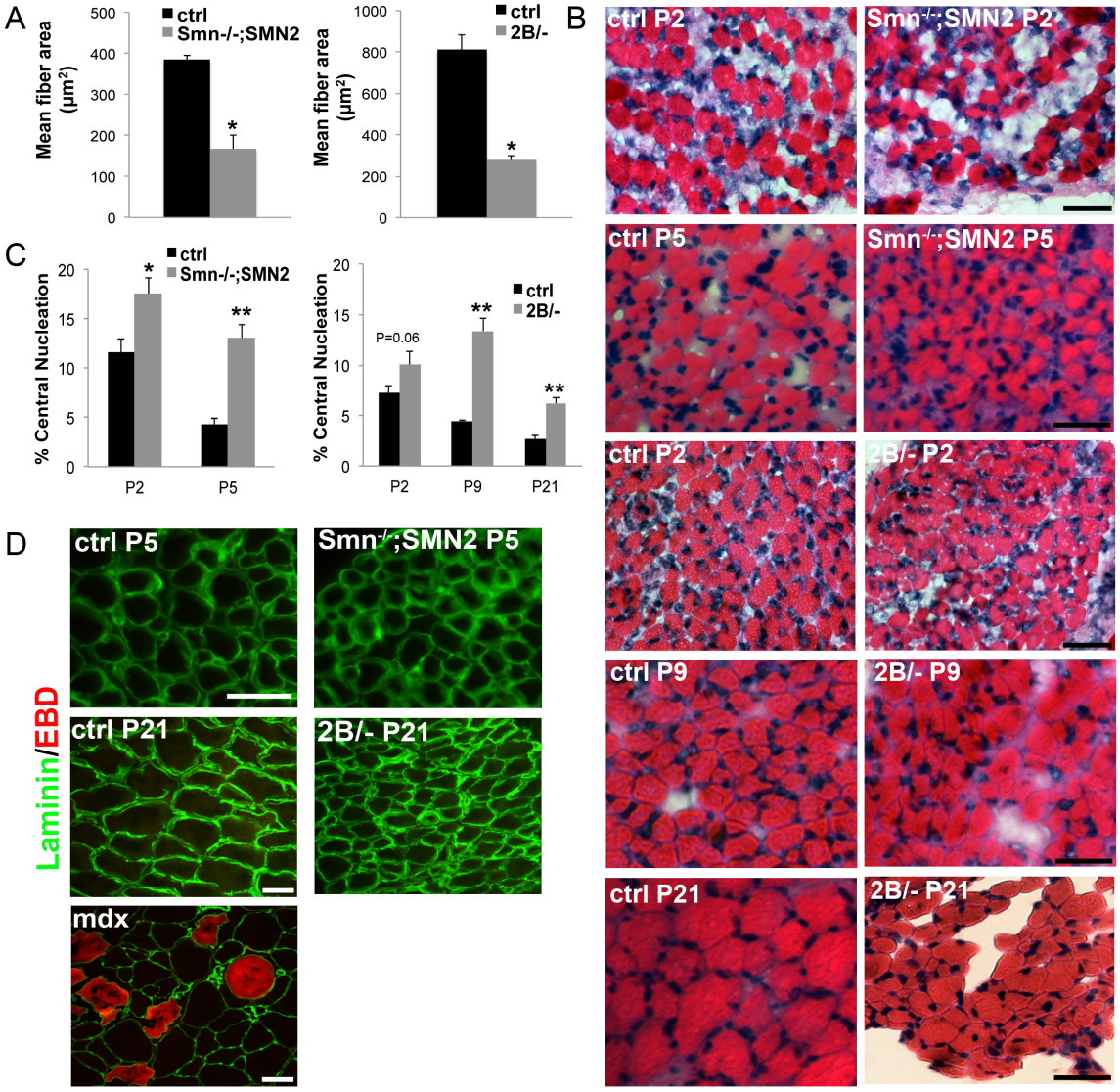
A
Mean fiber area (µm²)
ctrl
Smn-/-;SMN2
2B/-
B
ctrl P2
Smn-/-;SMN2 P2
ctrl P5
Smn-/-;SMN2 P5
2B/- P2
ctrl P9
2B/- P9
ctrl P21
2B/- P21
C
% Central Nucleation
P=0.06
P2
P5
P9
P21
D
Laminin/EBD
ctrl P5
Smn-/-;SMN2 P5
ctrl P21
2B/- P21
mdx

Figure 3.5. Decreased myofiber size and increased number of immature myofibers in mouse models of SMA.

(A) Cross-sectional area measurements revealed smaller fibers in both mouse models at phenotype stage. Cross-sections of TA muscles from *Smn*$^{-/-}$*;SMN2* and *Smn*$^{2B/-}$ mice were taken at P5 and P21 respectively. (B) Representative images of hematoxylin and eosin stained cross-sections from control, pre-phenotype P2 *Smn*$^{-/-}$*;SMN2*, P2 and P9 *Smn*$^{2B/-}$ mice, and phenotype stage P5 *Smn*$^{-/-}$*;SMN2* and P21 *Smn*$^{2B/-}$ TA muscles. Scale bars for P2 samples = 50 μm and scale bars for P5, P9 and P21 samples = 100 μm. (C) Quantification revealed an increased number of centrally located nuclei in both P2 and P5 *Smn*$^{-/-}$*;SMN2* muscles. No change in the proportion of immature myofibers was observed at P2 in *Smn*$^{2B/-}$ mice however, an increase in myofibers with centrally localized nuclei was observed in P9 and P21 samples. (D) Evan's blue dye (EBD) is taken up by degenerating fibers and is detected as a red fluorescence signal. Representative images demonstrating the absence of EBD uptake in control and phenotypic *Smn*$^{-/-}$*;SMN2* and *Smn*$^{2B/-}$ mice. TA muscle sections from the *mdx* muscular dystrophy mouse were used as a positive control for EBD uptake. Scale bar for P5 samples = 100 μm and the scale bar for P21 and *mdx* samples = 50 μm. N = 3 for all experiments. *, $p < 0.05$; **, $p < 0.01$.

Muscle denervation correlates with the degree of change in the protein expression of the myogenic program in mouse models of SMA

We wondered whether the mis-regulation of the myogenic program in SMA model mice was in part, due to the innervation status of the muscle. To address this question, we have taken advantage of our $Smn^{2B/-}$ mouse model in which there is a distinct vulnerability to denervation in various muscles. For instance, the cranial muscles are fully innervated while the RA and the TVA are both muscles with pronounced denervation in $Smn^{2B/-}$ mice (Bowerman et al. 2012). Therefore, we assessed the levels of Pax7, MyoD and myogenin in these muscles at P21 phenotype stage. Pax7 and MyoD levels were significantly increased in all three $Smn^{2B/-}$ muscle types tested compared to controls (Fig. 3.6). However, the degree to which Pax7 and MyoD were altered is much greater in the more vulnerable TVA and RA muscles (Fig. 3.6). Interestingly, the level of myogenin was not statistically different between control and $Smn^{2B/-}$ muscles from the three groups despite muscle denervation being significantly present in the TVA and RA muscles (Fig. 3.6). A clear association between the degree of denervation present and the change in Pax7 and MyoD protein expression can be observed.

To further investigate whether Pax7 and MyoD levels could change following motor neuron denervation, we experimentally denervated wild type mice and performed immunoblots. Denervation did not impact on Pax7 and MyoD expression 1 and 7 days post-denervation but rather, caused a pronounced increase in myogenin levels as early as 1 day post-denervation (Fig. 3.6A). Thus, our results show that although the increase in Pax7 and MyoD correlates with the degree of denervation in $Smn^{2B/-}$ mice, severe

denervation does not influence the levels of Pax7 and MyoD. Therefore, denervation is unlikely to be the cause of the altered myogenic program.

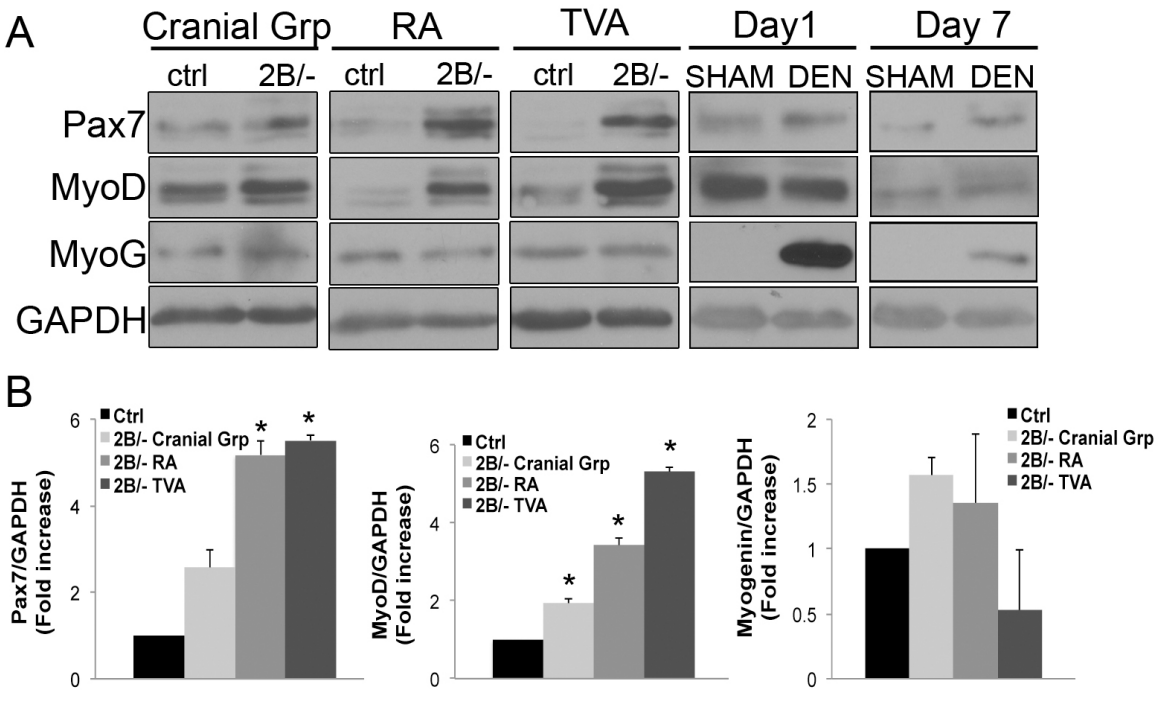

Figure 3.6. Motor neuron denervation is not the cause of the altered myogenic program expression in mouse models of SMA.

(A) Representative immunoblots showing altered protein levels of Pax7 and MyoD in innervated (cranial) and denervated (RA and TVA) muscles of *Smn*$^{2B/-}$ mice. Interestingly, Pax7 and MyoD levels are unaffected in muscles following experimental denervation, at one or seven days post-surgery. By comparison, a robust increase in myogenin expression can be detected as early as one day post-denervation and persists to seven days following denervation. (B) Quantification analyses revealed differences in Pax7 and MyoD protein expression in all three muscle groups. The expression of myogenin however, was similar between control and *Smn*$^{2B/-}$ mice for innervated and denervated muscles. (Myogenin; MyoG, Denervated; DEN).

Discussion

Previous studies have focused on uncovering the reasons for the motor neuron vulnerability in SMA and developing therapeutic approaches aimed at increasing SMN levels in motor neurons. In this study, we demonstrate that Smn deficiency leads to delayed postnatal skeletal muscle development in primary myoblasts from *Smn*$^{2B/-}$ mice and in multiple mouse models of SMA with varying phenotypes.

Delayed expression of the myogenic program in mouse models of SMA

A delay in muscle development had previously been suggested based on morphological studies in mice (Dachs et al. 2011, Lee et al. 2011). As well, delayed myotube growth has been reported in type 1 SMA patient muscles (Martinez-Hernandez et al. 2009). This led us to investigate whether the myogenic program was altered in muscles from mouse models of SMA. We show that the levels of Pax7, MyoD, myogenin and MRF4 were altered in both primary *Smn*$^{2B/-}$ myoblasts and in SMA model mice. Pax7 is essential for the proper maintenance and function of satellite cells (Seale et al. 2000) while myogenic regulatory factors like MyoD (myoblast commitment), myogenin and MRF4 (myoblast differentiation) regulate muscle growth and differentiation (Braun and Gautel 2011). The expression of these myogenic genes decreases over time during postnatal development as the myofibers mature. Interestingly, the expression of Smn follows a similar profile, as levels drop dramatically in muscles of P21 mice. This observation suggests that Smn is likely to play an important role in muscle development rather than in muscle structure maintenance.

In hindlimb muscles of *Smn*$^{-/-}$;*SMN2* mice, we demonstrate a decrease in Pax7, MyoD and myogenin. These changes are likely to be independent of denervation since the change in expression of myogenin was opposite to what has been described in denervated muscle. In addition to decreased Pax7 protein levels in *Smn*$^{-/-}$;*SMN2* mice, we also show fewer satellite cells in P5 TA muscle. Satellite cells contribute to early postnatal muscle growth and the decrease in their numbers could account, in part, to the smaller myofiber size observed. We have ruled out the possibility that the difference in the number of Pax7 positive cells is attributed to changes in miR-206 expression. This microRNA has previously been shown to inhibit Pax7 expression by binding to its three prime untranslated region (Chen et al. 2010). Interestingly, the expression levels of miR-206 were reminiscent of those we observed for the myogenic regulatory factors, that is miR-206 was decreased in P5 *Smn*$^{-/-}$;*SMN2* mice and increased in P21 *Smn*$^{2B/-}$ mice. Regulation of Pax7 expression by miR-206 in *Smn*$^{-/-}$;*SMN2* could only be explained by an up-regulation while the opposite applies to the *Smn*$^{2B/-}$ model. Therefore, it is unlikely that the altered Pax7 levels are the result of abnormal miR-206 expression in SMA model mice.

In *Smn*$^{2B/-}$ hindlimb muscles, levels of all myogenic proteins assessed were low at early pre-symptomatic (P2) stage and appeared to increase at the phenotype stage (P21), which is much later than in normal mice. Immunoblot analyses performed on late pre-symptomatic muscle revealed a shift in levels of Pax7 and MyoD, as they were increased in P9 *Smn*$^{2B/-}$ mice while myogenin and MRF4, which are markers of differentiation, remained low. In our study, Pax7 and MyoD appear to be most affected and their mis-regulation is likely the reason for the aberrant expression of myogenin and MRF4. Our

time course analysis reveals that indeed the protein expression of MyoD peaks at P9 and that the impaired muscle maturation is likely the result of this delay in expression. Whether Smn regulates one or more genes involved in the myogenic program is unknown and warrants future research.

In both mouse models studied, we show that the expression of the developmentally regulated MHC isoforms is altered in a pattern that matches the molecular profile of the myogenic program for each mouse model. A decrease in the expression of the myogenic program in phenotypic *Smn*$^{-/-}$*;SMN2* mice resulted in decreased expression of the MHC isoforms. By comparison, the delayed up-regulation of the myogenic program in phenotype stage *Smn*$^{2B/-}$ mice correlated with the delay in increased expression of the early MHC isoforms. This result suggests a profound delay in muscle development in mouse models of SMA. Given the aberrant expression of the embryonic and neonatal MHC isoforms in SMA model mice, it is plausible that other neonatal rather than adult isoforms of proteins important for muscle contractions are expressed in muscles of SMA model mice. This would in turn have a profound impact on proper muscle force production. Impaired myofiber development would lead to defects in the maturation of the neuromuscular junction endplate, which in turn would hinder its function. Indeed, several studies have highlighted defects at the postsynaptic endplate that support a delay in development, namely increased expression of the fetal acetylcholine receptor isoform and immature acetylcholine receptor morphology (Kong et al. 2009, Dachs et al. 2011, Lee et al. 2011, Bowerman et al. 2012).

Does the mis-regulation of the myogenic program lead to differential vulnerability in

mouse models of SMA?

We have taken advantage of the fact that the cranial muscles, the RA and the TVA show differences in their innervation status. We demonstrate subtle molecular changes in the innervated cranial muscle, while the differential expression of the myogenic program was apparent in the RA and TVA muscles and correlated with the degree of denervation. We had hypothesized that muscle denervation was influencing the expression of the myogenic program, however given our results, we suggest that the disruption in the myogenic program could be responsible for the differential muscle vulnerability observed. Although, we show that experimental denervation does not affect the levels of Pax7 and MyoD, we cannot rule out the possible contributions that pre-degenerative changes in motor neurons or at the NMJ in SMA model mice might lead to the changes observed in the muscle. Regardless of whether the mis-regulation of the myogenic program is intrinsic or not, muscle defects are present in mouse models of SMA and can be targeted therapeutically to increase muscle function.

A Smn threshold is required for skeletal muscle development

In *Smn*$^{-/-}$*;SMN2* skeletal muscle, it would appear that the level of Smn is too low at the required time point to fulfill its function(s) in muscle, and that this in turn leads to a robust decrease in the myogenic program and to immature myofibers. In *Smn*$^{2B/-}$ muscle however, our time-course analysis suggests that the myogenic program peaks at P9 instead of P0-P2 like in control mice. This delay ultimately has a profound impact on muscle morphology of *Smn*$^{2B/-}$ mice as we observed decreased cross-sectional myofiber area and increased immature myofibers from P9-P21. Therefore in *Smn*$^{2B/-}$ mice, the level

of full-length Smn protein appears to be sufficient to allow the progression of skeletal development albeit in a delayed manner.

In summary, the present study demonstrates early and persistent delayed muscle development in mouse models of SMA. The depletion of Smn hinders the normal maturation of skeletal muscle at the molecular and morphological level, and likely contributes to the SMA phenotype. Future studies should focus on elucidating the functions of Smn during perinatal and early postnatal life, in particular addressing how Smn depletion leads to the mis-regulation of the myogenic program. The study of muscle in SMA research allows for a better understanding of the contributions of this tissue in the pathophysiology of the disease and highlights the importance of including muscle as a target tissue in therapeutic development.

Acknowledgments

We are exceptionally grateful for the critical feedback of Dr. Lyndsay Murray. We thank Dr. Michael Rudnicki for the *mdx* mice used as a positive control in the EBD assay. This project was funded by grants from the Canadian Institutes of Health Research (CIHR) and The Muscular Dystrophy Association (USA) to R.K. J.G.B. is a recipient of a Frederick Banting and Charles Best CIHR Doctoral Research Award and R.K. is a recipient of a University Health Research Chair from the University of Ottawa.

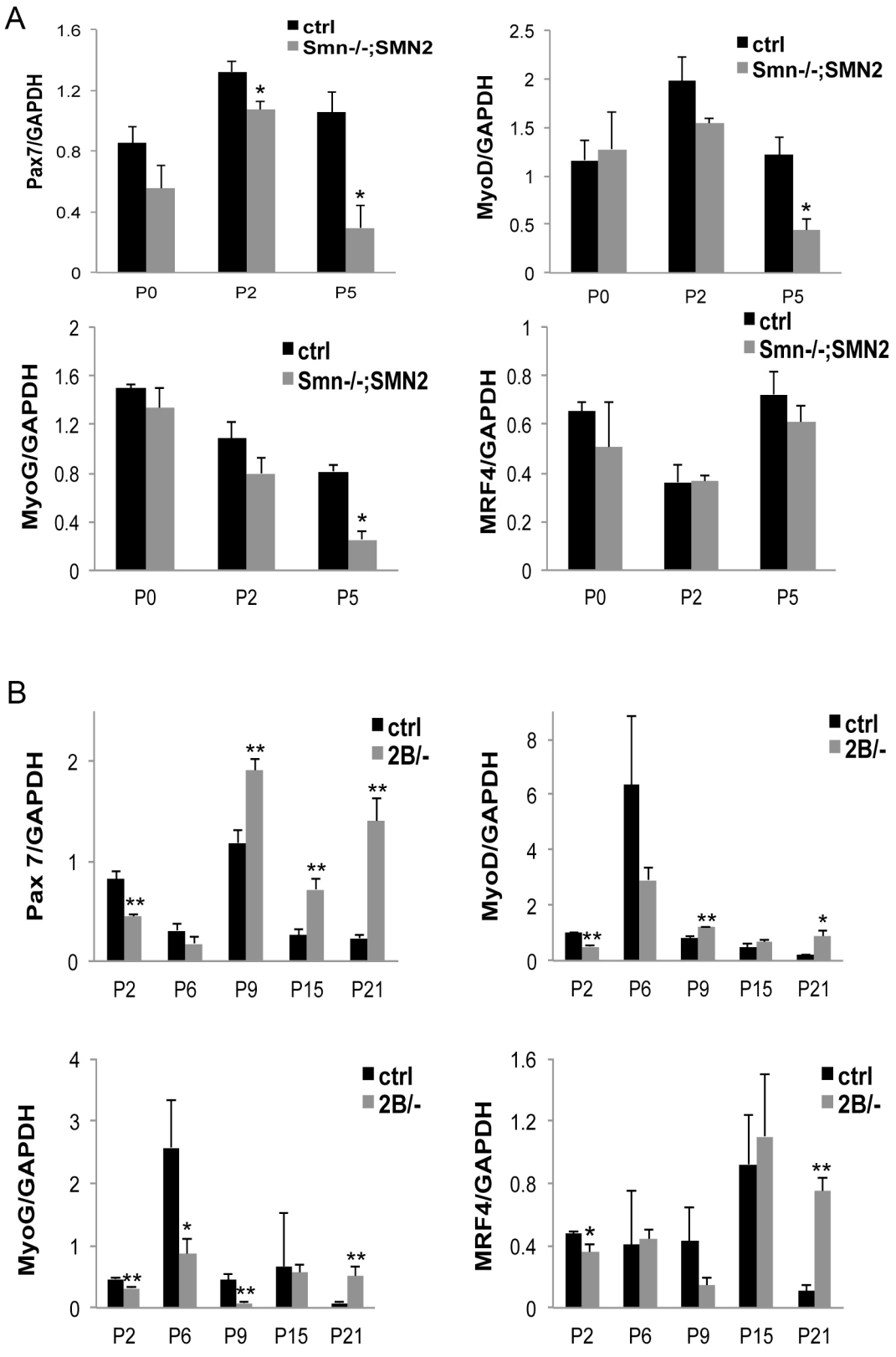
A
Pax7/GAPDH
ctrl
Smn-/-;SMN2
P0
P2
P5
MyoD/GAPDH
MyoG/GAPDH
MRF4/GAPDH
B
Pax 7/GAPDH
2B/-
P2
P6
P9
P15
P21
MyoD/GAPDH
MyoG/GAPDH
MRF4/GAPDH

Supplemental Figure 3.1. Altered expression of the myogenic program in mouse models of SMA.

(A) Quantification of immunoblot analyses for the *Smn*$^{-/-}$*;SMN2* mouse model. We observed a 19% decrease in Pax7 levels at P2 and a 72% decrease in Pax7 levels at P5 in *Smn*$^{-/-}$*;SMN2* model mice. In *Smn*$^{-/-}$*;SMN2* skeletal muscle, MyoD protein levels were decreased by 64% and those of myogenin were down by 69%. (B) Graphs showing the quantification results of immunoblots assessing the expression of the myogenic program in *Smn*$^{2B/-}$ mice. In *Smn*$^{2B/-}$ mice, Pax7 protein levels were down 47% at P2, however we observed a 1.6-fold increase in Pax7 levels at P9, a 2.8-fold increase at P15 and a 6.1-fold increase at P21. We demonstrate a 49% decrease in MyoD expression in P2 *Smn*$^{2B/-}$ mice. We observed a 1.5-fold and a 4.5-fold increase in MyoD protein levels in P9 and P21 *Smn*$^{2B/-}$ mice respectively. In *Smn*$^{2B/-}$ mice, myogenin protein levels were decrease by 30% at P2, 67% at P6 and 82% at P9. At P21 in *Smn*$^{2B/-}$ mice, myogenin protein levels were 6.3-fold higher than controls. MRF4 protein expression was 25% lower at P2 and 6.7-fold higher at P21 in *Smn*$^{2B/-}$ mice compared to controls. *, $p < 0.05$; **, $p < 0.01$. (Myogenin, MyoG).

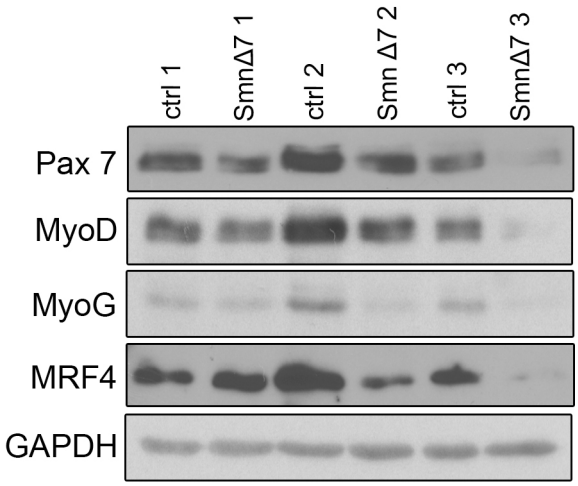

Supplemental Figure 3.2. Altered expression of the myogenic program in *Smn*$^{-/-}$*;SMN2;Δ7* mice.

Immunoblot analysis revealed a decrease in the protein levels of Pax7, MyoD, myogenin and to a lesser extent MRF4. Analysis was performed using hindlimb skeletal muscle from three independent phenotype stage P13 *Smn*$^{-/-}$*;SMN2;Δ7* mice. (Myogenin, MyoG).

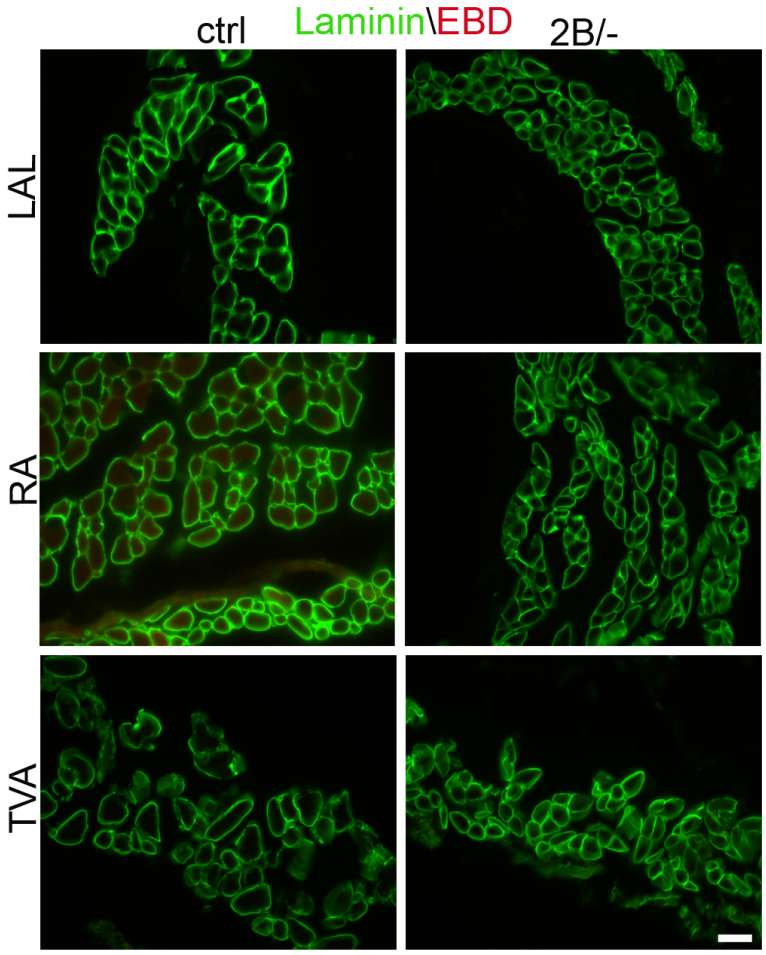

Supplemental Figure 3.3. Absence of degenerating myofibers in skeletal muscles from *Smn*$^{2B/-}$ mice.

Phenotypic P21 *Smn*$^{2B/-}$ mice were injected with Evan's blue dye to investigate whether any degenerating myofibers were present in the cranial levator auris longus (LAL), rectus abdominis (RA), and transversus abdominis (TVA) muscles. No degenerating myofibers were detected in control and *Smn*$^{2B/-}$ muscle. Scale bar = 20 μm.

Supplemental Table 3.1. Primers used for Quantitative Real-Time Polymerase Chain Reaction

Targets	**Sense (Forward) primer 5'-3'**	**Antisense (Reverse) primer 5'-3'**	**T_a**
Gapdh	TGAAGGGGTCGTTGATGG	AAAATGGTGAAGGTCGGTGT	62
Pax7	GACGACGAGGAAGGAGACAA	CGGGTTCTGATTCCACATCT	62
MyoD	TGGCATGATGGATTACAGCG	CCACTATGCTGGACAGGCAGT	62
MyoG	CATCCAGTACATTGAGCGCCTACA	AGCAAATGATCTCCTGGGTTGGGA	59
MRF4	CAAGCAAGAAATTCTTGAGGG	CGTTCCTCTGAAGAAATACTGTC	63
Neonatal MHC	TCGCTGGCTTTGAGATCTTT	ACGAACATGTGGTGGTTGAA	62
Embryonic MHC	GCAGATTCAGAAACTGGAGAC	CCTTAACACGCCGCTCATAC	62

T_a: annealing temperature

Chapter 4

Muscle weakness occurs prior to motor neuron loss and denervation in mouse models of spinal muscular atrophy

Author Contributions

JGB and RK conceived of and designed the project. JGB performed and analyzed most of the experiments and was assisted by KS for figure 4.1 and 4.3, and by YDR for panels A-C of figure 4.2. LMM performed experiments and analyzed the data in panels E-G of figure 4.2. JMR supervised KS and helped analyzed the data in figure 4.1. JGB wrote the paper and RK revised and edited the manuscript.

Muscle weakness occurs prior to motor neuron loss and denervation in mouse models of spinal muscular atrophy

Justin G. Boyer[1, 2], Lyndsay M. Murray[1], Kyle Scott[2], Yves De Repentigny[1], Jean-Marc Renaud[2], and Rashmi Kothary[1, 2, 3#]

[1]Ottawa Hospital Research Institute, Regenerative Medicine Program, Ottawa, ON, Canada K1H 8L6
[2]Department of Cellular and Molecular Medicine, University of Ottawa, Ottawa, ON, Canada K1H 8M5
[3]Department of Medicine, University of Ottawa, Ottawa, ON, Canada K1H 8M5

[#]To whom correspondence should be addressed

Abstract

The childhood neuromuscular disease spinal muscular atrophy (SMA) is caused by mutations or deletions of the survival motor neuron (*SMN1*) gene. Although SMA has traditionally been considered a motor neuron disease, the muscle-specific requirement for SMN has never been fully defined. The purpose of this study was to investigate intrinsic muscle defects in two different models of SMA, the severe *Smn*$^{-/-}$*;SMN2* mice and the less severe *Smn*$^{2B/-}$ mice. We report that tibialis anterior (TA) muscles of phenotype stage *Smn*$^{-/-}$*;SMN2* mice generate 39% less maximal force than control muscles independent of aberrant motor neuron signal transmission. In addition, during muscle fatigue, the *Smn*$^{-/-}$*;SMN2* muscle shows early onset and increased unstimulated force compared to controls. Muscle weakness in mouse models of SMA was associated with a delay in the transition of neonatal to adult isoforms of proteins important for proper muscle contractions such as ryanodine receptors and sodium channels. Immunoblot analyses of extracts from hindlimb skeletal muscle revealed aberrant levels of the sarcoplasmic reticulum Ca^{2+} ATPase. Moreover, we demonstrate a significant decrease in force production in muscles from pre-symptomatic *Smn*$^{-/-}$*;SMN2* and *Smn*$^{2B/-}$ mice, indicating that muscle weakness is an early event occurring prior to any motor neuron loss and motor neuron denervation. The findings from this study reveal a delay in the appearance of mature isoforms of proteins important for muscle contractions which leads to muscle weakness independent of aberrant motor neuron signal in mouse models of SMA, thus highlighting the contributions of skeletal muscle defects to the SMA phenotype.

Key words: spinal muscular atrophy, SMA, SMN, motor neuron disease, skeletal muscle

Introduction

With an overall carrier frequency of 1:40, spinal muscular atrophy (SMA) is a major leading genetic cause of infant deaths affecting 1 in 6,000-10,000 births (Pearn 1978, Ogino et al. 2002, Prior et al. 2010). SMA is an autosomal recessive disorder traditionally classified into different types based on the clinical severity of the symptoms (Boyer et al. 2010). In 1995, the SMA-determining gene was identified and named the survival motor neuron (*SMN*) gene (Lefebvre et al. 1995). This gene is located on chromosome 5q13 in humans. This region contains an inverted duplication of 500 kilobase pairs resulting in two virtually identical copies of the *SMN* gene. A telomeric copy, *SMN1*, and a centromeric copy, *SMN2*, which is unique to humans (Melki et al. 1990, Brzustowicz et al. 1993, Lefebvre et al. 1995, Rochette et al. 2001).

In the mouse, the *Smn* gene is present as a single copy, and homozygous loss of function leads to a pre-implantation lethality (Schrank et al. 1997). However, when this is coupled with low levels of human SMN expressed from a *SMN2* transgene, a severe phenotype approximating type I SMA is observed (Monani et al. 2000). We have previously generated a milder mouse model of SMA termed $Smn^{2B/-}$. These mice do not harbor the *SMN2* transgene but rather harbor one null allele and a second allele with a 3-nucleotide substitution in the of exon 7 of the mouse *Smn* gene (*2B* mutation) (Hammond et al. 2010). $Smn^{2B/-}$ model mice display a milder SMA phenotype due to slightly higher Smn protein levels than the severe model (Bowerman et al. 2012).

Motor neuron cell loss and muscle denervation are considered two pathological hallmarks of SMA. How SMN depletion leads to motor neuron degeneration is unclear and remains the focus of intense research. However, recent advances in the field have

highlighted the involvement of other tissues in the pathophysiology of SMA of which skeletal muscle appears to be a main contributor (Boyer et al. 2010, Hamilton and Gillingwater 2013).

In a Drosophila model of SMA, Smn was discovered to be a sarcomeric protein interacting with α-actinin, a cross-linking protein that stabilizes actin microfilaments (Rajendra et al. 2007). Walker and colleagues (2008) later confirmed these findings and specifically identified Smn as a Z-disc component in skeletal and cardiac muscle of mice. In fact, the authors suggest that a large proportion of the Smn complex is distributed to Z-discs and that the calpain protease is responsible for the removal of Smn from the Z-discs. At present, the function of Smn at this adhesion site is unknown but Smn is likely to have a specific function other than snRNP biogenesis in muscle (Walker et al. 2008). A Smn interacting protein screen in C2C12 myoblasts suggests that the function of Smn in muscle is dynamic and likely differs during varying stages of myogenesis based on its protein interactome (Shafey et al. 2010). A proteomic screen performed by Mutsaers et al. (2011) identified an increase in proteins involved in programmed cell death in pre-symptomatic *Smn*$^{-/-}$*;SMN2* mice. Several reports have highlighted the possibility of delayed myogenesis in mouse models of SMA. The basis of this notion comes from muscle morphological studies demonstrating a lack of increase in myofiber size and the increased expression levels of embryonic and neonatal myosin heavy chain (MHC) isoforms (Kong et al. 2009, Dachs et al. 2011, Lee et al. 2011). However, if and how impaired muscle growth contributes to muscle weakness in SMA is not known, since at present no comprehensive analysis has been performed relating to muscle force production in mouse models of SMA.

Here, we show previously unreported pathophysiological muscle defects in severe (*Smn*$^{-/-}$;*SMN2*) and less severe (*Smn*$^{2B/-}$) mouse models of SMA. We report pronounced intrinsic muscle weakness in these mice. These observations were associated with altered expression of proteins that are developmentally regulated and impact proper physiological muscle function. Furthermore, we show that muscle weakness is an early feature, observed prior to motor neuron loss and muscle denervation in mouse models of SMA. Thus, we conclude that intrinsic muscle defects contribute to the phenotype in SMA mouse models. Uncovering skeletal muscle defects in the context of SMA is of the utmost importance to better understand the SMA phenotype and for the development of targeted therapeutics.

Materials and Methods

Mouse models

The *Smn*$^{-/-}$*;SMN2* (Jackson Labs) and *Smn*$^{2B/-}$ (Bowerman et al. 2012) mice were housed and cared for according to the Canadian Council on Animal Care (CCAC) guidelines and the University of Ottawa Animal Care Committee protocols. Tissues from pre-symptomatic mice were collected at postnatal day (P) 2 for severe *Smn*$^{-/-}$*;SMN2* mice, and P9 for the *Smn*$^{2B/-}$ mice. Tissues were collected for phenotype analyses of *Smn*$^{-/-}$*;SMN2* and *Smn*$^{2B/-}$ mice at P5 and P21, respectively. Muscles used for RNA and protein analysis were flash frozen in liquid nitrogen and stored at -80°C.

Hindlimb denervation

Denervation surgeries were performed in accordance with the guidelines set by the CCAC. Young adult mice were anaesthetized by inhalation of isofluorane. Experimental denervation was achieved by revealing the sciatic nerve and removing of 2-3 mm of the nerve in the thigh section to cease neural input and prevent nerve regrowth. A sham procedure was performed in parallel to serve as control and consisted of exposing the mice to identical experimental conditions except for cutting the nerve. Hind leg muscles were collected and flash frozen from denervated and sham operated mice seven days following surgery.

Immunoblotting

Total tissue lysate extract was obtained by grinding flash frozen tissues in a liquid nitrogen pre-cooled mortar and pestle. The concentration of each sample was determined

by Bradford assay. Samples were subjected to sodium dodecyl sulfate polyacrylamide gel electrophoresis and examined by immunoblot as previously described (Shafey et al. 2010). Primary antibodies used were: calsequestrin (Abcam), glyceraldehyde-3-phosphate dehydrogenase (GAPDH, Abcam), $Na_v1.4$ (Alomone), $Na_v1.5$ (Alomone), nuclear factor 1 (Abcam), sarcoplasmic reticulum Ca^{2+} ATPase (SERCA1a, Cell Signaling), and zinc-finger E box-binding protein (ZEB) (Novus Biologicals). The protein expression signal was detected using enhanced chemiluminescence (Thermo). Densitometric analyses were performed using ImageJ software. Immunoblot data were normalized to GAPDH to control for possible loading differences.

Force measurements and fatigue protocol

TA muscles were dissected from P2 and P5 control and severe *Smn*$^{-/-}$*;SMN2* mice, and from P9 control and *Smn*$^{2B/-}$ mice. Muscles were constantly immersed in physiological saline solution containing 118.5 mM NaCl, 4.7 mM KCl, 2.4 mM $CaCl_2$, 3.1 mM $MgCl_2$, 25 mM $NaHCO_3$, 2 mM NaH_2PO_4, and 5.5 mM D-glucose. Solutions were continuously bubbled with 95% O_2, 5% CO_2 for a pH of 7.4. Solutions containing 30 μM of tubocurarine hydrochloride pentahydrate (Sigma) were prepared by adding the appropriate amount directly to the physiological solution. The flow of physiological solution below and above muscles was maintained at a total of 15 mL/min and a temperature of 37°C. Tetanic contractions were elicited with electrical stimulations applied across two platinum wires (4 mm apart) located on opposite sides of the muscle. Electrodes were connected to a Grass S88 stimulator and a Grass SIU5 isolation unit (Grass Technologies/Astro-Med Inc.). Tetanic contractions were elicited with 200 ms

trains of 0.3 ms, 12 V (supramaximal voltage) pulses at a frequency of 200 Hz. For all experiments, muscle length was adjusted to achieve maximal force production and muscles were allowed a 30 min equilibration period during which a tetanic contraction was elicited every second. Maximal force production was determined by increasing frequencies from 1 to 200 Hz. Muscles were then fatigued by increasing the contraction rate to 1 per sec for 180 sec. Twitch (obtained when stimulated with one square pulse) or tetanic force was defined as the force that developed during stimulation and was calculated as the difference between the maximum force during contraction and the force measured 5 ms before the contraction. Unstimulated force was defined as the force being generated by muscles in the absence of electrical stimulation and was observed during fatigue when muscles failed to relax between contractions; it was calculated as the difference in the baseline 5 ms before a contraction and the baseline 5 ms before fatigue was elicited. Muscle weight and length were used to calculate the cross-sectional area of the muscle that was used to normalize force measurements in each experiment.

RNA isolation

Total RNA was isolated from skeletal muscle tissue using a homogenizer and the RNeasy kit (Qiagen) according to the manufacturer's instructions. RNA samples were treated with DNase (gDNA wipeout buffer, Qiagen) to eliminate DNA contamination and concentrations were determined using a Nanophotometer spectrophotometer (MBI Lab Equipment).

Reverse-transcription polymerase chain reaction (PCR)

RNA was reverse-transcribed using the quantitect reverse transcription kit (Qiagen). Primer sequences and PCR conditions used to detect the spliced variants of the RyR1 gene were identical to those previously described (Kimura et al. 2005). A negative control in which water was added instead of cDNA was prepared in parallel for every PCR.

Immunofluorescence

Neuromuscular junction (NMJ) immunofluorescence and quantification was performed as described previously (Murray et al. 2008). Post-synaptic acetylcholine receptors were labeled with alpha-bungarotoxin (Molecular Probes) while the pre-synaptic terminal was labeled with anti-neurofilament and anti-synaptic vesicle protein 2 (both from Developmental Studies Hybridoma Bank). All secondary antibodies were purchased from Jackson Labs. Immunofluorescence images were captured using a Zeiss Confocal microscope (LSM 510 Meta DuoScan).

Histological analysis

The lumbar (L1-L2) region of the spinal cord was collected from control, pre-symptomatic *Smn*$^{-/-}$*;SMN2* and *Smn*$^{2B/-}$ mice. Tissues were fixed in 4% paraformaldehyde for 24 hrs, embedded in paraffin, cut in sections (10 μm) and stained with hematoxylin and eosin. Motor neurons were identified by their shape and size within the ventral horn region of the spinal cord. Motor neuron quantification was performed on every 5th section within the L1-L2 region on 3 mice from each genotype.

Statistical analyses

Data are presented as the mean ± standard error of the mean. Analysis of variance (ANOVA) was used to determine significant differences in the fatigue data. ANOVA calculations were made using the version 9.0 GLM (General Linear Model) procedures of the Statistical Analysis Software (SAS Institute Inc). A student's t-test was performed using Excel to compare the means of all other data. Significance was set at $p < 0.05$.

Results

Intrinsic skeletal muscle weakness in Smn$^{-/-}$;SMN2 mice

To date, no physiological studies have been performed on muscles from a severe SMA model mice. To this end, we have analyzed the twitch and peak tetanic force produced by direct stimulation of TA muscles of *Smn$^{-/-}$;SMN2* mice and control littermates at P5. In order to account for variations in muscle size, all force values were normalized to muscle cross sectional area. Compared to control muscles, *Smn$^{-/-}$;SMN2* mice produced 47% less twitch force measured after one stimulation and 39% less maximum peak tetanic force measured at 200 Hz (Fig. 4.1A, B).

Aberrant NMJ morphology and function have previously been highlighted in several mouse models of SMA (Kariya et al. 2008, Murray et al. 2008, Kong et al. 2009, Murray et al. 2012). In isolated muscle preparations, many fibers receive an indirect stimulation via the remaining nerve stump. Although it has previously been demonstrated that the TA muscle is fully innervated in SMA model mice (Kong et al. 2009, Bowerman et al. 2010), one possible explanation for the observed decrease in force is that the applied stimulus enters the residual nerve before reaching the myofibers. Thus, if poorly functioning NMJs were present in the preparation, it would negatively impact the force because fewer fibers would be stimulated. To address this possibility, we measured the maximal force production in muscles from control and mutant mice in the presence or absence of tubocurarine, which blocks acetylcholine receptors. Should aberrant NMJs negatively affect TA muscle force production, it would be expected that the relative force produced by muscles from *Smn$^{-/-}$;SMN2* mice would be equal to the control values in the presence of tubocurarine. The force production of control muscles was not affected by the

presence of tubocurarine nor did we observe an increase in force production in *Smn*$^{-/-}$*;SMN2* muscles after the addition of tubocurarine to the preparation compared to non-treated muscles (data not shown). Furthermore, in 5 independent experiments, the force production from *Smn*$^{-/-}$*;SMN2* muscle was lower than that of controls (Fig. 4.1C). These data show that aberrant NMJs did not impact *Smn*$^{-/-}$*;SMN2* TA muscle force production and that mechanisms of stimulus propagation may be compromised in muscles from *Smn*$^{-/-}$*;SMN2* mice.

Smn$^{-/-}$*;SMN2 muscles respond abnormally to induced muscle fatigue*

To determine whether *Smn*$^{-/-}$*;SMN2* muscles respond differently to muscle fatigue, we measured the decline in force with repeated tetanic stimulation for 180 seconds. The decrease in peak tetanic force recorded in *Smn*$^{-/-}$*;SMN2* muscles was similar to control littermates (Fig. 4.1D). During the fatigue protocol we also measured the unstimulated force, which is defined as the force being measured 100 ms before a contraction is elicited. The TA muscles of both control and *Smn*$^{-/-}$*;SMN2* P5 mice generated an increase in unstimulated force as they failed to completely relax between contractions (Fig. 4.1E). However, the *Smn*$^{-/-}$*;SMN2* muscle produced significantly more unstimulated force than control counterparts. The unstimulated force of control TA muscles had a mean time of appearance at 133 sec and was equivalent to 4.4% of the pre-fatigue tetanic force by the end of the protocol (Fig. 4.1E and F). However, for the P5 *Smn*$^{-/-}$*;SMN2* TA muscles, the average time of appearance started significantly sooner, i.e. at 49 sec, with a final mean of 8.2% (Fig. 4.1E and F). Therefore, our results suggest the presence of a defect in *Smn*$^{-/-}$*;SMN2* muscles to recover from muscle fatigue over time.

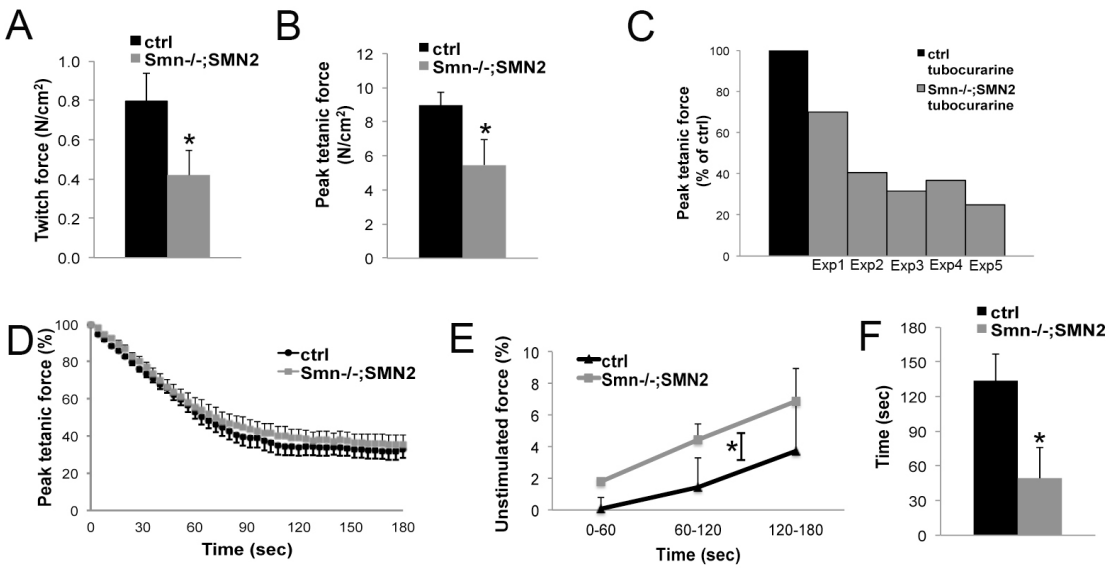
A
ctrl
Smn-/-;SMN2
Twitch force (N/cm²)
1.0
0.8
0.6
0.4
0.2
0.0
*
B
ctrl
Smn-/-;SMN2
Peak tetanic force (N/cm²)
12
10
8
6
4
2
0
*
C
ctrl tubocurarine
Smn-/-;SMN2 tubocurarine
Peak tetanic force (% of ctrl)
100
80
60
40
20
0
Exp1 Exp2 Exp3 Exp4 Exp5
D
ctrl
Smn-/-;SMN2
Peak tetanic force (%)
100
80
60
40
20
0
0 30 60 90 120 150 180
Time (sec)
E
ctrl
Smn-/-;SMN2
Unstimulated force (%)
10
8
6
4
2
0
*
0-60 60-120 120-180
Time (sec)
F
ctrl
Smn-/-;SMN2
Time (sec)
180
150
120
90
60
30
0
*

Figure 4.1. Intrinsic muscle weakness in muscle from *Smn*$^{-/-}$*;SMN2* mice.

(A) TA muscle preparations from P5 *Smn*$^{-/-}$*;SMN2* mice and control littermates were used to assess tetanic and twitch force normalized to the muscle cross-sectional area. Bar graph showing that P5 *Smn*$^{-/-}$*;SMN2* TA muscles produce significantly less twitch force than control littermates. (B) Bar graph demonstrating a reduction in normalized maximal peak tetanic force in P5 *Smn*$^{-/-}$*;SMN2* TA muscle compared to controls. (C) Administration of tubocurarine to block NMJs did not influence relative force production in *Smn*$^{-/-}$*;SMN2* muscles. In five independent experiments, *Smn*$^{-/-}$*;SMN2* mice produced less force than controls following treatment with tubocurarine. (D) Graph showing similar relative force decreases in *Smn*$^{-/-}$*;SMN2* and control mice during fatigue elicited with one tetanic contraction every sec for 3 min. Peak tetanic forces are expressed as a percentage of the pre-fatigue force. (E) Unstimulated force occurred when muscles failed to relax between contractions and is expressed as a percentage of the pre-fatigue peak tetanic force. During a fatigue protocol, P5 *Smn*$^{-/-}$*;SMN2* TA muscles show increased unstimulated force compared to controls. (F) The unstimulated force appeared much sooner in *Smn*$^{-/-}$*;SMN2* TA muscles compared to controls. N = 5-6; *, $p < 0.05$.

Pre-symptomatic muscle weakness in Smn$^{-/-}$;SMN2 and Smn$^{2B/-}$ mice

Whilst we observed a significant decrease in force production in muscles from phenotypic *Smn$^{-/-}$;SMN2* mice, which was independent of aberrant nerve transmission, it remains possible that the muscle weakness observed could be attributed to motor neuron degeneration occurring prior to the stage of our analyses. We therefore assessed the peak tetanic force in pre-symptomatic mice. For this, we have extended our analysis to include both *Smn$^{-/-}$;SMN2* and *Smn$^{2B/-}$* mouse models. This analysis was performed at pre-phenotypic time point of P2 and P9, respectively. In order to confirm that these time points preceded neurodegenerative events, we assessed motor neuron number and NMJ connectivity. At P2 in *Smn$^{-/-}$;SMN2* mice, and P9 in *Smn$^{2B/-}$* mice, there was no difference in the number of motor neuron cell bodies compared to controls (Fig. 4.2A-D). Furthermore, the percentage of fully occupied endplates was unchanged between each mouse model of SMA and the respective controls (Fig. 4.2E-H). During NMJ development, endplates are poly-innervated followed by a process of synapse elimination that occurs during postnatal NMJ maturation. Synapse elimination requires NMJ activity, thus compromised synaptic activity may lead to an increased number of neuronal inputs. Equally, the poly-innervation seen at these time points means that neuronal inputs can be lost, but the terminal can still appear fully innervated. For this reason, both increases and decreases in poly-innervation can be indicative of NMJ defects. Importantly, in both mouse models, quantification of the number of neuronal inputs revealed no significant difference between each mouse model of SMA and the respective controls (Fig 4.2I, J).

Despite the fact that we observed no disruption in motor neuron connectivity, in both models at pre-symptomatic stage, we observed a significant decrease in peak tetanic

force. TA muscles from P2 *Smn*$^{-/-}$*;SMN2* mice produced 67% lower peak tetanic force compared to control littermates (Fig. 4.3A). TA muscles from P9 *Smn*$^{2B/-}$ mice produced 61% lower peak tetanic force compared to control littermates (Fig. 4.3B). The peak forces were normalized to the cross-sectional area of each muscle, however at this stage, we did not observe any significant difference in mean fiber area between mutant and control muscle in either *Smn*$^{2B/-}$ or *Smn*$^{-/-}$*;SMN2* mice (Fig. 4.3C, D). Taken together, these data demonstrate that in two different mouse models of SMA, intrinsic muscle weakness is an early feature, occurring prior to any motor neuron loss and denervation.

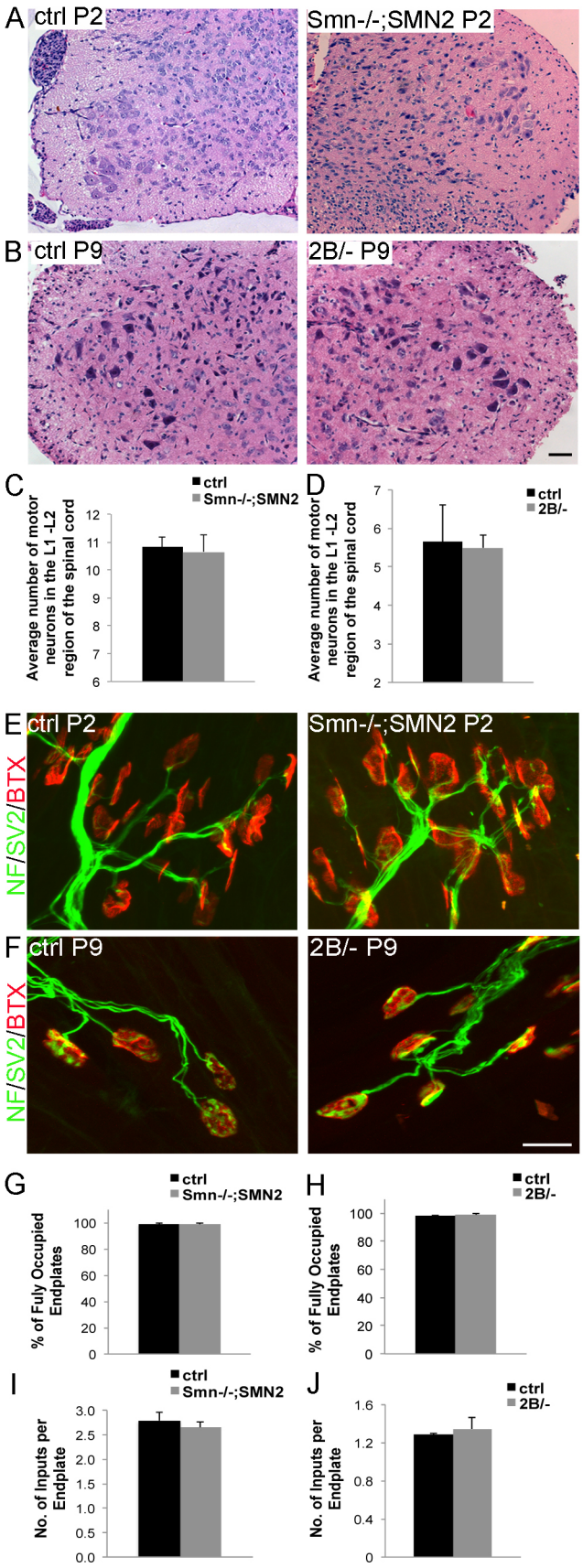
A
ctrl P2
Smn-/-;SMN2 P2
B
ctrl P9
2B/- P9
C
ctrl
Smn-/-;SMN2
Average number of motor neurons in the L1 -L2 region of the spinal cord
12
11
10
9
8
7
6
D
ctrl
2B/-
Average number of motor neurons in the L1 -L2 region of the spinal cord
7
6
5
4
3
2
E
ctrl P2
Smn-/-;SMN2 P2
NF/SV2/BTX
F
ctrl P9
2B/- P9
NF/SV2/BTX
G
ctrl
Smn-/-;SMN2
% of Fuly Occupied Endplates
100
80
60
40
20
0
H
ctrl
2B/-
% of Fully Occupied Endplates
100
80
60
40
20
0
I
ctrl
Smn-/-;SMN2
No. of Inputs per Endplate
3.0
2.5
2.0
1.5
1.0
0.5
0.0
J
ctrl
2B/-
No. of Inputs per Endplate
1.6
1.2
0.8
0.4
0

Figure 4.2. Normal motor neuron counts and intact NMJ connectivity in P2 *Smn*$^{-/-}$*;SMN2* and P9 *Smn*$^{2B/-}$ mice.

(A, B) Representative images of hematoxylin and eosin staining of motor neurons in the ventral horn region of the L1-L2 spinal cord region of P2 control and *Smn*$^{-/-}$*;SMN2* mice, and P9 control and *Smn*$^{2B/-}$ mice. Scale bar = 50 μm. (C, D) Quantification of the number of motor neurons within the ventral horn of the lumbar (L1-L2) region of the spinal cord for control and pre-symptomatic *Smn*$^{-/-}$*;SMN2*, and *Smn*$^{2B/-}$ mice. (E, F) Representative images showing fully intact NMJs from TA muscles of control and pre-symptomatic *Smn*$^{-/-}$*;SMN2* (E) and *Smn*$^{2B/-}$ (F) mice. Post-synaptic acetylcholine receptors were labeled with alpha-bungarotoxin (BTX, red) while the pre-synaptic terminal was labeled with anti-neurofilament (NF, green) and anti-synaptic vesicle protein 2 (SV2, green). Scale bar = 20 μm. (G, H) Quantification of the percentage of fully occupied endplates revealed no difference between control and pre-symptomatic *Smn*$^{-/-}$*;SMN2* and *Smn*$^{2B/-}$ mice. (I, J) Quantification of the number of inputs per endplate revealed no difference between control and pre-symptomatic *Smn*$^{-/-}$*;SMN2* and *Smn*$^{2B/-}$ mice. N = 3 for all experiments.

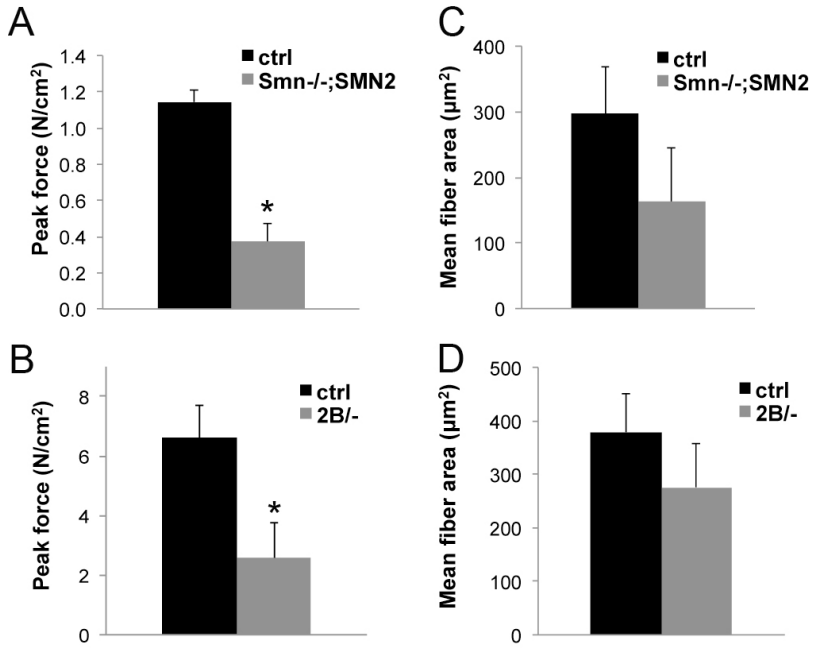

Figure 4.3. Pre-symptomatic muscle weakness in *Smn*$^{-/-}$*;SMN2* and *Smn*$^{2B/-}$ mice.

(A) P2 *Smn*$^{-/-}$*;SMN2* force measurements revealed a 67% decrease in maximal tetanic force production compared to controls. Force data were normalized to the muscle cross-sectional area. (B) The average peak tetanic force was reduced by 61% in P9 pre-symptomatic *Smn*$^{2B/-}$ TA muscles compared to control littermates. (C) Bar graph showing the mean fiber area of P2 TA muscles from *Smn*$^{-/-}$*;SMN2* and control mice. (D) The average fiber cross-sectional area was calculated for P9 *Smn*$^{2B/-}$ and control TA muscle. N = 3 for all experiments, *, $p < 0.05$.

Decreased expression of mature ryanodine receptor 1 expression in SMA muscle

The results from our physiology experiments led us to investigate possible causes for the decrease in force production form *Smn*$^{-/-}$*;SMN2* muscle. During a muscle contraction, calcium is released from the sarcoplasmic reticulum to the sarcomere to allow for the actin-myosin cross-bridge cycling to occur. The calcium release is mediated by the ryanodine receptor 1 (RyR1) which is the predominant ryanodine receptor expressed in mature muscle (Van Petegem 2012). Several splice variants of the RyR1 gene exist. For example, one variant is called ASI and is expressed without exon 70 [ASI (-)] in neonatal muscle and transitions to an alternatively spliced variant that includes exon 70 in mature skeletal muscle [ASI (+)] (Futatsugi et al. 1995). The second RyR1 splice variant is ASII, which is further spliced to exclude exon 83 in immature muscle [ASII (-)] or to include that exon in mature muscle [ASII (+)] (Futatsugi et al. 1995, Kimura et al. 2005). Using PCR primers designed to target the mature and immature variants, we assessed the RyR1 transcripts in hindlimb skeletal muscle RNA extracts from mouse models of SMA and in controls. A time course analysis demonstrates the dominant expression of ASII (+) in mature muscle (P21) over the ASII (-) variant in wild type mice (Fig. 4.4A). At P5, the predominant ASII isoform in control mice was ASII (+), while in *Smn*$^{-/-}$*;SMN2* muscle there was a relative increase in the proportion of the neonatal variant ASII (-) (Fig. 4.2B). In control P21 mice, we only observed the adult ASII (+) variant and not the neonatal ASII (-) transcript (Fig. 4.4C). Interestingly, the ASII (+) transcript level was decreased in P21 *Smn*$^{2B/-}$ muscle and we now detected the neonatal ASII (-) transcript variant in P21 *Smn*$^{2B/-}$ skeletal muscle (Fig. 4.4C).

Using the same PCR approach, we assessed the transcript levels of ASI using primers targeting both the neonatal and adult ASI splice variant. We did not observe any differences in neonatal versus adult transcript levels of the ASI variant for the *Smn*$^{-/-}$*;SMN2* mice (data not shown). In P21 *Smn*$^{2B/-}$ mice however, we detected the presence of the neonatal ASI (-) transcript that was not detectable in P21 control muscles. Furthermore, we observed a decrease in the mature ASI (+) transcript in *Smn*$^{2B/-}$ samples compared to controls (data not shown). Thus, both the ASII and ASI variants are aberrantly expressed in P21 *Smn*$^{2B/-}$ model mice. Collectively, the expression pattern of the RyR1 transcripts suggests a delay in muscle development in mouse models of SMA.

Muscle denervation at the NMJ is a widespread pathological feature observed in mouse models of SMA. Although the postsynaptic compartment of hindlimb muscles is occupied in these mice, we nonetheless investigated whether denervation would influence the expression the RyR1 transcript. To do so, we experimentally denervated the hind legs of young wild type mice and examined the expression of RyR1 in denervated samples compared to sham controls. Seven days post-denervation, we did not detect any changes in the splicing pattern of the RyR1 ASII variant in denervation compared to control samples (Fig. 4.4D). This result suggests that the changes in the RyR1 transcript pattern that we observed in muscles from the mouse models of SMA are not attributable to denervation and are therefore muscle-intrinsic.

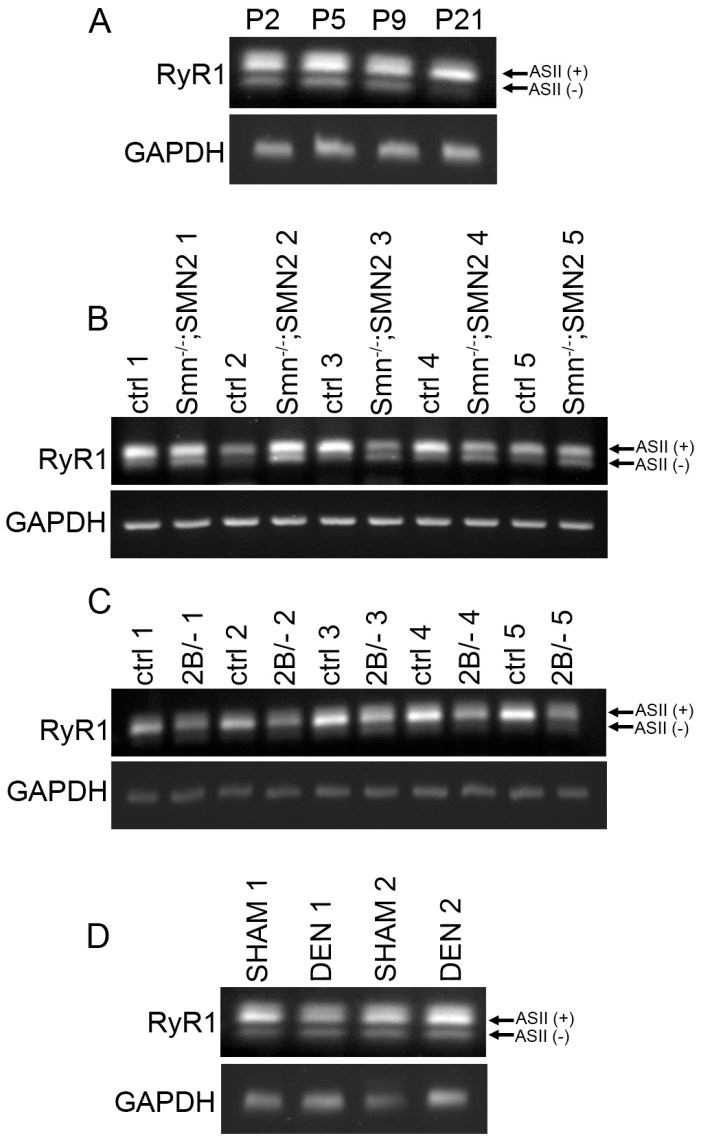
A
P2
P5
P9
P21
RyR1
ASII (+)
ASII (-)
GAPDH
B
ctrl 1
Smn-/-;SMN2 1
ctrl 2
Smn-/-;SMN2 2
ctrl 3
Smn-/-;SMN2 3
ctrl 4
Smn-/-;SMN2 4
ctrl 5
Smn-/-;SMN2 5
RyR1
ASII (+)
ASII (-)
GAPDH
C
ctrl 1
2B/- 1
ctrl 2
2B/- 2
ctrl 3
2B/- 3
ctrl 4
2B/- 4
ctrl 5
2B/- 5
RyR1
ASII (+)
ASII (-)
GAPDH
D
SHAM 1
DEN 1
SHAM 2
DEN 2
RyR1
ASII (+)
ASII (-)
GAPDH

Figure 4.4. Delayed expression of the adult RyR1 mRNA splice variant in muscles from mouse models of SMA.

(A) Image shows results of RT-PCR on RNA from hindlimb muscle from wild type mice with primers directed against ASII+ and ASS- with GAPDH to confirm starting cDNA levels were equivalent. Note that relative levels of ASII+ increase from P2 to P21 (upper band) with a corresponding relative decrease in ASII- (lower band). (B, C) Decreased expression of ASII (+) and sustained expression of ASII (-) in muscle samples from P5 *Smn*$^{-/-}$*;SMN2* (B) and *Smn*$^{2B/-}$ (D) P21 mice relative to controls. N = 5. (D) The expression the adult and neonatal ASII RyR1 transcript variants are not altered in young adult mice 7 days post-denervation. N = 2.

Altered sodium channel levels in SMA mice

In excitable cells types, such as neurons and myocytes, the action potential is propagated by sodium channels. Sodium channel expression is a developmentally regulated process in which an isoform switch, $Na_v1.5$ to $Na_v1.4$, occurs during postnatal development in the mouse (David et al. 2008, Morel et al. 2010). $Na_v1.4$, the predominant sodium channel isoform in adult skeletal muscle (Kallen et al. 1993), must be expressed at the correct time point during development to fulfil its role. A delay in expression of the $Na_v1.4$ isoform could negatively impact muscle force production (Hebert et al. 2007).

As expected, we observed a robust increase in $Na_v1.4$ levels in wild type muscle during postnatal development from P2 to P21 (Fig. 4.5A). Interestingly, in two independent mouse models of SMA, there is a decrease in the levels of $Na_v1.4$ compared to control mice. Specifically, in P5 *Smn*$^{-/-}$*;SMN2* mice there was a 51% decrease in $Na_v1.4$ levels in hindlimb skeletal muscle compared to control counterparts (Fig. 4.5B). Similarly, in muscle from phenotype stage P21 *Smn*$^{2B/-}$ mice, there was a 65% decrease in $Na_v1.4$ levels compared to controls (Fig. 4.5C). In addition to the decrease in $Na_v1.4$, we observed an increase in $Na_v1.5$ levels in *Smn*$^{2B/-}$ muscle (Fig. 4.5C). Sodium channel $Na_v1.5$ is the predominant isoform expressed in the adult heart and in early stages of skeletal muscle development (Morel et al. 2010).

To gain a better understanding on how $Na_v1.4$ is mis-regulated in SMA mice, we assessed the status of proteins known to regulate sodium channel expression. Hebert and colleagues (2007) have previously demonstrated that the transcription factor nuclear factor 1 (NF1) is recruited to the $Na_v1.4$ gene promoter by myogenic regulatory factors to enhance its expression. We did not observe any differences in the levels of NF1 in muscle

from *Smn*$^{2B/-}$ mice compared to controls (Fig. 4.5D). Another transcription factor, zinc-finger E box-binding protein (ZEB), is a $Na_v1.4$ repressor. As with NF1, we did not observe any change in ZEB levels in muscle from *Smn*$^{2B/-}$ mice (Fig. 4.5D).

To investigate whether the observed changes in $Na_v1.4$ were muscle-intrinsic, we evaluated whether $Na_v1.4$ expression was influenced by experimental denervation. There was no change in $Na_v1.4$ levels one-day post-denervation (Fig. 4.5E). However, a significant decrease was observed seven days following denervation, in agreement with previous studies (Lupa et al. 1995, Rich et al. 1999). Therefore, although the muscles used in the $Na_v1.4$ expression analysis are not morphologically denervated, we cannot rule out the possibility that functional synaptic defects at the NMJ influence sodium channel expression in muscles from mouse models of SMA.

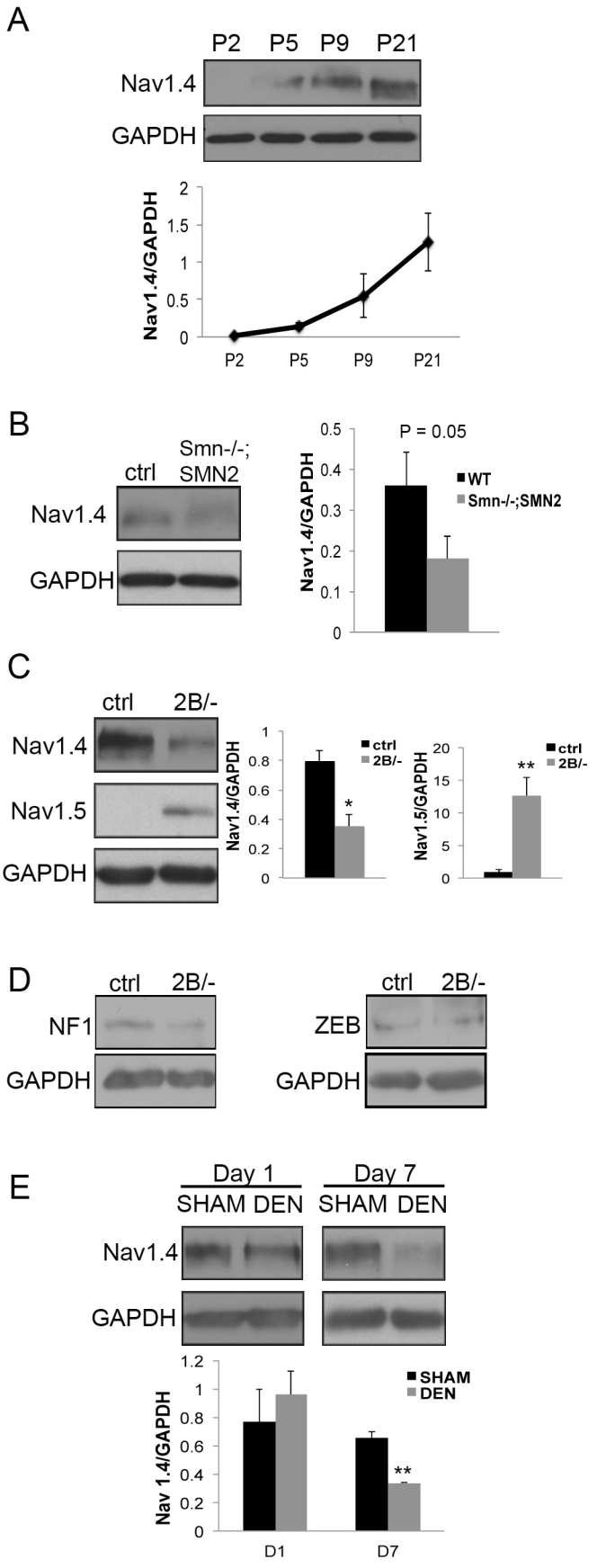
A
P2 P5 P9 P21
Nav1.4
GAPDH
Nav1.4/GAPDH
2
1.5
1
0.5
0
P2 P5 P9 P21
B
ctrl
Smn-/-;
SMN2
Nav1.4
GAPDH
P = 0.05
WT
Smn-/-;SMN2
Nav1.4/GAPDH
0.5
0.4
0.3
0.2
0.1
0
C
ctrl 2B/-
Nav1.4
Nav1.5
GAPDH
Nav1.4/GAPDH
ctrl
2B/-
*
Nav1.5/GAPDH
**
D
ctrl 2B/-
NF1
GAPDH
ZEB
E
Day 1
Day 7
SHAM DEN SHAM DEN
Nav1.4
GAPDH
Nav 1.4/GAPDH
SHAM
DEN
**
D1
D7

Figure 4.5. $Na_v1.4$ protein levels are decreased in muscles from mouse models of SMA. (A) Immunoblot analysis was performed using muscle lysate from P2, P5, P9 and P21 wild type mice. Nav1.4 protein levels increase during postnatal muscle development and it is the predominant sodium channel expressed in mature skeletal muscle (N = 3). (B) Representative immunoblot with quantification showing a decrease in levels of sodium channel $Na_v1.4$ in P5 *Smn*$^{-/-}$;*SMN2* hindlimb muscle compared to controls (N = 4). (C) Quantification of immunoblot analyses in P21 *Smn*$^{2B/-}$ and control hindlimb muscles revealed a decrease in $Na_v1.4$ levels. Early in postnatal muscle development, the $Na_v1.5$ sodium channel isoform is the most predominant. In P21 *Smn*$^{2B/-}$ mice, the protein levels of $Na_v1.5$ are higher compared to controls (N = 3). (D) The protein level of the $Na_v1.4$ positive regulator, nuclear factor 1 (NF1), is not altered in muscles from P21 *Smn*$^{2B/-}$ mice. Similarly, there was no change detected in the protein levels of the $Na_v1.4$ repressor ZEB. (E) Expression of sodium channel $Na_v1.4$ in control sham and denervated samples 1 and 7 days post-denervation was assessed by immunoblot (N = 3). A decrease in the levels of $Na_v1.4$ in muscle was noted at 7 days post-denervation. *, $p < 0.05$; **, $p < 0.01$.

SERCA1a protein expression is altered in Smn$^{-/-}$;SMN2 mice

One possible mechanism that can cause increased unstimulated force production is an incomplete removal of Ca^{2+} from the sarcoplasm because of decreased levels of the Ca^{2+} ATPase pump. The protein responsible for the Ca^{2+} uptake following a muscle contraction is the sarcoplasmic reticulum Ca^{2+} ATPase (SERCA), of which SERCA1a is the predominant isoform found in fast-twitch muscles such as the TA muscle (Beard et al. 2004). The protein expression of SERCA1a is developmentally regulated. It peaks by P9 and drops slightly at P21 (Fig. 4.6A). Immunoblot analysis revealed a decrease in SERCA1a protein levels in hindlimb skeletal muscles from P5 *Smn$^{-/-}$;SMN2* mice compared to control samples (Fig. 4.6B). Interestingly, levels of calsequestrin, a protein that binds and stores Ca^{2+} in the sarcoplasmic reticulum, was unchanged in *Smn$^{-/-}$;SMN2* muscle compared to controls (Fig. 4.6B), indicating that a Ca^{2+} handling defect was likely limited to the sarcoplasmic reticulum pump.

To address whether the decrease in SERCA1a was attributed to motor neuron denervation leading up to the analysis, we measured the influence of denervation on SERCA1a protein levels. Protein lysate from gastrocnemius muscles was collected from denervated and sham operated mice. SERCA1a protein levels were unchanged in skeletal muscle from denervated mice compared to controls, suggesting that the observed decrease in SERCA1a in muscle from *Smn$^{-/-}$;SMN2* mice is likely to be a muscle-intrinsic phenomenon (Fig. 4.6C).

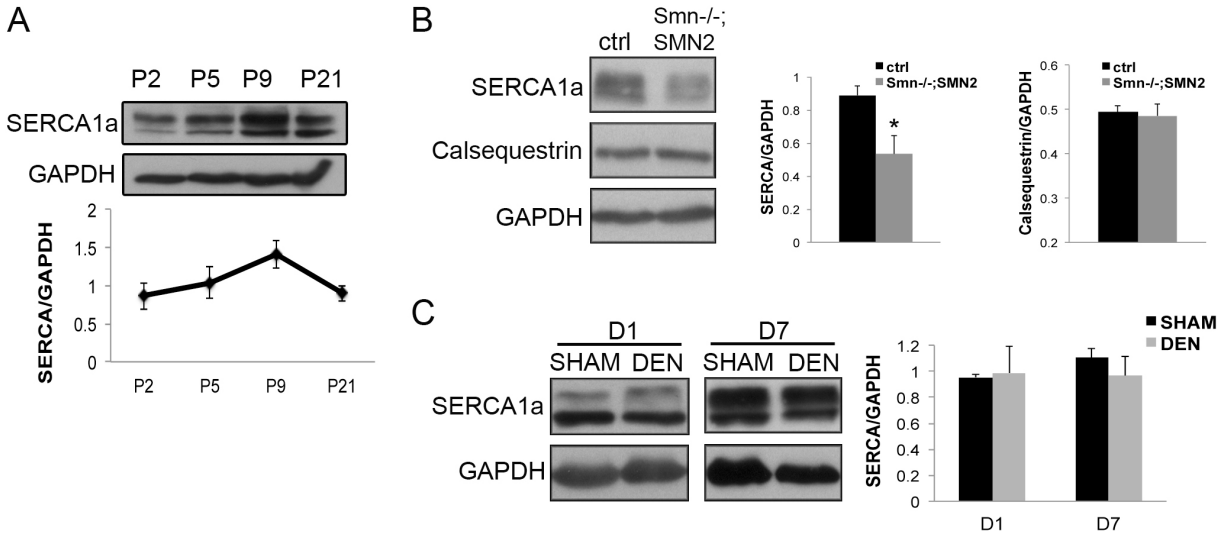

Figure 4.6. SERCA1a protein level is altered in muscles from *Smn*$^{-/-}$*;SMN2* mice.

(A) Whole muscle lysate was collected from P2, P5, P9, and P21 wild type mice and immunoblot analysis was performed to assess SERCA1a protein levels. SERCA1a levels increase over time and peak at P9 (N = 3). (B) Immunoblot with quantification showing a decrease in SERCA1a, but not calsequestrin, in hindlimb muscle from P5 *Smn*$^{-/-}$*;SMN2* mice compared to control. (C) Immunoblots were performed on muscle lysates collected from experimentally denervated (DEN) and sham operated (SHAM) muscle to assess whether the changes in SERCA1a protein levels were muscle-intrinsic. No change in SERCA1a levels was observed. N = 3, *, $p < 0.05$.

Discussion

It has long been assumed that the muscle weakness evident in SMA is coupled to the motor neuron cell loss and denervation-induced muscle atrophy. Here, we show muscle weakness occurs early and independently of motor neuron cell loss and denervation in two different mouse models of SMA. This physiological defect was associated with delayed expression of mature isoforms of proteins important for muscle function. Our results therefore point to delayed muscle development induced weakness and provide new insight into the pathophysiology underlying SMA.

Intrinsic muscle weakness in SMA mice

We have employed an *ex vivo* method in which the muscle is excised and placed in a chamber where it can be directly stimulated to contract. By doing so, we minimize the negative contribution that degenerating motor neurons might have in eliciting a contraction. We show a decrease in normalized peak tetanic force in muscle from phenotype stage *Smn*$^{-/-}$*;SMN2* mice. Importantly, we show a similar decrease in muscle force from pre-symptomatic *Smn*$^{-/-}$*;SMN2* and *Smn*$^{2B/-}$ mice prior to motor neuron loss and denervation. Furthermore, our physiological results were normalized to the cross-sectional area of each muscle tested. Therefore, the overt decrease in muscle size observed in P5 *Smn*$^{-/-}$*;SMN2* mice cannot explain the decrease in force production. In addition, our experiments performed on pre-symptomatic mice allow us to rule out the possibility that smaller myofibers are the reason for the decrease in relative force production since no significant difference was observed in muscle size between pre-symptomatic and control mice. However, the maturity of SMA muscle may influence muscle force production irrespective of size. As we have observed a decrease in the

mature isoforms of a number of muscle proteins, we suggest that a decrease in muscle maturity in P2 *Smn*$^{-/-}$*;SMN2* and P9 *Smn*$^{2B/-}$ mice could contribute to a marked decrease in force production.

Delayed expression of mature isoforms of muscle function proteins in mouse models of SMA

Several groups have indirectly demonstrated impaired muscle growth in mouse models of SMA by measuring the cross-sectional area of developing myofibers (Kong et al. 2009, Dachs et al. 2011, Lee et al. 2011). These analyses suggest that shortly after birth, muscle development is significantly impaired. During postnatal muscle development, as myotubes grow to become myofibers with sarcomeres, a switch in expression from neonatal to adult protein isoforms occurs for many muscle function proteins. A delay in the molecular events underlying myogenesis could potentially lead to a delay in the transition to the mature isoform expression of contractile proteins. Such may be the case with the expression of MHC in which the embryonic and perinatal MHC isoforms are predominantly expressed in SMA muscle (Kong et al. 2009, Lee et al. 2011). Therefore, we hypothesized that several other proteins important for generating muscle contractions could be aberrantly expressed, with juvenile isoforms predominating rather than adult ones, which could lead to muscle weakness in mouse models of SMA. We focused on proteins that are directly involved in the regulation of muscle contraction, that is, proteins important for calcium regulation and action potential propagation.

RyR1 expression in muscle from mouse models of SMA

Results from our RT-PCR analysis revealed a delay in the expression of the mature RyR1 splice variants in skeletal muscle from mouse models of SMA. In phenotype stage *Smn*$^{2B/-}$ mice, we observed a mis-regulation of both the ASI and ASII alternatively spliced variants. At P5 in the *Smn*$^{-/-}$*;SMN2* model, a change in expression was evident for the ASII variant but not the ASI. During development, the transition from ASII (-) to ASII (+) begins at P0 and is complete by P21 (Futatsugi et al. 1995). For the ASI variant, the transition from the neonatal ASI (-) to the adult ASI (+) form begins only at P8. Therefore, the timing of the ASI transition likely explains why we observed the delay in P21 *Smn*$^{2B/-}$ mice but not in P5 *Smn*$^{-/-}$*;SMN2* mice. The functional studies performed by Kimura et al. (2005) demonstrate that the neonatal RyR1 is less active than the adult RyR1 as it binds ryanodine with less affinity than the adult form, and for that reason releases less calcium. Therefore, the persistent expression of the neonatal RyR1 variants in mouse models of SMA likely leads to decreased Ca^{2+} release from the sarcoplasmic reticulum to the sarcomere, and subsequently results in weaker muscle contractions.

Sodium channel expression in muscle from mouse models of SMA

In skeletal muscle, action potentials are generated and propagated by voltage-gated sodium channels. $Na_v1.4$ is the predominant pore-conducting channel in adult muscle. Its expression significantly increases in mice in the first two weeks after birth (Kallen et al. 1993, David et al. 2008). Here we show that $Na_v1.4$ levels are decreased in muscles from two different mouse models of SMA. This may explain in part the lower force generation since there would have been an insufficient number of available $Na_v1.4$

channels to generate action potentials during a train. Furthermore, this time period after birth coincides with a period of dramatic muscle growth, and $Na_v1.5$ is the major sodium channel expressed during early muscle development. Upon denervation of skeletal muscle, the expression of sodium channels reverts back to that which occurs during development (Kallen et al. 1993). The expression of $Na_v1.5$ increases and that of $Na_v1.4$ decreases in denervated muscle. Indeed, we observed a decrease in $Na_v1.4$ levels in experimentally denervated muscles (day 7), as well as in muscles from both SMA mouse models studied. As such, we cannot rule out the possibility that the mis-regulation of $Na_v1.4$ is due to denervation in muscle from the symptomatic mice.

The expression of $Na_v1.4$ is positively regulated by the transcription factor nuclear factor 1 and is repressed by the transcription factor ZEB (Hebert et al. 2007). We did not observe any differences in the expression of these two transcription factors in *Smn*$^{2B/-}$ mice. The recruitment of the nuclear factor 1 protein to the $Na_v1.4$ promoter is mediated through two transcription factors that are important for muscle differentiation, namely myogenin and muscle-specific regulatory factor 4 (MRF4). It can be envisaged that a delay in the expression of myogenic regulatory factors such as myogenin and MRF4, or others even more up-stream of myogenin and MRF4, may explain the deferred $Na_v1.4$ expression in SMA mice.

Decreased SERCA1a expression in Smn$^{-/-}$*;SMN2 mice*

The results from our fatigue protocol demonstrate an increase in unstimulated force and a decrease in the time of unstimulated force onset in *Smn*$^{-/-}$*;SMN2* mice. This observation may be indicative of a defect in Ca^{2+} uptake from the sarcomere to the

sarcoplasmic reticulum, which is supported by the muscle intrinsic decrease in levels of the SERCA1a Ca^{2+} pump in muscles of *Smn*$^{-/-}$*;SMN2* mice. Defects in Ca^{2+} handling have previously been reported in mouse models of muscular dystrophies (Kimura et al. 2005, Millay et al. 2009). Specifically, defects related to Ca^{2+} uptake and SERCA1 function have been described in a mouse model of Duchenne's muscular dystrophy (Divet and Huchet-Cadiou 2002). Indeed, the overexpression of SERCA1 in skeletal muscles led to robust improvements in muscle function and attenuated muscle pathology in mouse models of muscular dystrophy (Goonasekera et al. 2011). Furthermore, RyR1 splicing defects resulting in the expression of the neonatal variants contribute to the pathogenesis of the neuromuscular disease myotonic dystrophy type 1 (Kimura et al. 2005). Thus, the defects we report in muscles from SMA model mice are reminiscent of those that occur in muscle-intrinsic diseases.

In summary, the present study demonstrates early and profound intrinsic muscle weakness, and aberrant expression of muscle proteins in two different mouse models of SMA, which may contribute to the SMA phenotype. Our results provide significant insight into a previously underappreciated component of SMA pathophysiology and suggest that including skeletal muscle as a therapeutic target in SMA is warranted.

Acknowledgements

This project was funded by grants from the Canadian Institutes of Health Research (CIHR) and The Muscular Dystrophy Association (USA) to R.K. J.G.B. is a recipient of a Frederick Banting and Charles Best CIHR Doctoral Research Award, L.M.M is a recipient of a Multiple Sclerosis Society of Canada Postdoctoral Fellowship, and R.K. is a recipient of a University Health Research Chair from the University of Ottawa.

Chapter 5

General Discussion

Impaired muscle growth leads to intrinsic muscle weakness in SMA model mice

During normal muscle development, the hierarchical expression of myogenic transcription factors is crucial for proper timing of developmental milestones (Bentzinger et al. 2012). Depletion of satellite cells during early postnatal muscle growth, a phase of intense satellite cell proliferation and differentiation, leads to impaired muscle development, thus demonstrating a role for satellite cells in muscle growth (Seale et al. 2000). Over time, the satellite cell population decreases owing to a diminished need for growth. In mature muscle, a residual satellite cell population is maintained for muscle regeneration following injury. As the expression of the myogenic program progresses, a transition in the expression from neonatal to adult isoforms of proteins important for muscle function ensues (Schiaffino and Reggiani 1996). The changes at the molecular level lead to an overt morphological transformation in which mature myofibers appear and grow in size. Ultimately, the growth and maturity of the myofibers lead to increased force production capacity. A schematic representing the transformations occurring in postnatal muscle development is presented in Figure 5.1A.

Using mouse models of SMA, namely the *Smn*$^{-/-}$*;SMN2* and the *Smn*$^{2B/-}$ models, the data herein provides strong evidence to support the hypothesis that the pathological reduction of Smn leads to impaired muscle development (Fig. 5.1B). As early as the second day after birth, molecular differences in the expression pattern of the myogenic program were observed. In *Smn*$^{-/-}$*;SMN2* muscle, myogenic program expression continues to decrease over time while in *Smn*$^{2B/-}$ muscle, a delay in expression is evident with a later than normal up-regulation of myogenic transcription factors at P21. To determine whether the mis-regulation of the myogenic program was a cell-intrinsic effect, we

performed experiments using *Smn*$^{2B/-}$ primary myoblasts to eliminate the negative contributions that diseased motor neurons might have on skeletal muscles. Indeed, we show that the myogenic program is mis-regulated in primary myoblasts isolated from *Smn*$^{2B/-}$ mice, suggesting that the aberrant levels of the myogenic regulatory factors were due to muscle-intrinsic defects. At the histological level, an increased proportion of myofibers with centrally located nuclei was apparent, as was a decrease in myofiber size in both models. Although we assessed the expression of muscle function proteins at phenotype stage in both models, we hypothesize that the aberrant transition from neonatal to adult isoforms coincides with the mis-regulation of the myogenic regulatory factors starting at P2 in both models. Finally, we observed a relative decrease in force production at P2 in *Smn*$^{-/-}$*;SMN2* mice which persisted to P5 phenotype stage. We observed muscle weakness at P9 in *Smn*$^{2B/-}$ mice, however a decrease in force could be envisaged at the same time as the appearance of immature fibers (~P3) and would likely persist to P21 where a significant population of immature myofibers is still present. The changes to skeletal muscle development that occur in mouse models of SMA are graphically represented in Figure 5.1B.

Taken together, our data suggest a robust correlation between the early molecular alterations and the physiological defects that we report in mouse models of SMA. Therefore, the following scenario is proposed where the mis-regulation of Pax7 and myogenic regulatory factors leads to the aberrant expression of mature isoforms of proteins important for muscle function. Moreover, delayed expression of the myogenic program leads to an increased proportion of immature myofibers and smaller myofibers.

These defects, in turn, impact on muscle force production and lead to muscle weakness in mouse models of SMA.

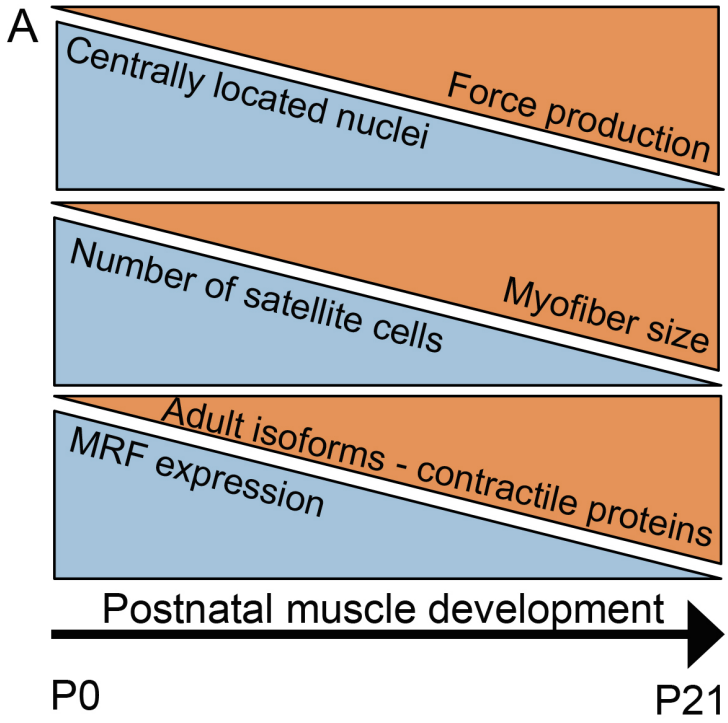
A
Centrally located nuclei
Force production
Number of satellite cells
Myofiber size
Adult isoforms - contractile proteins
MRF expression
Postnatal muscle development
P0
P21

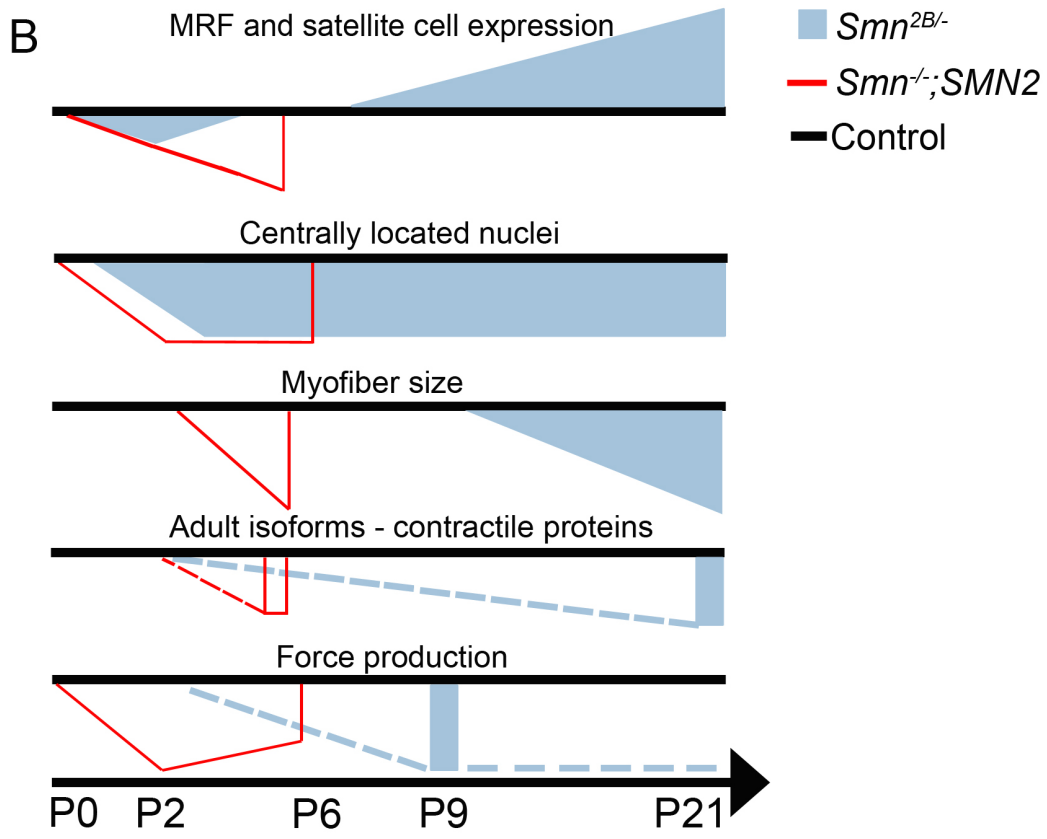
B
MRF and satellite cell expression
Centrally located nuclei
Myofiber size
Adult isoforms - contractile proteins
Force production
P0
P2
P6
P9
P21
Smn2B/-
Smn-/-;SMN2
Control

Figure 5.1. Aberrant postnatal muscle development in mouse models of SMA.

(A) During postnatal muscle development, the need for satellite cells decreases over time, as does the expression level of myogenic regulatory factors (MRF). As such, a transition from neonatal to adult isoforms of proteins important for muscle function occurs. With growth, muscle adopts a more mature phenotype characterized by fewer myofibers with centrally located nuclei and larger sized myofibers. Ultimately, these changes allow the muscle to function properly and produce force. (B) Muscles from mouse models of SMA are characterized by developmental changes at the molecular, histological and functional level. The results obtained from *Smn*$^{2B/-}$ mice are represented by the blue shapes and those from *Smn*$^{-/-}$*;SMN2* mice are depicted by red lines. These results are illustrated relative to control mice represented by the black horizontal lines. In *Smn*$^{2B/-}$ mice, the levels of MRFs and number of satellite cells decrease at P2 and are up-regulated from P9-P21. In *Smn*$^{-/-}$*;SMN2* mice, the levels of MRFs and number of satellite cells are down-regulated shortly after birth, and continue to decrease until end-stage. The high proportion of immature fibers with centrally located nuclei fails to decrease from birth and persists to phenotype stage in *Smn*$^{-/-}$*;SMN2* mice. Increased immature fibers in *Smn*$^{2B/-}$ muscles compared to controls are prominent at P9 and high numbers are sustained until P21. The cross-sectional area of the muscle fibers is smaller than controls after P2 in *Smn*$^{-/-}$*;SMN2* mice and after P9 in *Smn*$^{2B/-}$ mice. The mis-regulation of adult isoforms of proteins important for muscle function was assessed at phenotype stage of *Smn*$^{-/-}$*;SMN2* and *Smn*$^{2B/-}$ mice at P5 and P21 respectively. We hypothesize that the mis-regulation of the adult isoforms begins at P2 in both models when the aberrant expression of MRFs is detected. A dashed line is used to represent this assumption. Finally, the force

production is negatively affected relative to control muscles from P2-P5 in *Smn*$^{-/-}$;*SMN2* mice. And, although we observed a relative decrease in force production at P9 in *Smn*$^{2B/-}$ muscles, we hypothesize that the decrease in force production corresponds to the increase in immature myofiber number at ~P3 and persists to P21 (represented by the dashed line).

Function(s) of Smn in skeletal muscle

The muscle intrinsic defects that we observed support the notion that Smn plays a key role in muscle development. To begin addressing the possible function(s) of Smn in skeletal muscle, we have performed a protein interaction screen to identify Smn-associated proteins during varying stages of development in C2C12 muscle cells. Our findings suggest that the nature of the Smn-interacting proteins varies during growth, early differentiation and late differentiation (Shafey et al. 2010). The levels of snRNP assembly activity significantly decrease during C2C12 myoblast differentiation, suggesting unique functions for Smn other than snRNP assembly (Gabanella et al. 2005). For this reason, we postulate that the function of Smn in muscle is dynamic in nature.

The mis-regulation of myogenic genes at P2 in mouse models of SMA indicates that Smn in required early during postnatal muscle development. The abnormal number of satellite cells in muscles from mouse models of SMA suggests that Smn impacts on Pax7 levels. Furthermore, Smn negatively impacts on the expression of the myogenic regulatory factors. Although it is likely that aberrant MyoD expression leads to altered expression patterns of myogenin and MRF4, at the moment, it is unclear whether altered Pax7 expression influences MyoD levels in the context of SMA. However, it can be envisaged that Smn acts on Pax7 and MyoD independently from one another either directly or indirectly. This would suggest that Smn plays a role in satellite cells and a separate role in committed myoblasts. Alternatively, Smn may regulate the expression of another transcription factor important for muscle development such as myocyte enhancer factor-2 (Mef2) or possibly a protein with a novel function in skeletal muscle. Interestingly, it has previously been demonstrated that Mef2 can regulate MyoD,

myogenin and MRF4 levels (Black and Olson 1998). Expressing Pax7 and MyoD back to wild type levels in primary myoblasts are rescue experiments that may provide insight as to when Smn is required during myogenesis. For the moment, based on the early presence of muscle defects and the expression pattern of Smn in muscle, it appears that the function Smn is developmentally regulated. The importance of Smn during development has previously been highlighted by the complete absence of the gene in mice which leads to pre-implantation lethality (Schrank et al. 1997). Furthermore, a neurodevelopmental component of the pathogenesis of SMA has previously been suggested (Boyer et al. 2010). Therefore, although we postulate that the defects in muscle are attributed to a muscle-specific function of Smn, it is possible that the pathological reduction of Smn leads to a more general defect in the development of multiple tissues.

As such, we cannot rule out that the depletion of Smn in skeletal muscle leads to widespread defects in cellular processes. Given the known function of Smn in the assembly of the spliceosome, aberrant gene splicing may lead to altered levels of myogenic genes which could profoundly impact on muscle development. Smn activity in snRNP assembly is at its highest during proliferation compared to differentiation in C2C12 cells (Gabanella et al. 2005). Further supporting this point, we identified an interaction between Smn and Sm proteins in C2C12 cells during stages of growth but not differentiation (Shafey et al. 2010). The increase in Smn mediated snRNPs likely reflects a greater need for RNA transcription during proliferation compared to differentiation. Therefore, alternative-splicing events early during myogenesis may trigger a progression of aberrantly expressed myogenic regulatory factors ultimately leading to physiological

defects. Splicing defects have never been assessed in muscle but should be investigated to rule out the possible mis-splicing of transcription factors essential for proper myogenesis.

Our interaction screen highlighted the association of Smn with several sarcomeric contractile proteins. We identified known sarcomeric Smn associated protein such as α-actin as well several novel sarcomeric proteins like isoforms of tropomyosin and myosin regulatory light chain (Shafey et al. 2010). The significance of the interactions between Smn and contractile proteins is unclear at the moment however, the loss of these interactions in skeletal muscle from mouse models of SMA may impact on force production and lead to weaker muscles.

Are defects observed in mouse models of SMA present in other motor neuron diseases?

Amyotrophic lateral sclerosis (ALS) is a an adult-onset neurodegenerative disease characterized by the degeneration of motor neurons which leads to muscle weakness, paralysis and ultimately death (Manzano et al. 2013). Most cases of ALS are sporadic in nature, only 10% of patients have a familial type of ALS and a small subset of these cases are associated with mutations in the *Cu/Zn superoxide dismutase 1* (*SOD1*) gene. A growing body of evidence suggests that muscle intrinsic defects are a primary component of the disease. This is best illustrated by the use of conditional mouse models in which *SOD1* mutations restricted to skeletal muscle lead to motor neuron degeneration (Wong and Martin 2010).

Altered expression of the myogenic program has previously been reported in a mouse model of ALS. Similar to $Smn^{2B/-}$ muscles, the protein levels of Pax7 and myogenic regulatory factors were increased in ALS model mice at the onset of symptoms

(Manzano et al. 2011). However, unlike the profile we observed in P2 and P9 *Smn*$^{2B/-}$ muscle, the levels of myogenic genes were not differentially expressed in early and late pre-symptomatic ALS mice compared to controls. In a separate study, primary myoblasts isolated from ALS patients and induced to differentiate into myotubes showed decreased expression of MHC and fusion defects (Pradat et al. 2011). These results are reminiscent of what we observed in *Smn*$^{2B/-}$ myotubes. Therefore, the notion of delayed expression of myogenic proteins *in vivo* appears to be specific to mouse models of SMA. However in culture, primary myoblasts from ALS patients behave like those isolated from *Smn*$^{2B/-}$ mice and from SMA patients (Arnold et al. 2004).

Spinal bulbar muscular atrophy (SBMA) is caused by expansion of a polyglutamine (polyQ)-encoding CAG trinucleotide repeat in the first exon of the gene coding for the androgen receptor (AR) (Malena et al. 2013). These repeats are toxic and lead to motor neuron death causing respiratory weakness in adult SBMA patients (Bricceno et al. 2012). Proliferation and differentiation are not affected in primary myoblasts isolated from SBMA patients (Malena et al. 2013). In a mouse model of SBMA, defects such as altered levels of myogenic regulatory factors and decreased expression of the muscle chloride channel 1 and the $Na_v1.4$ sodium channel have been reported (Yu et al. 2006). Furthermore, the muscle-specific overexpression of the androgen receptor in mice led to motor neuron defects and denervation-induced muscle defects (Monks et al. 2007). Thus, this would suggest that muscle toxicity leads to diseased motor neurons. Unlike in mouse models of SMA, muscle defects in SBMA are demonstrated to be caused by muscle degeneration and denervation rather than impaired

muscle development. Therefore, the defects that we report in mouse models of SMA appear to be unique in nature when compared to other motor neuron diseases.

Closing remarks

By taking advantage of model mice we provide tremendous insight into the contributions of skeletal muscle defects in SMA. Importantly, we have done so in a way that highlights intrinsic defects in the context of disease pathology. The results from the physiological experiments reveal that profound muscle weakness is an early feature present in mouse models of SMA. We have for the first time, demonstrated how muscle defects can contribute to the disease phenotype independently of motor neuron pathology. Our work should lead the field to re-evaluate the classification of SMA, which has long been strictly considered a motor neuron disease.

Understanding how Smn regulates the expression of myogenic transcription factors will provide valuable knowledge regarding the disease pathogenesis and may lead to novel therapeutics. The myogenic contributions to SMA appear to be unique when compared to other motor neuron diseases. This observation highlights an important factor to consider in the development of therapeutics tailored specifically for SMA. Given our findings, it is imperative that skeletal muscles be considered as a therapeutic target when developing strategies to rescue SMA.

References

Aebersold, R. and M. Mann (2003). "Mass spectrometry-based proteomics." Nature **422**(6928): 198-207.

Arnold, A. S., M. Gueye, S. Guettier-Sigrist, I. Courdier-Fruh, G. Coupin, P. Poindron and J. P. Gies (2004). "Reduced expression of nicotinic AChRs in myotubes from spinal muscular atrophy I patients." Lab Invest **84**(10): 1271-1278.

Battle, D. J., M. Kasim, J. Yong, F. Lotti, C. K. Lau, J. Mouaikel, Z. Zhang, K. Han, L. Wan and G. Dreyfuss (2006). "The SMN complex: an assembly machine for RNPs." Cold Spring Harb Symp Quant Biol **71**: 313-320.

Baümer, D., S. Lee, G. Nicholson, J. L. Davies, N. J. Parkinson, L. M. Murray, T. H. Gillingwater, O. Ansorge, K. E. Davies and K. Talbot (2009). "Alternative splicing events are a late feature of pathology in a mouse model of spinal muscular atrophy." PLoS Genet **5**(12): e1000773.

Beard, N. A., D. R. Laver and A. F. Dulhunty (2004). "Calsequestrin and the calcium release channel of skeletal and cardiac muscle." Prog Biophys Mol Biol **85**(1): 33-69.

Bentzinger, C. F., Y. X. Wang and M. A. Rudnicki (2012). "Building muscle: molecular regulation of myogenesis." Cold Spring Harb Perspect Biol **4**(2).

Black, B. L. and E. N. Olson (1998). "Transcriptional control of muscle development by myocyte enhancer factor-2 (MEF2) proteins." Annu Rev Cell Dev Biol **14**: 167-196.

Boisvert, F. M., J. Cote, M. C. Boulanger, P. Cleroux, F. Bachand, C. Autexier and S. Richard (2002). "Symmetrical dimethylarginine methylation is required for the localization of SMN in Cajal bodies and pre-mRNA splicing." J Cell Biol **159**(6): 957-969.

Boon, K. L., S. Xiao, M. L. McWhorter, T. Donn, E. Wolf-Saxon, M. T. Bohnsack, C. B. Moens and C. E. Beattie (2009). "Zebrafish survival motor neuron mutants exhibit presynaptic neuromuscular junction defects." Hum Mol Genet **18**(19): 3615-3625.

Bowerman, M., C. L. Anderson, A. Beauvais, P. P. Boyl, W. Witke and R. Kothary (2009). "SMN, profilin IIa and plastin 3: A link between the deregulation of actin dynamics and SMA pathogenesis." Mol Cell Neurosci.

Bowerman, M., C. L. Anderson, A. Beauvais, P. P. Boyl, W. Witke and R. Kothary (2009). "SMN, profilin IIa and plastin 3: a link between the deregulation of actin dynamics and SMA pathogenesis." Mol Cell Neurosci **42**(1): 66-74.

Bowerman, M., A. Beauvais, C. L. Anderson and R. Kothary (2010). "Rho-kinase inactivation prolongs survival of an intermediate SMA mouse model." Hum Mol Genet **19**(8): 1468-1478.

Bowerman, M., L. M. Murray, A. Beauvais, B. Pinheiro and R. Kothary (2012). "A critical smn threshold in mice dictates onset of an intermediate spinal muscular atrophy phenotype associated with a distinct neuromuscular junction pathology." Neuromuscul Disord **22**(3): 263-276.

Bowerman, M., L. M. Murray, J. G. Boyer, C. L. Anderson and R. Kothary (2012). "Fasudil improves survival and promotes skeletal muscle development in a mouse model of spinal muscular atrophy." BMC Med **10**: 24.

Bowerman, M., D. Shafey and R. Kothary (2007). "Smn depletion alters profilin II expression and leads to upregulation of the RhoA/ROCK pathway and defects in neuronal integrity." J Mol Neurosci **32**(2): 120-131.

Boyer, J. G., K. Bhanot, R. Kothary and C. Boudreau-Lariviere (2010a). "Hearts of dystonia musculorum mice display normal morphological and histological features but show signs of cardiac stress." PLoS One **5**(3): e9465.

Boyer, J. G., M. Bowerman and R. Kothary (2010). "The many faces of SMN: deciphering the function critical to spinal muscular atrophy pathogenesis." Future Neurology **5**(6): 873-890.

Brahe, C., O. Clermont, S. Zappata, F. Tiziano, J. Melki and G. Neri (1996). "Frameshift mutation in the survival motor neuron gene in a severe case of SMA type I." Hum Mol Genet **5**(12): 1971-1976.

Braun, S., B. Croizat, M. C. Lagrange, J. M. Warter and P. Poindron (1995). "Constitutive muscular abnormalities in culture in spinal muscular atrophy." Lancet **345**(8951): 694-695.

Braun, T. and M. Gautel (2011). "Transcriptional mechanisms regulating skeletal muscle differentiation, growth and homeostasis." Nat Rev Mol Cell Biol **12**(6): 349-361.

Bray, D. and K. Chapman (1985). "Analysis of microspike movements on the neuronal growth cone." J Neurosci **5**(12): 3204-3213.

Bricceno, K. V., K. H. Fischbeck and B. G. Burnett (2012). "Neurogenic and myogenic contributions to hereditary motor neuron disease." Neurodegener Dis **9**(4): 199-209.

Brzustowicz, L. M., C. Merette, P. W. Kleyn, T. Lehner, L. H. Castilla, G. K. Penchaszadeh, K. Das, T. L. Munsat, J. Ott and T. C. Gilliam (1993). "Assessment of nonallelic genetic heterogeneity of chronic (type II and III) spinal muscular atrophy." Hum Hered **43**(6): 380-387.

Buhler, D., V. Raker, R. Luhrmann and U. Fischer (1999). "Essential role for the tudor domain of SMN in spliceosomal U snRNP assembly: implications for spinal muscular atrophy." Hum Mol Genet **8**(13): 2351-2357.

Buhler, D., V. Raker, R. Luhrmann and U. Fischer (1999). "Essential role for the tudor domain of SMN in spliceosomal U snRNP assembly: implications for spinal muscular atrophy." Hum Mol Genet **8**(13): 2351-2357.

Burghes, A. H. and C. E. Beattie (2009). "Spinal muscular atrophy: why do low levels of survival motor neuron protein make motor neurons sick?" Nat Rev Neurosci **10**(8): 597-609.

Burglen, L., S. Lefebvre, O. Clermont, P. Burlet, L. Viollet, C. Cruaud, A. Munnich and J. Melki (1996). "Structure and organization of the human survival motor neurone (SMN) gene." Genomics **32**(3): 479-482.

Bussaglia, E., O. Clermont, E. Tizzano, S. Lefebvre, L. Burglen, C. Cruaud, J. A. Urtizberea, J. Colomer, A. Munnich, M. Baiget and et al. (1995). "A frame-shift deletion in the survival motor neuron gene in Spanish spinal muscular atrophy patients." Nat Genet **11**(3): 335-337.

Campbell, L., K. M. Hunter, P. Mohaghegh, J. M. Tinsley, M. A. Brasch and K. E. Davies (2000). "Direct interaction of Smn with dp103, a putative RNA helicase: a role for Smn in transcription regulation?" Hum Mol Genet **9**(7): 1093-1100.

Carrel, T. L., M. L. McWhorter, E. Workman, H. Zhang, E. C. Wolstencroft, C. Lorson, G. J. Bassell, A. H. Burghes and C. E. Beattie (2006). "Survival motor neuron function in motor axons is independent of functions required for small nuclear ribonucleoprotein biogenesis." J Neurosci **26**(43): 11014-11022.

Cartegni, L., M. L. Hastings, J. A. Calarco, E. de Stanchina and A. R. Krainer (2006). "Determinants of exon 7 splicing in the spinal muscular atrophy genes, SMN1 and SMN2." Am J Hum Genet **78**(1): 63-77.

Cartegni, L. and A. R. Krainer (2002). "Disruption of an SF2/ASF-dependent exonic splicing enhancer in SMN2 causes spinal muscular atrophy in the absence of SMN1." Nat Genet **30**(4): 377-384.

Carvalho, T., F. Almeida, A. Calapez, M. Lafarga, M. T. Berciano and M. Carmo-Fonseca (1999). "The spinal muscular atrophy disease gene product, SMN: A link between snRNP biogenesis and the Cajal (coiled) body." J Cell Biol **147**(4): 715-728.

Chan, Y. B., I. Miguel-Aliaga, C. Franks, N. Thomas, B. Trulzsch, D. B. Sattelle, K. E. Davies and M. van den Heuvel (2003). "Neuromuscular defects in a Drosophila survival motor neuron gene mutant." Hum Mol Genet **12**(12): 1367-1376.

Chang, H. C., D. N. Dimlich, T. Yokokura, A. Mukherjee, M. W. Kankel, A. Sen, V. Sridhar, T. A. Fulga, A. C. Hart, D. Van Vactor and S. Artavanis-Tsakonas (2008). "Modeling spinal muscular atrophy in Drosophila." PLoS One **3**(9): e3209.

Chari, A., M. M. Golas, M. Klingenhager, N. Neuenkirchen, B. Sander, C. Englbrecht, A. Sickmann, H. Stark and U. Fischer (2008). "An assembly chaperone collaborates with the SMN complex to generate spliceosomal SnRNPs." Cell **135**(3): 497-509.

Charrasse, S., F. Comunale, Y. Grumbach, F. Poulat, A. Blangy and C. Gauthier-Rouviere (2006). "RhoA GTPase regulates M-cadherin activity and myoblast fusion." Mol Biol Cell **17**(2): 749-759.

Charroux, B., L. Pellizzoni, R. A. Perkinson, A. Shevchenko, M. Mann and G. Dreyfuss (1999). "Gemin3: A novel DEAD box protein that interacts with SMN, the spinal muscular atrophy gene product, and is a component of gems." J Cell Biol **147**(6): 1181-1194.

Charroux, B., L. Pellizzoni, R. A. Perkinson, J. Yong, A. Shevchenko, M. Mann and G. Dreyfuss (2000). "Gemin4. A novel component of the SMN complex that is found in both gems and nucleoli." J Cell Biol **148**(6): 1177-1186.

Chen, J. F., Y. Tao, J. Li, Z. Deng, Z. Yan, X. Xiao and D. Z. Wang (2010). "microRNA-1 and microRNA-206 regulate skeletal muscle satellite cell proliferation and differentiation by repressing Pax7." J Cell Biol **190**(5): 867-879.

Chen, Q., S. D. Baird, M. Mahadevan, A. Besner-Johnston, R. Farahani, J. Xuan, X. Kang, C. Lefebvre, J. E. Ikeda, R. G. Korneluk and A. E. MacKenzie (1998). "Sequence of a 131-kb region of 5q13.1 containing the spinal muscular atrophy candidate genes SMN and NAIP." Genomics **48**(1): 121-127.

Cherasse, Y., A. C. Maurin, C. Chaveroux, C. Jousse, V. Carraro, L. Parry, C. Deval, C. Chambon, P. Fafournoux and A. Bruhat (2007). "The p300/CBP-associated factor (PCAF) is a cofactor of ATF4 for amino acid-regulated transcription of CHOP." Nucleic Acids Res **35**(17): 5954-5965.

Cho, S. and G. Dreyfuss (2010). "A degron created by SMN2 exon 7 skipping is a principal contributor to spinal muscular atrophy severity." Genes Dev **24**(5): 438-442.

Cifuentes-Diaz, C., T. Frugier, F. D. Tiziano, E. Lacene, N. Roblot, V. Joshi, M. H. Moreau and J. Melki (2001). "Deletion of murine SMN exon 7 directed to skeletal muscle leads to severe muscular dystrophy." J Cell Biol **152**(5): 1107-1114.

Cifuentes-Diaz, C., S. Nicole, M. E. Velasco, C. Borra-Cebrian, C. Panozzo, T. Frugier, G. Millet, N. Roblot, V. Joshi and J. Melki (2002). "Neurofilament accumulation at the motor endplate and lack of axonal sprouting in a spinal muscular atrophy mouse model." Hum Mol Genet **11**(12): 1439-1447.

Cingolani, L. A. and Y. Goda (2008). "Actin in action: the interplay between the actin cytoskeleton and synaptic efficacy." Nat Rev Neurosci **9**(5): 344-356.

Cobb, M. S., F. F. Rose, H. Rindt, J. J. Glascock, M. Shababi, M. R. Miller, E. Y. Osman, P. F. Yen, M. L. Garcia, B. R. Martin, M. J. Wetz, C. Mazzasette, Z. Feng, C. P. Ko and C. L. Lorson (2013). "Development and characterization of an SMN2-based intermediate mouse model of Spinal Muscular Atrophy." Hum Mol Genet **22**(9): 1843-1855.

Côté, J. and S. Richard (2005). "Tudor domains bind symmetrical dimethylated arginines." J Biol Chem **280**(31): 28476-28483.

Crawford, T. O. and C. A. Pardo (1996). "The neurobiology of childhood spinal muscular atrophy." Neurobiol Dis **3**(2): 97-110.

da Silva, J. S. and C. G. Dotti (2002). "Breaking the neuronal sphere: regulation of the actin cytoskeleton in neuritogenesis." Nat Rev Neurosci **3**(9): 694-704.

Da Silva, J. S., M. Medina, C. Zuliani, A. Di Nardo, W. Witke and C. G. Dotti (2003). "RhoA/ROCK regulation of neuritogenesis via profilin IIa-mediated control of actin stability." J Cell Biol **162**(7): 1267-1279.

Dachs, E., M. Hereu, L. Piedrafita, A. Casanovas, J. Caldero and J. E. Esquerda (2011). "Defective neuromuscular junction organization and postnatal myogenesis in mice with severe spinal muscular atrophy." J Neuropathol Exp Neurol **70**(6): 444-461.

David, M., R. Martinez-Marmol, T. Gonzalez, A. Felipe and C. Valenzuela (2008). "Differential regulation of Na(v)beta subunits during myogenesis." Biochem Biophys Res Commun **368**(3): 761-766.

DiDonato, C. J., X. N. Chen, D. Noya, J. R. Korenberg, J. H. Nadeau and L. R. Simard (1997). "Cloning, characterization, and copy number of the murine survival motor neuron gene: homolog of the spinal muscular atrophy-determining gene." Genome Res **7**(4): 339-352.

Dillon, C. and Y. Goda (2005). "The actin cytoskeleton: integrating form and function at the synapse." Annu Rev Neurosci **28**: 25-55.

Divet, A. and C. Huchet-Cadiou (2002). "Sarcoplasmic reticulum function in slow- and fast-twitch skeletal muscles from mdx mice." Pflugers Arch **444**(5): 634-643.

Dubowitz, V. (1999). "Very severe spinal muscular atrophy (SMA type 0): an expanding clinical phenotype." Eur J Paediatr Neurol **3**(2): 49-51.

Elias, J. E., W. Haas, B. K. Faherty and S. P. Gygi (2005). "Comparative evaluation of mass spectrometry platforms used in large-scale proteomics investigations." Nat Methods **2**(9): 667-675.

Etienne-Manneville, S. and A. Hall (2002). "Rho GTPases in cell biology." Nature **420**(6916): 629-635.

Fan, L. and L. R. Simard (2002). "Survival motor neuron (SMN) protein: role in neurite outgrowth and neuromuscular maturation during neuronal differentiation and development." Hum Mol Genet **11**(14): 1605-1614.

Fifkova, E. and R. J. Delay (1982). "Cytoplasmic actin in neuronal processes as a possible mediator of synaptic plasticity." J Cell Biol **95**(1): 345-350.

Fischer, U., Q. Liu and G. Dreyfuss (1997). "The SMN-SIP1 complex has an essential role in spliceosomal snRNP biogenesis." Cell **90**(6): 1023-1029.

Futatsugi, A., G. Kuwajima and K. Mikoshiba (1995). "Tissue-specific and developmentally regulated alternative splicing in mouse skeletal muscle ryanodine receptor mRNA." Biochem J **305 (Pt 2)**: 373-378.

Gabanella, F., M. E. Butchbach, L. Saieva, C. Carissimi, A. H. Burghes and L. Pellizzoni (2007). "Ribonucleoprotein assembly defects correlate with spinal muscular atrophy severity and preferentially affect a subset of spliceosomal snRNPs." PLoS One **2**(9): e921.

Gabanella, F., C. Carissimi, A. Usiello and L. Pellizzoni (2005). "The activity of the spinal muscular atrophy protein is regulated during development and cellular differentiation." Hum Mol Genet **14**(23): 3629-3642.

Gavrilina, T. O., V. L. McGovern, E. Workman, T. O. Crawford, R. G. Gogliotti, C. J. DiDonato, U. R. Monani, G. E. Morris and A. H. Burghes (2008). "Neuronal SMN expression corrects spinal muscular atrophy in severe SMA mice while muscle-specific SMN expression has no phenotypic effect." Hum Mol Genet **17**(8): 1063-1075.

Giesemann, T., S. Rathke-Hartlieb, M. Rothkegel, J. W. Bartsch, S. Buchmeier, B. M. Jockusch and H. Jockusch (1999). "A role for polyproline motifs in the spinal muscular atrophy protein SMN. Profilins bind to and colocalize with smn in nuclear gems." J Biol Chem **274**(53): 37908-37914.

Giesemann, T., S. Rathke-Hartlieb, M. Rothkegel, J. W. Bartsch, S. Buchmeier, B. M. Jockusch and H. Jockusch (1999). "A role for polyproline motifs in the spinal muscular atrophy protein SMN. Profilins bind to and colocalize with smn in nuclear gems." J Biol Chem **274**(53): 37908-37914.

Giganti, A., J. Plastino, B. Janji, M. Van Troys, D. Lentz, C. Ampe, C. Sykes and E. Friederich (2005). "Actin-filament cross-linking protein T-plastin increases Arp2/3-mediated actin-based movement." J Cell Sci **118**(Pt 6): 1255-1265.

Glenney, J. R., Jr., P. Kaulfus, P. Matsudaira and K. Weber (1981). "F-actin binding and bundling properties of fimbrin, a major cytoskeletal protein of microvillus core filaments." J Biol Chem **256**(17): 9283-9288.

Gonsalvez, G. B., L. Tian, J. K. Ospina, F. M. Boisvert, A. I. Lamond and A. G. Matera (2007). "Two distinct arginine methyltransferases are required for biogenesis of Sm-class ribonucleoproteins." J Cell Biol **178**(5): 733-740.

Goonasekera, S. A., C. K. Lam, D. P. Millay, M. A. Sargent, R. J. Hajjar, E. G. Kranias and J. D. Molkentin (2011). "Mitigation of muscular dystrophy in mice by SERCA overexpression in skeletal muscle." J Clin Invest **121**(3): 1044-1052.

Hahnen, E., R. Forkert, C. Marke, S. Rudnik-Schoneborn, J. Schonling, K. Zerres and B. Wirth (1995). "Molecular analysis of candidate genes on chromosome 5q13 in autosomal recessive spinal muscular atrophy: evidence of homozygous deletions of the SMN gene in unaffected individuals." Hum Mol Genet **4**(10): 1927-1933.

Hahnen, E., J. Schonling, S. Rudnik-Schoneborn, H. Raschke, K. Zerres and B. Wirth (1997). "Missense mutations in exon 6 of the survival motor neuron gene in patients with spinal muscular atrophy (SMA)." Hum Mol Genet **6**(5): 821-825.

Hahnen, E., J. Schonling, S. Rudnik-Schoneborn, K. Zerres and B. Wirth (1996). "Hybrid survival motor neuron genes in patients with autosomal recessive spinal muscular atrophy: new insights into molecular mechanisms responsible for the disease." Am J Hum Genet **59**(5): 1057-1065.

Hamilton, G. and T. H. Gillingwater (2013). "Spinal muscular atrophy: going beyond the motor neuron." Trends Mol Med **19**(1): 40-50.

Hammond, S. M., R. G. Gogliotti, V. Rao, A. Beauvais, R. Kothary and C. J. DiDonato (2010). "Mouse survival motor neuron alleles that mimic SMN2 splicing and are inducible rescue embryonic lethality early in development but not late." PLoS One **5**(12): e15887.

Haramati, S., E. Chapnik, Y. Sztainberg, R. Eilam, R. Zwang, N. Gershoni, E. McGlinn, P. W. Heiser, A. M. Wills, I. Wirguin, L. L. Rubin, H. Misawa, C. J. Tabin, R. Brown, Jr., A. Chen and E. Hornstein (2010). "miRNA malfunction causes spinal motor neuron disease." Proc Natl Acad Sci U S A **107**(29): 13111-13116.

Hayhurst, M., A. K. Wagner, M. Cerletti, A. J. Wagers and L. L. Rubin (2012). "A cell-autonomous defect in skeletal muscle satellite cells expressing low levels of survival of motor neuron protein." Dev Biol **368**(2): 323-334.

Hebert, M. D., P. W. Szymczyk, K. B. Shpargel and A. G. Matera (2001). "Coilin forms the bridge between Cajal bodies and SMN, the spinal muscular atrophy protein." Genes Dev **15**(20): 2720-2729.

Hebert, S. L., C. Simmons, A. L. Thompson, C. S. Zorc, E. M. Blalock and S. D. Kraner (2007). "Basic helix-loop-helix factors recruit nuclear factor I to enhance expression of the NaV 1.4 Na+ channel gene." Biochim Biophys Acta **1769**(11-12): 649-658.

Hsieh-Li, H. M., J. G. Chang, Y. J. Jong, M. H. Wu, N. M. Wang, C. H. Tsai and H. Li (2000). "A mouse model for spinal muscular atrophy." Nat Genet **24**(1): 66-70.

Huber, J., U. Cronshagen, M. Kadokura, C. Marshallsay, T. Wada, M. Sekine and R. Luhrmann (1998). "Snurportin1, an m3G-cap-specific nuclear import receptor with a novel domain structure." EMBO J **17**(14): 4114-4126.

Jablonka, S., B. Schrank, M. Kralewski, W. Rossoll and M. Sendtner (2000). "Reduced survival motor neuron (Smn) gene dose in mice leads to motor neuron degeneration: an animal model for spinal muscular atrophy type III." Hum Mol Genet **9**(3): 341-346.

Jones, K. W., K. Gorzynski, C. M. Hales, U. Fischer, F. Badbanchi, R. M. Terns and M. P. Terns (2001). "Direct interaction of the spinal muscular atrophy disease protein SMN with the small nucleolar RNA-associated protein fibrillarin." J Biol Chem **276**(42): 38645-38651.

Kallen, R. G., S. A. Cohen and R. L. Barchi (1993). "Structure, function and expression of voltage-dependent sodium channels." Mol Neurobiol **7**(3-4): 383-428.

Kariya, S., G. H. Park, Y. Maeno-Hikichi, O. Leykekhman, C. Lutz, M. S. Arkovitz, L. T. Landmesser and U. R. Monani (2008). "Reduced SMN protein impairs maturation of the neuromuscular junctions in mouse models of spinal muscular atrophy." Hum Mol Genet **17**(16): 2552-2569.

Kashima, T. and J. L. Manley (2003). "A negative element in SMN2 exon 7 inhibits splicing in spinal muscular atrophy." Nat Genet **34**(4): 460-463.

Kashima, T., N. Rao, C. J. David and J. L. Manley (2007). "hnRNP A1 functions with specificity in repression of SMN2 exon 7 splicing." Hum Mol Genet **16**(24): 3149-3159.

Kimura, K., M. Ito, M. Amano, K. Chihara, Y. Fukata, M. Nakafuku, B. Yamamori, J. Feng, T. Nakano, K. Okawa, A. Iwamatsu and K. Kaibuchi (1996). "Regulation of myosin phosphatase by Rho and Rho-associated kinase (Rho-kinase)." Science **273**(5272): 245-248.

Kimura, T., M. Nakamori, J. D. Lueck, P. Pouliquin, F. Aoike, H. Fujimura, R. T. Dirksen, M. P. Takahashi, A. F. Dulhunty and S. Sakoda (2005). "Altered mRNA

splicing of the skeletal muscle ryanodine receptor and sarcoplasmic/endoplasmic reticulum Ca2+-ATPase in myotonic dystrophy type 1." Hum Mol Genet **14**(15): 2189-2200.

Knuesel, M., Y. Wan, Z. Xiao, E. Holinger, N. Lowe, W. Wang and X. Liu (2003). "Identification of novel protein-protein interactions using a versatile mammalian tandem affinity purification expression system." Mol Cell Proteomics **2**(11): 1225-1233.

Kong, L., X. Wang, D. W. Choe, M. Polley, B. G. Burnett, M. Bosch-Marce, J. W. Griffin, M. M. Rich and C. J. Sumner (2009). "Impaired synaptic vesicle release and immaturity of neuromuscular junctions in spinal muscular atrophy mice." J Neurosci **29**(3): 842-851.

Landis, D. M., A. K. Hall, L. A. Weinstein and T. S. Reese (1988). "The organization of cytoplasm at the presynaptic active zone of a central nervous system synapse." Neuron **1**(3): 201-209.

Le, T. T., L. T. Pham, M. E. Butchbach, H. L. Zhang, U. R. Monani, D. D. Coovert, T. O. Gavrilina, L. Xing, G. J. Bassell and A. H. Burghes (2005). "SMNDelta7, the major product of the centromeric survival motor neuron (SMN2) gene, extends survival in mice with spinal muscular atrophy and associates with full-length SMN." Hum Mol Genet **14**(6): 845-857.

Lee, Y. I., M. Mikesh, I. Smith, M. Rimer and W. Thompson (2011). "Muscles in a mouse model of spinal muscular atrophy show profound defects in neuromuscular development even in the absence of failure in neuromuscular transmission or loss of motor neurons." Dev Biol **356**(2): 432-444.

Lefebvre, S., L. Burglen, S. Reboullet, O. Clermont, P. Burlet, L. Viollet, B. Benichou, C. Cruaud, P. Millasseau, M. Zeviani and et al. (1995). "Identification and characterization of a spinal muscular atrophy- determining gene." Cell **80**(1): 155-165.

Lefebvre, S., L. Burglen, S. Reboullet, O. Clermont, P. Burlet, L. Viollet, B. Benichou, C. Cruaud, P. Millasseau, M. Zeviani and et al. (1995). "Identification and characterization of a spinal muscular atrophy-determining gene." Cell **80**(1): 155-165.

Lefebvre, S., P. Burlet, Q. Liu, S. Bertrandy, O. Clermont, A. Munnich, G. Dreyfuss and J. Melki (1997). "Correlation between severity and SMN protein level in spinal muscular atrophy." Nat Genet **16**(3): 265-269.

Lefebvre, S., P. Burlet, L. Viollet, S. Bertrandy, C. Huber, C. Belser and A. Munnich (2002). "A novel association of the SMN protein with two major non-ribosomal nucleolar proteins and its implication in spinal muscular atrophy." Hum Mol Genet **11**(9): 1017-1027.

Liu, H., D. Shafey, J. N. Moores and R. Kothary (2010). "Neurodevelopmental consequences of Smn depletion in a mouse model of spinal muscular atrophy." J Neurosci Res **88**(1): 111-122.

Liu, Q. and G. Dreyfuss (1996). "A novel nuclear structure containing the survival of motor neurons protein." Embo J **15**(14): 3555-3565.

Liu, Q., U. Fischer, F. Wang and G. Dreyfuss (1997). "The spinal muscular atrophy disease gene product, SMN, and its associated protein SIP1 are in a complex with spliceosomal snRNP proteins." Cell **90**(6): 1013-1021.

Lorson, C. L. and E. J. Androphy (1998). "The domain encoded by exon 2 of the survival motor neuron protein mediates nucleic acid binding." Hum Mol Genet **7**(8): 1269-1275.

Lorson, C. L., E. Hahnen, E. J. Androphy and B. Wirth (1999). "A single nucleotide in the SMN gene regulates splicing and is responsible for spinal muscular atrophy." Proc Natl Acad Sci U S A **96**(11): 6307-6311.

Lorson, C. L., H. Rindt and M. Shababi (2010). "Spinal muscular atrophy: mechanisms and therapeutic strategies." Hum Mol Genet **19**(R1): R111-118.

Lorson, C. L., J. Strasswimmer, J. M. Yao, J. D. Baleja, E. Hahnen, B. Wirth, T. Le, A. H. Burghes and E. J. Androphy (1998). "SMN oligomerization defect correlates with spinal muscular atrophy severity." Nat Genet **19**(1): 63-66.

Lotti, F., W. L. Imlach, L. Saieva, E. S. Beck, T. Hao le, D. K. Li, W. Jiao, G. Z. Mentis, C. E. Beattie, B. D. McCabe and L. Pellizzoni (2012). "An SMN-dependent U12 splicing event essential for motor circuit function." Cell **151**(2): 440-454.

Lupa, M. T., D. M. Krzemien, K. L. Schaller and J. H. Caldwell (1995). "Expression and distribution of sodium channels in short- and long-term denervated rodent skeletal muscles." J Physiol **483 (Pt 1)**: 109-118.

MacLeod, M. J., J. E. Taylor, P. W. Lunt, C. G. Mathew and S. A. Robb (1999). "Prenatal onset spinal muscular atrophy." Eur J Paediatr Neurol **3**(2): 65-72.

Malena, A., M. Pennuto, C. Tezze, G. Querin, C. D'Ascenzo, V. Silani, G. Cenacchi, A. Scaramozza, S. Romito, L. Morandi, E. Pegoraro, A. P. Russell, G. Soraru and L. Vergani (2013). "Androgen-dependent impairment of myogenesis in spinal and bulbar muscular atrophy." Acta Neuropathol.

Manzano, R., J. M. Toivonen, A. C. Calvo, S. Olivan, P. Zaragoza, C. Rodellar, D. Montarras and R. Osta (2013). "Altered in vitro proliferation of mouse SOD1-G93A skeletal muscle satellite cells." Neurodegener Dis **11**(3): 153-164.

Manzano, R., J. M. Toivonen, S. Olivan, A. C. Calvo, M. Moreno-Igoa, M. J. Munoz, P. Zaragoza, A. Garcia-Redondo and R. Osta (2011). "Altered expression of myogenic regulatory factors in the mouse model of amyotrophic lateral sclerosis." Neurodegener Dis **8**(5): 386-396.

Martinez, T. L., L. Kong, X. Wang, M. A. Osborne, M. E. Crowder, J. P. Van Meerbeke, X. Xu, C. Davis, J. Wooley, D. J. Goldhamer, C. M. Lutz, M. M. Rich and C. J. Sumner (2012). "Survival motor neuron protein in motor neurons determines synaptic integrity in spinal muscular atrophy." J Neurosci **32**(25): 8703-8715.

Martinez-Hernandez, R., C. Soler-Botija, E. Also, L. Alias, L. Caselles, I. Gich, S. Bernal and E. F. Tizzano (2009). "The developmental pattern of myotubes in spinal muscular atrophy indicates prenatal delay of muscle maturation." J Neuropathol Exp Neurol **68**(5): 474-481.

McKinnell, I. W., J. Ishibashi, F. Le Grand, V. G. Punch, G. C. Addicks, J. F. Greenblatt, F. J. Dilworth and M. A. Rudnicki (2007). "Pax7 activates myogenic genes by recruitment of a histone methyltransferase complex." Nat Cell Biol.

McWhorter, M. L., U. R. Monani, A. H. Burghes and C. E. Beattie (2003). "Knockdown of the survival motor neuron (Smn) protein in zebrafish causes defects in motor axon outgrowth and pathfinding." J Cell Biol **162**(5): 919-931.

Meister, G., D. Buhler, B. Laggerbauer, M. Zobawa, F. Lottspeich and U. Fischer (2000). "Characterization of a nuclear 20S complex containing the survival of motor neurons (SMN) protein and a specific subset of spliceosomal Sm proteins." Hum Mol Genet **9**(13): 1977-1986.

Meister, G., D. Buhler, R. Pillai, F. Lottspeich and U. Fischer (2001). "A multiprotein complex mediates the ATP-dependent assembly of spliceosomal U snRNPs." Nat Cell Biol **3**(11): 945-949.

Melki, J., S. Abdelhak, P. Sheth, M. F. Bachelot, P. Burlet, A. Marcadet, J. Aicardi, A. Barois, J. P. Carriere, M. Fardeau and et al. (1990). "Gene for chronic proximal spinal muscular atrophies maps to chromosome 5q." Nature **344**(6268): 767-768.

Melki, J., S. Lefebvre, L. Burglen, P. Burlet, O. Clermont, P. Millasseau, S. Reboullet, B. Benichou, M. Zeviani, D. Le Paslier and et al. (1994). "De novo and inherited deletions of the 5q13 region in spinal muscular atrophies." Science **264**(5164): 1474-1477.

Menell, J. S., G. M. Cesarman, A. T. Jacovina, M. A. McLaughlin, E. A. Lev and K. A. Hajjar (1999). "Annexin II and bleeding in acute promyelocytic leukemia." N Engl J Med **340**(13): 994-1004.

Michaud, M., T. Arnoux, S. Bielli, E. Durand, Y. Rotrou, S. Jablonka, F. Robert, M. Giraudon-Paoli, M. Riessland, M. G. Mattei, E. Andriambeloson, B. Wirth, M. Sendtner, J. Gallego, R. M. Pruss and T. Bordet (2010). "Neuromuscular defects and breathing disorders in a new mouse model of spinal muscular atrophy." Neurobiol Dis **38**(1): 125-135.

Millay, D. P., S. A. Goonasekera, M. A. Sargent, M. Maillet, B. J. Aronow and J. D. Molkentin (2009). "Calcium influx is sufficient to induce muscular dystrophy through a TRPC-dependent mechanism." Proc Natl Acad Sci U S A **106**(45): 19023-19028.

Monani, U. R., D. D. Coovert and A. H. Burghes (2000). "Animal models of spinal muscular atrophy." Hum Mol Genet **9**(16): 2451-2457.

Monani, U. R., M. Sendtner, D. D. Coovert, D. W. Parsons, C. Andreassi, T. T. Le, S. Jablonka, B. Schrank, W. Rossol, T. W. Prior, G. E. Morris and A. H. Burghes (2000). "The human centromeric survival motor neuron gene (SMN2) rescues embryonic lethality in Smn(-/-) mice and results in a mouse with spinal muscular atrophy." Hum Mol Genet **9**(3): 333-339.

Monani, U. R., M. Sendtner, D. D. Coovert, D. W. Parsons, C. Andreassi, T. T. Le, S. Jablonka, B. Schrank, W. Rossoll, T. W. Prior, G. E. Morris and A. H. Burghes (2000). "The human centromeric survival motor neuron gene (SMN2) rescues embryonic

lethality in Smn(-/-) mice and results in a mouse with spinal muscular atrophy." Hum Mol Genet **9**(3): 333-339.

Monks, D. A., J. A. Johansen, K. Mo, P. Rao, B. Eagleson, Z. Yu, A. P. Lieberman, S. M. Breedlove and C. L. Jordan (2007). "Overexpression of wild-type androgen receptor in muscle recapitulates polyglutamine disease." Proc Natl Acad Sci U S A **104**(46): 18259-18264.

Montes, J., A. M. Gordon, S. Pandya, D. C. De Vivo and P. Kaufmann (2009). "Clinical outcome measures in spinal muscular atrophy." J Child Neurol **24**(8): 968-978.

Morel, J., F. Rannou, H. Talarmin, M. A. Giroux-Metges, J. P. Pennec, G. Dorange and G. Gueret (2010). "Sodium channel Na(V)1.5 expression is enhanced in cultured adult rat skeletal muscle fibers." J Membr Biol **235**(2): 109-119.

Mouaikel, J., U. Narayanan, C. Verheggen, A. G. Matera, E. Bertrand, J. Tazi and R. Bordonne (2003). "Interaction between the small-nuclear-RNA cap hypermethylase and the spinal muscular atrophy protein, survival of motor neuron." EMBO Rep **4**(6): 616-622.

Munsat, T. L. and K. E. Davies (1992). "International SMA consortium meeting. (26-28 June 1992, Bonn, Germany)." Neuromuscul Disord **2**(5-6): 423-428.

Murray, L. M., A. Beauvais, K. Bhanot and R. Kothary (2012). "Defects in neuromuscular junction remodelling in the Smn(2B/-) mouse model of spinal muscular atrophy." Neurobiol Dis **49C**: 57-67.

Murray, L. M., L. H. Comley, D. Thomson, N. Parkinson, K. Talbot and T. H. Gillingwater (2008). "Selective vulnerability of motor neurons and dissociation of pre- and post-synaptic pathology at the neuromuscular junction in mouse models of spinal muscular atrophy." Hum Mol Genet **17**(7): 949-962.

Murray, L. M., S. Lee, D. Baumer, S. H. Parson, K. Talbot and T. H. Gillingwater (2010). "Pre-symptomatic development of lower motor neuron connectivity in a mouse model of severe spinal muscular atrophy." Hum Mol Genet **19**(3): 420-433.

Murray, L. M., K. Talbot and T. H. Gillingwater (2010). "Review: neuromuscular synaptic vulnerability in motor neurone disease: amyotrophic lateral sclerosis and spinal muscular atrophy." Neuropathol Appl Neurobiol **36**(2): 133-156.

Mutsaers, C. A., T. M. Wishart, D. J. Lamont, M. Riessland, J. Schreml, L. H. Comley, L. M. Murray, S. H. Parson, H. Lochmuller, B. Wirth, K. Talbot and T. H. Gillingwater (2011). "Reversible molecular pathology of skeletal muscle in spinal muscular atrophy." Hum Mol Genet.

Narayanan, U., T. Achsel, R. Luhrmann and A. G. Matera (2004). "Coupled in vitro import of U snRNPs and SMN, the spinal muscular atrophy protein." Mol Cell **16**(2): 223-234.

Narayanan, U., J. K. Ospina, M. R. Frey, M. D. Hebert and A. G. Matera (2002). "SMN, the spinal muscular atrophy protein, forms a pre-import snRNP complex with snurportin1 and importin beta." Hum Mol Genet **11**(15): 1785-1795.

Nicole, S., B. Desforges, G. Millet, J. Lesbordes, C. Cifuentes-Diaz, D. Vertes, M. L. Cao, F. De Backer, L. Languille, N. Roblot, V. Joshi, J. M. Gillis and J. Melki (2003). "Intact satellite cells lead to remarkable protection against Smn gene defect in differentiated skeletal muscle." J Cell Biol **161**(3): 571-582.

Nishiyama, T., I. Kii and A. Kudo (2004). "Inactivation of Rho/ROCK signaling is crucial for the nuclear accumulation of FKHR and myoblast fusion." J Biol Chem **279**(45): 47311-47319.

O'Rourke, J. R., S. A. Georges, H. R. Seay, S. J. Tapscott, M. T. McManus, D. J. Goldhamer, M. S. Swanson and B. D. Harfe (2007). "Essential role for Dicer during skeletal muscle development." Dev Biol **311**(2): 359-368.

Ogino, S., D. G. Leonard, H. Rennert, W. J. Ewens and R. B. Wilson (2002). "Genetic risk assessment in carrier testing for spinal muscular atrophy." Am J Med Genet **110**(4): 301-307.

Oprea, G. E., S. Krober, M. L. McWhorter, W. Rossoll, S. Muller, M. Krawczak, G. J. Bassell, C. E. Beattie and B. Wirth (2008). "Plastin 3 is a protective modifier of autosomal recessive spinal muscular atrophy." Science **320**(5875): 524-527.

Oskoui, M., G. Levy, C. J. Garland, J. M. Gray, J. O'Hagen, D. C. De Vivo and P. Kaufmann (2007). "The changing natural history of spinal muscular atrophy type 1." Neurology **69**(20): 1931-1936.

Palacios, I., M. Hetzer, S. A. Adam and I. W. Mattaj (1997). "Nuclear import of U snRNPs requires importin beta." EMBO J **16**(22): 6783-6792.

Park, G. H., S. Kariya and U. R. Monani (2010). "Spinal muscular atrophy: new and emerging insights from model mice." Curr Neurol Neurosci Rep **10**(2): 108-117.

Parsons, D. W., P. E. McAndrew, U. R. Monani, J. R. Mendell, A. H. Burghes and T. W. Prior (1996). "An 11 base pair duplication in exon 6 of the SMN gene produces a type I spinal muscular atrophy (SMA) phenotype: further evidence for SMN as the primary SMA-determining gene." Hum Mol Genet **5**(11): 1727-1732.

Paushkin, S., A. K. Gubitz, S. Massenet and G. Dreyfuss (2002). "The SMN complex, an assemblyosome of ribonucleoproteins." Curr Opin Cell Biol **14**(3): 305-312.

Pearn, J. (1978). "Incidence, prevalence, and gene frequency studies of chronic childhood spinal muscular atrophy." J Med Genet **15**(6): 409-413.

Pearn, J. (1980). "Classification of spinal muscular atrophies." Lancet **1**(8174): 919-922.

Pellizzoni, L., J. Baccon, B. Charroux and G. Dreyfuss (2001). "The survival of motor neurons (SMN) protein interacts with the snoRNP proteins fibrillarin and GAR1." Curr Biol **11**(14): 1079-1088.

Pellizzoni, L., B. Charroux and G. Dreyfuss (1999). "SMN mutants of spinal muscular atrophy patients are defective in binding to snRNP proteins." Proc Natl Acad Sci U S A **96**(20): 11167-11172.

Pellizzoni, L., B. Charroux, J. Rappsilber, M. Mann and G. Dreyfuss (2001). "A functional interaction between the survival motor neuron complex and RNA polymerase II." J Cell Biol **152**(1): 75-85.

Pellizzoni, L., N. Kataoka, B. Charroux and G. Dreyfuss (1998). "A novel function for SMN, the spinal muscular atrophy disease gene product, in pre-mRNA splicing." Cell **95**(5): 615-624.

Pellizzoni, L., J. Yong and G. Dreyfuss (2002). "Essential role for the SMN complex in the specificity of snRNP assembly." Science **298**(5599): 1775-1779.

Pradat, P. F., A. Barani, J. Wanschitz, O. Dubourg, A. Lombes, A. Bigot, V. Mouly, G. Bruneteau, F. Salachas, T. Lenglet, V. Meininger and G. Butler-Browne (2011). "Abnormalities of satellite cells function in amyotrophic lateral sclerosis." Amyotroph Lateral Scler **12**(4): 264-271.

Praveen, K., Y. Wen and A. G. Matera (2012). "A Drosophila model of spinal muscular atrophy uncouples snRNP biogenesis functions of survival motor neuron from locomotion and viability defects." Cell Rep **1**(6): 624-631.

Prior, T. W., P. J. Snyder, B. D. Rink, D. K. Pearl, R. E. Pyatt, D. C. Mihal, T. Conlan, B. Schmalz, L. Montgomery, K. Ziegler, C. Noonan, S. Hashimoto and S. Garner (2010). "Newborn and carrier screening for spinal muscular atrophy." Am J Med Genet A **152A**(7): 1608-1616.

Puig, O., F. Caspary, G. Rigaut, B. Rutz, E. Bouveret, E. Bragado-Nilsson, M. Wilm and B. Seraphin (2001). "The tandem affinity purification (TAP) method: a general procedure of protein complex purification." Methods **24**(3): 218-229.

Rajendra, T. K., G. B. Gonsalvez, M. P. Walker, K. B. Shpargel, H. K. Salz and A. G. Matera (2007). "A Drosophila melanogaster model of spinal muscular atrophy reveals a function for SMN in striated muscle." J Cell Biol **176**(6): 831-841.

Rando, T. A. and H. M. Blau (1994). "Primary mouse myoblast purification, characterization, and transplantation for cell-mediated gene therapy." J Cell Biol **125**(6): 1275-1287.

Rezniczek, G. A., P. Konieczny, B. Nikolic, S. Reipert, D. Schneller, C. Abrahamsberg, K. E. Davies, S. J. Winder and G. Wiche (2007). "Plectin 1f scaffolding at the sarcolemma of dystrophic (mdx) muscle fibers through multiple interactions with beta-dystroglycan." J Cell Biol **176**(7): 965-977.

Rich, M. M., S. D. Kraner and R. L. Barchi (1999). "Altered gene expression in steroid-treated denervated muscle." Neurobiol Dis **6**(6): 515-522.

Rigaut, G., A. Shevchenko, B. Rutz, M. Wilm, M. Mann and B. Seraphin (1999). "A generic protein purification method for protein complex characterization and proteome exploration." Nat Biotechnol **17**(10): 1030-1032.

Rochette, C. F., N. Gilbert and L. R. Simard (2001). "SMN gene duplication and the emergence of the SMN2 gene occurred in distinct hominids: SMN2 is unique to Homo sapiens." Hum Genet **108**(3): 255-266.

Rossoll, W., A. K. Kroning, U. M. Ohndorf, C. Steegborn, S. Jablonka and M. Sendtner (2002). "Specific interaction of Smn, the spinal muscular atrophy determining gene

product, with hnRNP-R and gry-rbp/hnRNP-Q: a role for Smn in RNA processing in motor axons?" Hum Mol Genet **11**(1): 93-105.

Sakaba, T. and E. Neher (2003). "Involvement of actin polymerization in vesicle recruitment at the calyx of Held synapse." J Neurosci **23**(3): 837-846.

Schiaffino, S. and C. Reggiani (1996). "Molecular diversity of myofibrillar proteins: gene regulation and functional significance." Physiol Rev **76**(2): 371-423.

Schrank, B., R. Gotz, J. M. Gunnersen, J. M. Ure, K. V. Toyka, A. G. Smith and M. Sendtner (1997). "Inactivation of the survival motor neuron gene, a candidate gene for human spinal muscular atrophy, leads to massive cell death in early mouse embryos." Proc Natl Acad Sci U S A **94**(18): 9920-9925.

Seale, P., L. A. Sabourin, A. Girgis-Gabardo, A. Mansouri, P. Gruss and M. A. Rudnicki (2000). "Pax7 is required for the specification of myogenic satellite cells." Cell **102**(6): 777-786.

Selenko, P., R. Sprangers, G. Stier, D. Buhler, U. Fischer and M. Sattler (2001). "SMN tudor domain structure and its interaction with the Sm proteins." Nat Struct Biol **8**(1): 27-31.

Shafey, D., J. G. Boyer, K. Bhanot and R. Kothary (2010). "Identification of novel interacting protein partners of SMN using tandem affinity purification." J Proteome Res **9**(4): 1659-1669.

Shafey, D., P. D. Cote and R. Kothary (2005). "Hypomorphic Smn knockdown C2C12 myoblasts reveal intrinsic defects in myoblast fusion and myotube morphology." Exp Cell Res **311**(1): 49-61.

Shafey, D., A. E. MacKenzie and R. Kothary (2008). "Neurodevelopmental abnormalities in neurosphere-derived neural stem cells from SMN-depleted mice." J Neurosci Res **86**(13): 2839-2847.

Sharma, A., A. Lambrechts, T. Hao le, T. T. Le, C. A. Sewry, C. Ampe, A. H. Burghes and G. E. Morris (2005). "A role for complexes of survival of motor neurons (SMN) protein with gemins and profilin in neurite-like cytoplasmic extensions of cultured nerve cells." Exp Cell Res **309**(1): 185-197.

Shupliakov, O., O. Bloom, J. S. Gustafsson, O. Kjaerulff, P. Low, N. Tomilin, V. A. Pieribone, P. Greengard and L. Brodin (2002). "Impaired recycling of synaptic vesicles

after acute perturbation of the presynaptic actin cytoskeleton." Proc Natl Acad Sci U S A **99**(22): 14476-14481.

Strasswimmer, J., C. L. Lorson, D. E. Breiding, J. J. Chen, T. Le, A. H. Burghes and E. J. Androphy (1999). "Identification of survival motor neuron as a transcriptional activator-binding protein." Hum Mol Genet **8**(7): 1219-1226.

Szczesna, D., J. Zhao, M. Jones, G. Zhi, J. Stull and J. D. Potter (2002). "Phosphorylation of the regulatory light chains of myosin affects Ca2+ sensitivity of skeletal muscle contraction." J Appl Physiol **92**(4): 1661-1670.

Talbot, K., C. P. Ponting, A. M. Theodosiou, N. R. Rodrigues, R. Surtees, R. Mountford and K. E. Davies (1997). "Missense mutation clustering in the survival motor neuron gene: a role for a conserved tyrosine and glycine rich region of the protein in RNA metabolism?" Hum Mol Genet **6**(3): 497-500.

Totsukawa, G., Y. Yamakita, S. Yamashiro, D. J. Hartshorne, Y. Sasaki and F. Matsumura (2000). "Distinct roles of ROCK (Rho-kinase) and MLCK in spatial regulation of MLC phosphorylation for assembly of stress fibers and focal adhesions in 3T3 fibroblasts." J Cell Biol **150**(4): 797-806.

Tucker, K. E., M. T. Berciano, E. Y. Jacobs, D. F. LePage, K. B. Shpargel, J. J. Rossire, E. K. Chan, M. Lafarga, R. A. Conlon and A. G. Matera (2001). "Residual Cajal bodies in coilin knockout mice fail to recruit Sm snRNPs and SMN, the spinal muscular atrophy gene product." J Cell Biol **154**(2): 293-307.

Ueda, K., M. Murata-Hori, M. Tatsuka and H. Hosoya (2002). "Rho-kinase contributes to diphosphorylation of myosin II regulatory light chain in nonmuscle cells." Oncogene **21**(38): 5852-5860.

van Bergeijk, J., K. Rydel-Konecke, C. Grothe and P. Claus (2007). "The spinal muscular atrophy gene product regulates neurite outgrowth: importance of the C terminus." Faseb J **21**(7): 1492-1502.

van der Steege, G., P. M. Grootscholten, J. M. Cobben, S. Zappata, H. Scheffer, J. T. den Dunnen, G. J. van Ommen, C. Brahe and C. H. Buys (1996). "Apparent gene conversions involving the SMN gene in the region of the spinal muscular atrophy locus on chromosome 5." Am J Hum Genet **59**(4): 834-838.

Van Petegem, F. (2012). "Ryanodine receptors: structure and function." J Biol Chem **287**(38): 31624-31632.

Vitte, J. M., B. Davoult, N. Roblot, M. Mayer, V. Joshi, S. Courageot, F. Tronche, J. Vadrot, M. H. Moreau, F. Kemeny and J. Melki (2004). "Deletion of murine Smn exon 7 directed to liver leads to severe defect of liver development associated with iron overload." Am J Pathol **165**(5): 1731-1741.

Waisman, D. M. (1995). "Annexin II tetramer: structure and function." Mol Cell Biochem **149-150**: 301-322.

Walker, M. P., T. K. Rajendra, L. Saieva, J. L. Fuentes, L. Pellizzoni and A. G. Matera (2008). "SMN complex localizes to the sarcomeric Z-disc and is a proteolytic target of calpain." Hum Mol Genet **17**(21): 3399-3410.

Wan, L., D. J. Battle, J. Yong, A. K. Gubitz, S. J. Kolb, J. Wang and G. Dreyfuss (2005). "The survival of motor neurons protein determines the capacity for snRNP assembly: biochemical deficiency in spinal muscular atrophy." Mol Cell Biol **25**(13): 5543-5551.

Will, C. L. and R. Luhrmann (2001). "Spliceosomal UsnRNP biogenesis, structure and function." Curr Opin Cell Biol **13**(3): 290-301.

Williams, A. H., G. Valdez, V. Moresi, X. Qi, J. McAnally, J. L. Elliott, R. Bassel-Duby, J. R. Sanes and E. N. Olson (2009). "MicroRNA-206 delays ALS progression and promotes regeneration of neuromuscular synapses in mice." Science **326**(5959): 1549-1554.

Wilm, M., A. Shevchenko, T. Houthaeve, S. Breit, L. Schweigerer, T. Fotsis and M. Mann (1996). "Femtomole sequencing of proteins from polyacrylamide gels by nano-electrospray mass spectrometry." Nature **379**(6564): 466-469.

Winkler, C., C. Eggert, D. Gradl, G. Meister, M. Giegerich, D. Wedlich, B. Laggerbauer and U. Fischer (2005). "Reduced U snRNP assembly causes motor axon degeneration in an animal model for spinal muscular atrophy." Genes Dev **19**(19): 2320-2330.

Wirth, B., L. Brichta, B. Schrank, H. Lochmuller, S. Blick, A. Baasner and R. Heller (2006). "Mildly affected patients with spinal muscular atrophy are partially protected by an increased SMN2 copy number." Hum Genet **119**(4): 422-428.

Wong, M. and L. J. Martin (2010). "Skeletal muscle-restricted expression of human SOD1 causes motor neuron degeneration in transgenic mice." Hum Mol Genet **19**(11): 2284-2302.

Yang, P., H. M. Sampson and H. M. Krause (2006). "A modified tandem affinity purification strategy identifies cofactors of the Drosophila nuclear receptor dHNF4." Proteomics **6**(3): 927-935.

Young, P. J., T. T. Le, N. thi Man, A. H. Burghes and G. E. Morris (2000). "The relationship between SMN, the spinal muscular atrophy protein, and nuclear coiled bodies in differentiated tissues and cultured cells." Exp Cell Res **256**(2): 365-374.

Young, P. J., N. T. Man, C. L. Lorson, T. T. Le, E. J. Androphy, A. H. Burghes and G. E. Morris (2000). "The exon 2b region of the spinal muscular atrophy protein, SMN, is involved in self-association and SIP1 binding." Hum Mol Genet **9**(19): 2869-2877.

Yu, Z., N. Dadgar, M. Albertelli, K. Gruis, C. Jordan, D. M. Robins and A. P. Lieberman (2006). "Androgen-dependent pathology demonstrates myopathic contribution to the Kennedy disease phenotype in a mouse knock-in model." J Clin Invest **116**(10): 2663-2672.

Zhang, H. L., F. Pan, D. Hong, S. M. Shenoy, R. H. Singer and G. J. Bassell (2003). "Active transport of the survival motor neuron protein and the role of exon-7 in cytoplasmic localization." J Neurosci **23**(16): 6627-6637.

Zhang, Z., F. Lotti, K. Dittmar, I. Younis, L. Wan, M. Kasim and G. Dreyfuss (2008). "SMN deficiency causes tissue-specific perturbations in the repertoire of snRNAs and widespread defects in splicing." Cell **133**(4): 585-600.

Appendix

1.0 Micro-RNA expression in Smn$^{-/-}$;SMN2 mice

Micro-RNAs (miRNAs) are short (~22 nucleotides) single-stranded RNAs that silence genes by binding to complementary mRNA sequences. Given the large number of predicted miRNA target genes, these molecules are likely key regulators of many cellular processes including maintaining neuronal cell integrity and skeletal muscle development (Wong and Martin 2010, Manzano et al. 2013). Interestingly, dysregulation of miRNAs has been observed in multiple neurodegenerative diseases and is the focus of intense study. The importance of miRNAs in motor neuron health and muscle development has previously been highlighted in conditional dicer knockout mouse models (O'Rourke et al. 2007, Haramati et al. 2010). The complete absence of miRNA activity in postmitotic motor neurons triggers severe pathology in mice which are phenotypically reminiscent of SMA model mice. Indeed, depletion of miRNA in motor neurons causes motor neuron loss, axonopathy and muscle atrophy that contribute to decreased motor function in mice (Haramati et al. 2010). We hypothesize that miRNAs are mis-regulated and play a role in the pathogenesis of SMA. To address this hypothesis, we performed miRNA microarray experiments using skeletal muscle and spinal cord samples from P5 control and *Smn$^{-/-}$;SMN2* mice. RNA was sent to the Centre for Applied Genomics (Toronto) for microarray processing. Microarray data analyses were performed in collaboration with Dr. Hang Yin in Dr. Michael Rudnicki's laboratory at the OHRI.

Our analyses revealed that 33 miRNAs appeared to be mis-regulated in spinal cords of *Smn$^{-/-}$;SMN2* mice (Fig. 1.1.). In skeletal muscle tissue, 61 miRNAs were identified as mis-regulated in *Smn$^{-/-}$;SMN2* samples compared to controls (Fig. 1.2.). We have cross-referenced our spinal cord microarray data with previously published gene

expression microarray data obtained from the same mouse model and time point (Murray et al. 2010). From the 33 abnormally expressed miRNAs in the spinal cord, 13 have corresponding mis-regulated target mRNA. Conversely, 27 out of 274 mis-regulated genes have corresponding differentially expressed miRNAs (Fig. 3.1.). Our data demonstrate that miRNA levels are altered in tissues of SMA model mice. This in turn could have an impact on gene regulation, which may play a role in the pathogenesis in SMA.

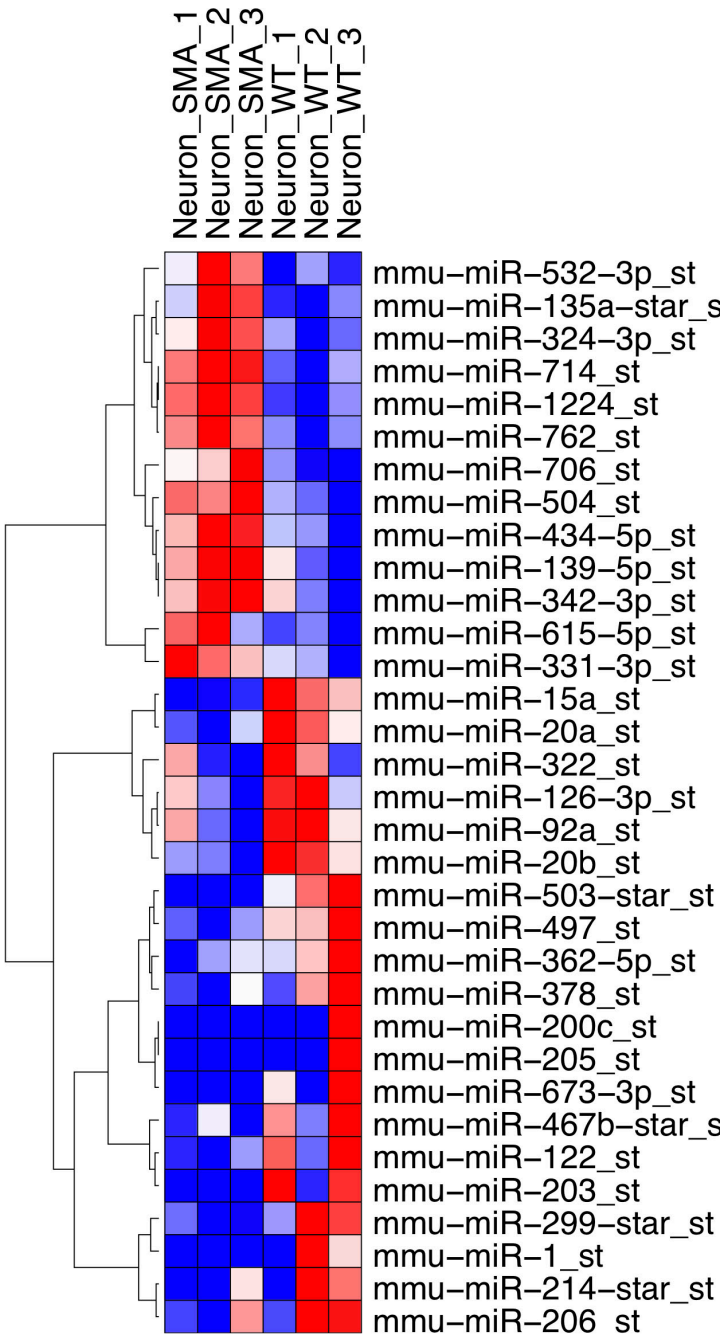
Neuron_SMA_1
Neuron_SMA_2
Neuron_SMA_3
Neuron_WT_1
Neuron_WT_2
Neuron_WT_3
mmu−miR−532−3p_st
mmu−miR−135a−star_s
mmu−miR−324−3p_st
mmu−miR−714_st
mmu−miR−1224_st
mmu−miR−762_st
mmu−miR−706_st
mmu−miR−504_st
mmu−miR−434−5p_st
mmu−miR−139−5p_st
mmu−miR−342−3p_st
mmu−miR−615−5p_st
mmu−miR−331−3p_st
mmu−miR−15a_st
mmu−miR−20a_st
mmu−miR−322_st
mmu−miR−126−3p_st
mmu−miR−92a_st
mmu−miR−20b_st
mmu−miR−503−star_st
mmu−miR−497_st
mmu−miR−362−5p_st
mmu−miR−378_st
mmu−miR−200c_st
mmu−miR−205_st
mmu−miR−673−3p_st
mmu−miR−467b−star_s
mmu−miR−122_st
mmu−miR−203_st
mmu−miR−299−star_st
mmu−miR−1_st
mmu−miR−214−star_st
mmu−miR−206_st

Figure 1. MiRNA profiling in spinal cords of *Smn*$^{-/-}$*;SMN2* and control mice.

Heat map and cluster analysis results showing 33 mis-regulated miRNAs that form distinct clusters between samples from controls and SMA model mice. A cutoff of 1.5 fold was used to analyze the data. $N = 3$, $p < 0.1$.

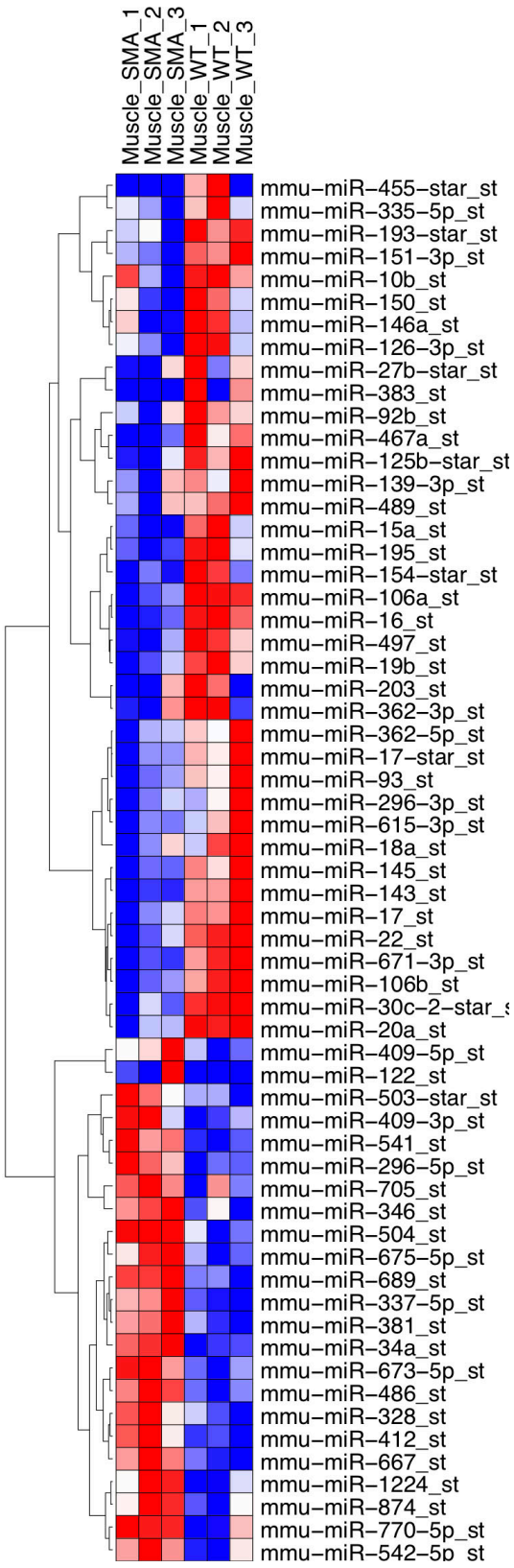
Muscle_SMA_1
Muscle_SMA_2
Muscle_SMA_3
Muscle_WT_1
Muscle_WT_2
Muscle_WT_3
mmu−miR−455−star_st
mmu−miR−335−5p_st
mmu−miR−193−star_st
mmu−miR−151−3p_st
mmu−miR−10b_st
mmu−miR−150_st
mmu−miR−146a_st
mmu−miR−126−3p_st
mmu−miR−27b−star_st
mmu−miR−383_st
mmu−miR−92b_st
mmu−miR−467a_st
mmu−miR−125b−star_st
mmu−miR−139−3p_st
mmu−miR−489_st
mmu−miR−15a_st
mmu−miR−195_st
mmu−miR−154−star_st
mmu−miR−106a_st
mmu−miR−16_st
mmu−miR−497_st
mmu−miR−19b_st
mmu−miR−203_st
mmu−miR−362−3p_st
mmu−miR−362−5p_st
mmu−miR−17−star_st
mmu−miR−93_st
mmu−miR−296−3p_st
mmu−miR−615−3p_st
mmu−miR−18a_st
mmu−miR−145_st
mmu−miR−143_st
mmu−miR−17_st
mmu−miR−22_st
mmu−miR−671−3p_st
mmu−miR−106b_st
mmu−miR−30c−2−star_
mmu−miR−20a_st
mmu−miR−409−5p_st
mmu−miR−122_st
mmu−miR−503−star_st
mmu−miR−409−3p_st
mmu−miR−541_st
mmu−miR−296−5p_st
mmu−miR−705_st
mmu−miR−346_st
mmu−miR−504_st
mmu−miR−675−5p_st
mmu−miR−689_st
mmu−miR−337−5p_st
mmu−miR−381_st
mmu−miR−34a_st
mmu−miR−673−5p_st
mmu−miR−486_st
mmu−miR−328_st
mmu−miR−412_st
mmu−miR−667_st
mmu−miR−1224_st
mmu−miR−874_st
mmu−miR−770−5p_st
mmu−miR−542−5p_st

Figure 1.2. MiRNA profiling in skeletal muscle of *Smn*$^{-/-}$*;SMN2* and control mice.

Heat map and cluster analysis results showing 61 mis-regulated miRNAs that form distinct clusters between samples from controls and SMA model mice. A cutoff of 1.5 fold was used to analyze the data. $N = 3$, $p < 0.1$.

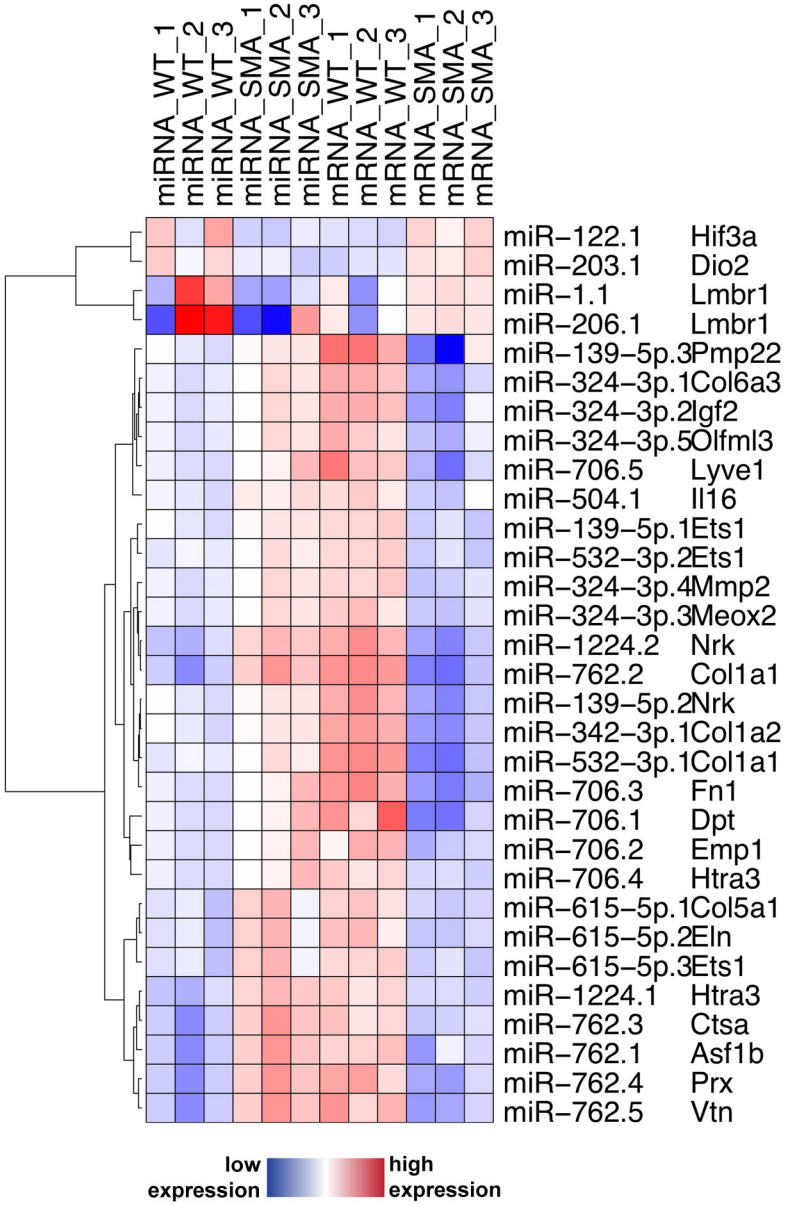

Figure 1.3. Association between microRNA and mRNA profiling in *Smn*$^{-/-}$*;SMN2* mice. Heat map and cluster results from spinal cord mis-regulated miRNAs and their associated mis-regulated putative mRNA targets. The putative target gene list of the mis-regulated miRNAs was cross-referenced with aberrantly expressed mRNA from *Smn*$^{-/-}$*;SMN2* spinal cords. From the 33 abnormally expressed miRNAs in *Smn*$^{-/-}$*;SMN2* spinal cords, 13 have corresponding targets that are aberrantly expressed. The predictions of miRNA targets are based on two programs (TargetScan v5 and Diana microT v3). N = 3, $p < 0.1$.